INFORMATION TO USERS

This manuscript has been reproduced from the microfilm master. UMI films the text directly from the original or copy submitted. Thus, some thesis and dissertation copies are in typewriter face, while others may be from any type of computer printer.

The quality of this reproduction is dependent upon the quality of the copy submitted. Broken or indistinct print, colored or poor quality illustrations and photographs, print bleedthrough, substandard margins, and improper alignment can adversely affect reproduction.

In the unlikely event that the author did not send UMI a complete manuscript and there are missing pages, these will be noted. Also, if unauthorized copyright material had to be removed, a note will indicate the deletion.

Oversize materials (e.g., maps, drawings, charts) are reproduced by sectioning the original, beginning at the upper left-hand corner and continuing from left to right in equal sections with small overlaps.

ProQuest Information and Learning
300 North Zeeb Road, Ann Arbor, MI 48106-1346 USA
800-521-0600

PROPERTIES OF LIGHT MESONS CALCULATED IN A RELATIVISTIC RANDOM-PHASE APPROXIMATION

By

HUANGSHENG WANG

A dissertation submitted to the Graduate Faculty in Physics in partial fulfillment of the requirements for the degree of Doctor of Philosophy, The City University of New York

2004

UMI Number: 3115302

UMI Microform 3115302

ProQuest Information and Learning Company
300 North Zeeb Road
P.O. Box 1346
Ann Arbor, MI 48106-1346

This manuscript has been read and accepted for the Graduate Faculty in Physics in satisfaction of the dissertation requirement for the degree of Doctor of Philosophy.

Jan 01, 2004
Date

Chair of Examining Committee

Jan 12, 2004
Date

Executive Officer

Carl M. Shakin

Louis S. Celenza

Ming-Kung Liou

Peter Lesser

William Shreiber

Supervisory Committee

The City University of New York

Abstract

PROPERTIES OF LIGHT MESONS CALCULATED IN A RELATIVISTIC RANDOM-PHASE APPROXIMATION

By

HUANGSHENG WANG

Advisor: Distinguished Professor Carl M. Shakin

In this work we report upon a large number of calculations made using a generalized Nambu – Jona-Lasinio (NJL) model that has been extended to include a covariant model of confinement. We discuss the properties of light mesons calculated in a covariant random-phase approximation (RPA). We describe the a_0, f_0, π, K, η, and η' mesons and their radial excitations. For the pseudoscalar mesons we include pseudoscalar – axial-vector coupling and report upon calculations of meson decay constants for all the meson states that we consider. In the case of the scalar mesons, the identification of the experimentally observed states with the states of our model is made complex due to the presence of "dynamically-generated" states such as the f_0(400-1200) and the κ(700-900). In this work we provide a precise definition of "intrinsic" and "dynamically-generated" states and present our suggestions for the distribution of scalar, vector and pseudoscalar states into nonets.

Acknowledgements

To Professor Carl M. Shakin, my thesis advisor, I wish to express my deepest gratitude for his valuable guidance and constant encouragement throughout this thesis work.

I would also like to express my sincere gratitude to Professor Louis S. Celenza of Brooklyn College of CUNY for many useful discussion and for help given to me during the course of this work.

I wish to acknowledge with gratitude the Department of Physics of Brooklyn College and the Research Foundation and The Graduate Center of CUNY for the financial support during the course of this work.

Table of Contents

List of Tables

List of Figures

Chapter 1

Introduction

In a series of papers, calculations of the properties of a very large number of states of light mesons have been reported. These works made use of a Nambu - Jona-Lasinio (NJL) model that has been generalized to include a covariant model of confinement. The previous work, did not take full advantage of the symmetries of the formalism and made a few approximations that obscured the relation of the model to many-body calculations made in the random-phase-approximation (RPA). We remedy that defect in this thesis and show that our calculations may be understood as being covariant RPA calculations of the properties of $q\bar{q}$ mesons. The introduction of confinement has been made in such a fashion as to allow for a simple presentation of results of Tamm-Dancoff Approximation (TDA) calculations and RPA calculations for the properties of mesons other than the pion and the kaon. (Proper calculations of Goldstone boson properties may only be made in the RPA.) In Chapter 2 we study the $a_0(980)$ and its radial excitations. The parameters of the model are known, so that the calculation of the properties of the a_0 mesons are parameter-free. We find, in one example, that the $a_0(980)$ mass is 1075 MeV in the TDA and 991 MeV in the RPA.(Addtional dispersive effects move the RPA result for the mass to 949 MeV.) This result strongly suggests that the $a_0(980)$ is mainly a $1\ ^3P_0\ n\bar{n}$ state which is

coupled to the $\pi\eta$ and $K\bar{K}$ continuum channels. We also discuss the results of the model for the f_0 mesons. In that case, we find that the use of the RPA rather than the TDA places the $f_0(980)$ at 980 MeV. That again suggests that, in a first approximation, the $f_0(980)$ is the $1\,^3P_0\ n\bar{n}$ state. Since the $f_0(980)$ resonance is rather distant in energy from the scalar glueball, which is expected to be in the range of 1500-1700 MeV, we do not believe that quarkonium-glueball mixing will be an important effect for the $f_0(980)$ resonance. However, we are not able to assess the importance of mixing with $q\bar{q}q\bar{q}$ states at this stage in the development of the model.

In Chapter 3 we consider pseudoscalar mesons and derive the equations of a relativistic random-phase approximation (RPA) for a study of the wave functions of the isovector pseudoscalar mesons. The inclusion of pseudoscalar - axial-vector coupling leads to doublets of states bound in the confining field. When the Nambu – Jona-Lasinio interaction is included, one member of each doublet moves down in energy, with the low-lying nodeless state representing the $\pi(138)$. The states affected in this manner may be termed "pionlike", while the other states, whose vertex structure is dominated by the $\gamma_0\gamma_5$ terms, may be designated as "mixed" states. Our formalism allows us to calculate the decay constants of the pionlike and mixed states. In the case of the pion we sum a series of vacuum-polarization diagrams which lead to a value of 0.769 for the axial charge of the pion. With that value we obtain a pion decay constant of $F_\pi = 134$ MeV which may be compared to the experimental value of 92.4 MeV. (We have not performed a parameter search to improve upon our result, but have used parameters that we have previously used in our study of light mesons.

A modest change in the regulator parameter from the value used previously reduces F_π to 124 MeV.) We find excited pionlike states at 1391, 1717 and 1960 MeV with decay constants of 30.5, 27.7 and 27.5 MeV, respectively. We find mixed states at 1325, 1652, 1890 and 2080 MeV with decay constants of 55.1, 49.0, 42.2 and 30.4 MeV, respectively. We also exhibit the wave functions for a number of pionlike and mixed states and compare the pion wave function obtained in our model with and without our covariant model of confinement.

The RPA provides wave functions whose structure is readily apparent, even in the case of the η mesons, where the RPA wave functions are expressed in terms of eight amplitudes. In Chapter 4 we describe the spectrum of the $T = 0$ $J^{PC} = 0^{-+}$ mesons up to 2.6 GeV. (However, we have not as yet studied η-glueball mixing.) We calculate the singlet and octet decay constants for the twenty-eight states we study and also present wave functions for the six states of lowest energy. For the $\eta(547)$ we find $F_\eta^{(0)}$ = 50.8 MeV and $F_\eta^{(8)}$ = 118 MeV. For the $\eta'(958)$ we find $F_{\eta'}^{(0)}$ = 109 MeV and $F_{\eta'}^{(8)}$ = 69.5 MeV. It is found that the $\eta(1295)$ and $\eta(1440)$ are almost entirely of $n\bar{n}$ character. The $\eta(1440)$ is a $2\ ^3S_0$ $n\bar{n}$ state with a very small $\gamma_0\gamma_5$ vertex component, while the $\gamma_0\gamma_5$ vertex is dominant in the $\eta(1295)$ wave function.

In Chapter 5 we present RPA wave functions for the $\pi(138)$, $K(495)$, $a_0(980)$, $a_0(1450)$ and $K_0^*(1430)$ mesons. For the a_0 and K_0^* mesons we calculate the decay constants using the definitions introduced by Maltman. We find that the use of the RPA rather than the TDA leads to a modest enhancement of the decay constants of the a_0 mesons and a small decrease in the case of the K_0^* mesons. On the whole, our values

are in reasonable agreement with those obtained by Maltman using QCD sum rules and other techniques in his analysis. One possible interpretation of our results is that the $a_0(980)$ wave function has an important $K\bar{K}$ component, since we overestimate the decay constant by about a factor of 2. Our results also suggest that the $a_0(980)$ and $K_0^*(1430)$ should be placed in the same nonet of scalar states.

It is well known that the RPA equations yield wave functions that are naturally separated into "large" and "small" components. These components are similar in magnitude for the pion, while the small components become progressively smaller as we consider mesons of increasing mass. However, even for the more massive mesons considered, the small components make non-negligible contributions when calculating decay constants. (We suspect that they will also be of significance in the calculation of other transition rates.)

Recent work by Maltman has given us confidence that our assignment of scalar meson states to various nonets based upon the generalized Nambu - Jona-Lasinio model is correct. (For example, in our model the $a_0(980)$ and the $f_0(980)$ are in the same nonet as the $K_0^*(1430)$). In Chapter 6 we make use of the model to provide a precise definition of "preexisting" resonances and "dynamically-generated" resonances when considering various scalar mesons. (This distinction has been noted by Meissner in his characterization of the $f_0(400\text{-}1200)$ as non-preexisting.) We define preexisting (or intrinsic) resonances as those that appear as singularities of the $q\bar{q}$ T matrix and are in correspondence with $q\bar{q}$ states bound in the confining field. (Additional singularities may be found when studying the T matrices describing π-π or π-K scattering, for

example. Such features may be seen to arise, in part, from t-channel and u-channel ρ exchange in the case of π-π scattering, leading to the introduction of the σ(500-600). In addition, threshold effects in the $q\bar{q}$ T matrix can give rise to significant broad cross section enhancements. The latter is, in part, responsible for the introduction of the κ(900) in a study of π-K scattering, for example.) We suggest that it is only the *intrinsic* resonances which correspond to $q\bar{q}$ quark-model states, and it is only the intrinsic states that are to be used to form quark-model $q\bar{q}$ nonets of states. (While the κ(900) and σ(500-600) could be placed in a nonet of *dynamically-generated* states, it is unclear whether there is evidence that requires the introduction of other members of such a nonet.) In this work we show how the phenomena related to the introduction of the σ(500-600) and the κ(900) are generated in studies of π-π and π-K scattering, making use of our generalized Nambu - Jona-Lasinio model.

Chapter 2

Covariant RPA Calculations of the Properties of Light Mesons

2.1 Introduction

In a series of works we have studied the properties of light mesons, making use of our generalized Nambu - Jona-Lasinio (NJL) model [Ce99a, Ce00]. In reference [Ce99a] we studied the pseudoscalar, vector, scalar and axial-vector nonets, while Ref.[Ce00] was mainly concerned with the properties of the f_0 mesons. References [Ce99b] and [Ce99c] were devoted to a study of the $a_0(980)$ and $K(495)$ mesons and their radial excitations, respectively.

The Lagrangian of our model is

$$\begin{aligned}\mathcal{L} = &\bar{q}(i\partial - m^0)q + \frac{G_S}{2}\sum_{i=0}^{8}\left[(\bar{q}\lambda^i q)^2 + (\bar{q}i\gamma_5\lambda^i q)^2\right] \\ &- \frac{G_V}{2}\sum_{i=0}^{8}\left[(\bar{q}\gamma^\mu\lambda^i q)^2 + (\bar{q}\gamma^\mu\gamma_5\lambda^i q)^2\right] \\ &+ \frac{G_D}{2}\left\{\det[\bar{q}(1+\gamma_5)q] + \det[\bar{q}(1-\gamma_5)q]\right\} \\ &+ \mathcal{L}_{tensor} + \mathcal{L}_{conf}\ .\end{aligned} \tag{2.1.1}$$

Here, the fourth term is the 't Hooft interaction, $\mathcal{L}_{tensor}$ denotes interactions added to study tensor mesons, while $\mathcal{L}_{conf}$ denotes our model of Lorentz-vector confinement. In

Eq.(2.1.1) m^0 is the current quark mass matrix $m^0 = \mathrm{diag}(m_u^0, m_d^0, m_s^0)$, the λ_i (i = 1, ...8) are the Gell-Mann matrices, and $\lambda_0 = \sqrt{2/3}\ \mathbb{I}$, with $\mathbb{I}$ being the unit matrix in flavor space.

2.2 Confinement Potential and Vertex Functions

Our model of confinement is based upon the coordinate-space potential $V(r) = \kappa r \exp[-\mu r]$, where μ is a small parameter introduced to facilitate our momentum-space calculations. Note that we do not have absolute confinement in our model. However, the $q\bar{q}$ states in the confining field are readily separated into states inside the potential barrier and scattering states that show little barrier penetration. We have $V_{max} = \kappa/\mu e$, which for κ = 0.055 GeV^2 and μ = 0.010 GeV, yields V_{max} = 2.023 GeV. Thus, we can find bound states in the interior region of the potential up to $E_{max} = m_a + m_{\bar{b}} + 2.023\,\mathrm{GeV}$. For constituent masses $m_u = m_d$ = 0.364 GeV and m_s = 0.565 GeV, E_{max} = 2.751 GeV, if we study $n\bar{n}$ systems, and E_{max} = 2.952 GeV for $n\bar{s}$ systems. Smaller values of μ may be used if we wish to increase the value of E_{max}. For μ = 0.010 GeV, we can find from 8 to 10 states bound in the confining field when we study scalar mesons, for example. (Barrier penetration is of no importance in this model.)

The Fourier transform of $V(r)$ is

$$V^C(\vec{k}-\vec{k}') = -8\pi\kappa \left[\frac{1}{\left[(\vec{k}-\vec{k}')^2 + \mu^2\right]^2} - \frac{4\mu^2}{\left[(\vec{k}-\vec{k}')^2 + \mu^2\right]^3} \right] . \qquad (2.2.1)$$

The model is made covariant through the use of the four-vectors

$$\hat{k}^{\mu} = k^{\mu} - \frac{(k\cdot P)P^{\mu}}{P^2} \ , \qquad (2.2.2)$$

and

$$\hat{k}'^{\mu} = k'^{\mu} - \frac{(k'\cdot P)P^{\mu}}{P^2} \ , \qquad (2.2.3)$$

since in the meson rest frame ($\vec{P} = 0$) $\hat{k}^{\mu} - \hat{k}'^{\mu} = [0, \vec{k} - \vec{k}']$. Thus, we may write

$$V^C(k-k') = -8\pi\kappa \left[\frac{1}{\left[-(\hat{k}-\hat{k}')^2 + \mu^2\right]^2} - \frac{4\mu^2}{\left[-(\hat{k}-\hat{k}')^2 + \mu^2\right]^3} \right] \ . \qquad (2.2.4)$$

We use the confining interaction to construct equations for various vertex functions [Ce99a, Ce00]. Let us consider the case of the scalar vertex for equal mass quarks. In the meson rest frame we may write

$$\bar{\Gamma}^S(P,k) = 1 - i\int \frac{d^4k'}{(2\pi)^4}\left[\gamma^{\rho} S(P/2+k')\bar{\Gamma}^S(P,k')S(-P/2+k')\gamma_{\rho}\right] V^C(\vec{k}-\vec{k}'), \qquad (2.2.5)$$

[See Fig.2.1.] Here, $\bar{\Gamma}^S(P,k)$ has a matrix structure. The Dirac matrices γ^{ρ} and γ_{ρ} appear in Eq.(2.2.5) because we are using Lorentz-vector confinement. It is useful to introduce functions Γ_S^{+-} and Γ_S^{-+} [Ce99a, Ce00]. First, we define the projection operators

$$\Lambda^{(+)}(\vec{k}) = \frac{\not{k} + m}{2m} \ , \qquad (2.2.6)$$

and

$$\Lambda^{(-)}(-\vec{k}) = \frac{\tilde{\not{k}} + m}{2m} \ , \tag{2.2.7}$$

with $k^{\mu} = [E(\vec{k}),\ \vec{k}]$ and $\tilde{k}^{\mu} = [-E(\vec{k}),\ \vec{k}]$. Then, we write (for $\vec{P} = 0$)

$$\Lambda^{(+)}(\vec{k})\,\bar{\Gamma}^{S}(P,k)\,\Lambda^{(-)}(-\vec{k}) = \Gamma_{S}^{+-}(P,k)\,\Lambda^{(+)}(\vec{k})\,\Lambda^{(-)}(-\vec{k}) \ , \tag{2.2.8}$$

and

$$\Lambda^{(-)}(-\vec{k})\,\bar{\Gamma}^{S}(P,k)\,\Lambda^{(+)}(\vec{k}) = \Gamma_{S}^{-+}(P,k)\,\Lambda^{(-)}(-\vec{k})\,\Lambda^{(+)}(\vec{k}) \ . \tag{2.2.9}$$

In our work we obtained the following equations for $\Gamma_{S}^{+-}(P,k)$ and $\Gamma_{S}^{-+}(P,k)$ in the frame where $\vec{P} = 0$,

$$\begin{aligned}\Gamma_{S}^{+-}(P^0,k) = 1 + \frac{1}{(2\pi)^2}\int k'^2 dk' \left[2k'^2k^2V_0^C(k,k') + m^2kk'V_1^C(k,k')\right] \\ \times \frac{1}{k^2E^2(\vec{k}')}\,\frac{\Gamma_{S}^{+-}(P^0,k')}{P^0 - 2E(\vec{k}')} \ ,\end{aligned} \tag{2.2.10}$$

and

$$\begin{aligned}\Gamma_{S}^{-+}(P^0,k) = 1 - \frac{1}{(2\pi)^2}\int k'^2 dk' \left[2k'^2k^2V_0^C(k,k') + m^2kk'V_1^C(k,k')\right] \\ \times \frac{1}{k^2E^2(\vec{k}')}\,\frac{\Gamma_{S}^{-+}(P^0,k')}{P^0 + 2E(\vec{k}')} \ .\end{aligned} \tag{2.2.11}$$

Here $k = |\vec{k}|$ and $k' = |\vec{k}'|$. With $x = \cos\theta$, we have

$$V_l^C(k,k') = \frac{1}{2}\int_{-1}^{1} dx\, P_l(x)\, V^C(\vec{k} - \vec{k}') \ , \tag{2.2.12}$$

where $P_l(x)$ is a Legendre polynomial. This formalism may be used to obtain covariant expressions for the vertex [Ce99a, Ce00]. We write

$$\bar{\Gamma}_S(P,k) = a_1(P,k) + \hat{k}\, a_2(P,k) \ , \qquad (2.2.13)$$

where $\hat{k}^\mu$ was defined previously in Eq.(2.2.2). We have

$$\Gamma_S^{+-}(P,k) = a_1(P,k) + m_q a_2(P,k) \ , \qquad (2.2.14)$$

$$\Gamma_S^{-+}(P,k) = a_1(P,k) - \frac{\vec{k}^2}{m_q} a_2(P,k) \ . \qquad (2.2.15)$$

Note that we can write $a_1(P,k) = a_1(P^2, \sqrt{-\hat{k}^2}\,)$ and $a_2(P,k) = a_2(P^2, \sqrt{-\hat{k}^2}\,)$. The Lorentz invariants a_1 and a_2 may be determined by relating them to the rest-frame values of $\Gamma_S^{+-}(P^0, |\vec{k}|)$ and $\Gamma_S^{-+}(P^0, |\vec{k}|)$ [Ce99a, Ce00]. (The case where the quark masses are different is discussed in great detail in [Ce99a].) Using this formalism, vacuum polarization diagrams and meson decay amplitudes may be calculated in any Lorentz frame and we have made a number of such calculations.

2.3 Vacuum Polarization Functions and Quark T Matrices

The vacuum polarization function seen in Fig.2.2a is given by the integral

$$-iJ^S(P^2) = -2n_C \int \frac{d^4k}{(2\pi)^4} \mathrm{Tr}\left[iS(P/2+k)\bar{\Gamma}^S(P,k) iS(-P/2+k) \right] \ , \qquad (2.3.1)$$

where the factor 2 arises from the flavor trace. In Eq.(2.3.1) $S(P/2+k)$ and $S(-P/2+k)$ are propagators for constituent quarks of mass m, $S(p) = \left[\not{p} - m + i\eta \right]^{-1}$. (The case of unequal mass values for the quarks is discussed in [Ce99a] and [Ce00].) We have

$$J^S(P^2) = -4n_c \int \frac{d^3k}{(2\pi)^3} \left[\frac{\vec{k}^2}{E^2(\vec{k})} \right] e^{-\vec{k}^2/\alpha^2} \times \left[\frac{\Gamma_S^{+-}(P^0, |\vec{k}|)}{P^0 - 2E(\vec{k})} - \frac{\Gamma_S^{-+}(-P^0, |\vec{k}|)}{P^0 + 2E(\vec{k})} \right] . \tag{2.3.2}$$

In Eq.(2.3.2) we have included a Gaussian regulator, $\exp[-\vec{k}^2/\alpha^2]$, which can be written in a covariant form using the four-vector $\hat{k}^\mu$ of Eq.(2.2.2). (In our earlier work [Ce00,Ce99b,Ce99c] we have used $\alpha = 0.605$ GeV.)

It is important for this work to note that from Eqs.(2.2.10) and (2.2.11), we have

$$\Gamma_S^{-+}(-P^0, |\vec{k}|) = \Gamma_S^{+-}(P^0, |\vec{k}|) , \tag{2.3.3}$$

so that Eq.(2.3.2) becomes

$$J^S(P^2) = -4n_c \int \frac{d^3k}{(2\pi)^3} \left[\frac{\vec{k}^2}{E^2(\vec{k})} \right] e^{-\vec{k}^2/\alpha^2} \times \Gamma_S^{+-}(P^0, |\vec{k}|) \left[\frac{1}{P^0 - 2E(\vec{k})} - \frac{1}{P^0 + 2E(\vec{k})} \right] . \tag{2.3.4}$$

In some of our calculations we have kept only the first term in the bracket of Eq.(2.3.4). That procedure defines the TDA, while the complete expression defines the RPA. [See Fig.2.3.]

We now turn to a definition of $q\bar{q}$ T matrices [Ce99a, Ce00]. We may write, for a single-channel problem,

$$t^{\mathrm{TDA}}(P^2) = -\frac{G}{1 - GJ^S_{\mathrm{TDA}}(P^2)} \tag{2.3.5}$$

and

$$t^{\mathrm{RPA}}(P^2) = -\frac{G}{1 - GJ^S_{\mathrm{RPA}}(P^2)} \ . \tag{2.3.6}$$

We may find the meson mass values by solving the equation

$$G^{-1} - J^S(P^2) = 0 \ , \tag{2.3.7}$$

for $J^S(P^2)$ equal to $J^S_{\mathrm{RPA}}(P^2)$ or $J^S_{\mathrm{TDA}}(P^2)$. More generally, we may include $K^S(P^2)$ of Fig.2.2b and write

$$t(P^2) = -\frac{G}{1 - G\left[J^S(P^2) + K^S(P^2)\right]} \tag{2.3.8}$$

$$= -\frac{1}{G^{-1} - \left[J^S(P^2) + \mathrm{Re}K^S(P^2)\right] - i\,\mathrm{Im}K^S(P^2)} . \tag{2.3.9}$$

(Note that $J^S(P^2)$ is of order n_C and $K^S(P^2)$ is of order 1.)

We may then solve

$$G^{-1} - \left[J^S(P^2) + \mathrm{Re}K^S(P^2)\right] = 0 \tag{2.3.10}$$

to obtain the mass values. The extension of this formalism to include singlet-octet coupling, as is appropriate in the study of the f_0 mesons, is given in [Ce00]. In that case, the coupling constants G_{88}, G_{08} and G_{00} appear. These may be related to the values of G_S, G_D and the matrix elements defining the vacuum condensates $\langle \bar{u}u \rangle$, $\langle \bar{d}d \rangle$ and $\langle \bar{s}s \rangle$ [Ce00]. We remark that the complete $q\bar{q}$ T matrix, which

is defined in Ref.[Ce99d], is shown there to be represented by only $q\bar{q}$ bound-state wave functions in the case we have absolute confinement.

We use the notation $n\bar{n} = [u\bar{u} + d\bar{d}]/\sqrt{2}$. In Fig.2.4 we show values of $J^S_{n\bar{n}}(P^2)$ in both the TDA [dotted line] and the RPA [solid line]. Here $m_u = m_d = 0.364$ GeV, $\kappa = 0.055$ GeV^2 and $\alpha = 0.605$ GeV. In Fig.2.5 we show values of $J^S_{s\bar{s}}(P^2)$ for the value $m_s = 0.565$ GeV and the same value of α. It is seen that the effects due to the use of the RPA rather than the TDA become relatively less important with increasing P^2. That may also be seen in Figs.2.6 and 2.7, where we compare the two approximations, TDA and RPA, for $J^S_{n\bar{n}}(P^2)$ and $J^S_{s\bar{s}}(P^2)$ in the range $0 < P^2 < 5$ GeV^2.

2.4 Choice of Parameters and the Properties of the a_0 Mesons

In order to determine the coupling constant for octet states, G_{88}, we consider the $K(495)$ meson using the formalism of [Ce99c]. (See Appendix A.) In Ref.[Ce99c] we include pseudoscalar - axial-vector mixing for the kaon and its radial excitations. With a Gaussian regulator parameter of $\alpha = 0.605$ GeV, we found the $K(495)$ at 495 MeV, if $G_{88} = 13.10$ GeV^{-2} and $G_V = 12.46$ GeV^{-2} [Ce99c]. In the absence of such mixing we may solve

$$G_{88}^{-1} - J_{PP}(P^2) = 0 \ , \qquad (2.4.1)$$

where $J^{PP}(P^2)$ was defined in [Ce99c] and in Appendix A. The solution of Eq.(2.4.1) yields $G_{88} = 12.77$ GeV^{-2}, which is quite close to the value 13.10 GeV^{-2} quoted above. In our earlier work we found that $G_{88} - G_{00} \simeq 2.00$ GeV^{-2} gave satisfactory results, so when we consider the f_0 mesons, we will use $G_{88} = 13.10$ GeV^{-2} and G_{00}

$= 11.10\ \text{GeV}^{-2}$.

As in some of our previous studies, we will neglect G_{08}, which is quite small. (The difference between G_{88} and G_{00} arises from the 't Hooft interaction.) At this point we wish to present the results of our calculations in such a way as to make the relation to RPA calculations of particle-hole dynamics in nuclear physics [Fe71, Ro70] more transparent. For example, in Fig.2.8 we show $J^S_{n\bar{n}}(P^0)$ calculated in the RPA. (The symmetry between positive and negative values of the energy is characteristic of the RPA [Fe71, Ro70].) We also show a dotted line which represents the value $G_{88}^{-1} = 0.07634\ \text{GeV}^2$, corresponding to the value $G_{88} = 13.10\ \text{GeV}^{-2}$ given above. In this manner we obtain the results given in Table I. It is seen there that the use of the RPA rather than the TDA improves upon the TDA results presented in [Ce99b] and brings the $a_0(980)$ mass to within 7 MeV of the experimental value.

Inclusion of $\text{Re}K^S(P^2)$ leads to a value of 949 MeV for the mass of the $a_0(980)$. [See Table 2.1.] The values of $K^S(P^2)$ used for this calculation are shown in Fig.2.9. The values for the individual channels, $\pi\eta$, $K\bar{K}$ and $\pi\eta'$ are given in Ref.[Ce99b]. For the present work we have divided $\text{Re}K(P^2)$ and $\text{Im}K(P^2)$, calculated for the $K\bar{K}$ channel, by 4, since the values given in Ref.[Ce99b] for these functions represent a significant overestimate. Note that $K(P^2)$ for $K\bar{K}$ intermediate states depends upon g^4_{Kqq}, where g_{Kqq} is the kaon-quark coupling constant.

2.5 Properties of the f_0 Mesons

In [Ce00] we presented the results of an extensive study of the f_0 mesons made in the TDA. As may be seen from Fig.11 of [Ce00], the state we identified as the

$f_0(980)$ resonance was found at about 1120 MeV. It was necessary to appeal to various dispersive effects to bring the energy of the state down to 980 MeV. To obtain this downward energy shift, we added a parameter to the model. We will now see that, just as in the case of the $a_0(980)$, a parameter-free RPA calculation provides the necessary downward shift in the mass of the $f_0(980)$ without the need of additional parameters.

In Fig.2.10 we show the result of our calculation with $G_{88} = 13.10$ GeV^{-2} and $G_{00} = 11.10$ GeV^{-2} of the absolute square of the $\pi\pi$ scattering matrix $|T_{\pi\pi}(E)|^2$ [Ce00]. The solid line has its peak value at $E = 980$ MeV. (Note that at that energy $|T_{\pi\pi}(E)|^2 = 1.0$.) The dotted curve is the result obtained when we put $\mathrm{Re}K^{\pi\pi}(P^2)$ and $\mathrm{Re}K^{K\bar{K}}(P^2)$ equal to zero. The peak of the dotted curve is at $E = 1060$ MeV. Thus, we see that $\mathrm{Re}K(P^2)$ induces a downward shift in energy of approximately 80 MeV. Combined with the use of the RPA rather than the TDA, we find satisfactory agreement with the experimental value of the mass of the $f_0(980)$.

In Fig.2.11 we show the absolute square of the T matrix describing $K\bar{K}$ scattering $|T_{K\bar{K}}(E)|^2$ [Ce00]. We find the $1\ ^3P_0\ s\bar{s}$ state at 1445 MeV in the RPA. In a first approximation, that neglects quarkonium-glueball mixing, we identify that state with the $f_0(1370)$, whose mass is not well determined. In Fig.2.12 we show $|T_{K\bar{K}}(E)|^2$ in more detail in the region where we find the $1\ ^3P_0\ s\bar{s}$ state. There, we see that the width of the state is about 40 MeV in the RPA. The dotted curve in the figure shows the result obtained when $\mathrm{Re}K(P^2) = 0$. The dotted curve has a peak at 1469 MeV indicating that inclusion of $\mathrm{Re}K^{\pi\pi}(P^2)$ and $\mathrm{Re}K^{K\bar{K}}(P^2)$ results in a downward shift of only 24 MeV in this case.

In Fig.2.13 we show various results obtained in our study of the f_0 mesons. Column a) shows the energies of the $n\bar{n}$ states bound in the confining field, while column c) shows the $s\bar{s}$ bound-state energies. Inclusion of the short-range NJL interaction and $\mathrm{Re}K^S(P^2)$ yields the values in column b). Since we have approximate ideal mixing, we indicate the states of mainly $s\bar{s}$ character by dotted lines. In column d) we show some of the states found in experiment. There is definitely a state at 1770 MeV, while the state at 1710 MeV may have $J = 0$ or $J = 2$ [Bu00].

The scalar glueball is thought to be in the region of 1.5-1.7 GeV before quarkonium-glueball mixing. Mixing of the glueball with the $q\bar{q}$ states is probably an essential feature of scalar meson dynamics in the region above 1 GeV. For example, the $s\bar{s}$ state that we found at 1445 MeV will probably mix significantly with the glueball and with the 2 $^3P_0$ $n\bar{n}$ state that we find at 1550 MeV. Such mixing is necessary to account for the fact that the $f_0(1370)$ decays mainly to the 4π continuum. It is not clear at this time whether the $f_0(1500)$, $f_J(1710)$ or the $f_0(1770)$ resonance has the main glueball component after quarkonium-glueball mixing is taken into account.

2.6 Discussion

The organization of scalar $q\bar{q}$ states into nonets is a subject of some controversy. For example, if the $a_0(980)$ and $f_0(980)$ are taken to be $K\bar{K}$ "molecules" [Ja95], one might chose the $f_0(1370)$ as mainly the 1 $^3P_0$ $n\bar{n}$ state, with the $f_0(1500)$ as mainly the 1 $^3P_0$ $s\bar{s}$ state. Then, the $f_0(1710)$ would have a large glueball component. Alternatively, the $f_0(1500)$ may be taken to have the major glueball component with the $f_0(1710)$ having a large $s\bar{s}$ component. One or the other of these

choices are considered in [Cl00] or in [Le99, Le00].

Other assignments of scalar states to various nonets are suggested in the literature. For example, Schechter and collaborators [Sa95, Bl98, Bl99, Bl00] place the σ(500-600), a_0(980), f_0(980) and κ(700-900) in the same nonet. Then the a_0(1450) is in the same nonet as the K_0^* (1430). These assignments lead to various problems with the energetics as described in [Bl00]. For example, one does not see the expected increase in energy when a u or d quark is replaced by a s quark in the passage from the a_0(1450) to the K_0^* (1430). These and other problems are discussed in Ref.[Bl00] and a model involving configuration mixing of the a_0(980) and K_0^* (1430) with two other states, possibly of $q\bar{q}q\bar{q}$ character, is introduced in an attempt to overcome the problems raised by the above mentioned assignment of configurations. (In our analysis the σ(500-600) and κ(700-900) are "dynamically generated" states [Sh00], which appear as poles in the $\pi\pi$ and πK T matrices, but which do not correspond to $q\bar{q}$ states.)

We find that the a_0(980), K_0^* (1430), f_0(980) and f_0(1370) should be placed in the same 1 $^3P_0$ nonet of states before quarkonium-glueball mixing modifies the properties of the f_0(1370). Supporting arguments for placing the a_0(980) and K_0^* (1430) in the same nonet have recently been presented by Maltman [Ma99, Ma00]. He calculated the scalar decay constants of the a_0(980) and K_0^* (1430) using QCD sum rule techniques and other methods. He found similar values of the decay constants, suggesting that these resonances belong in the same nonet. In Chapter 5, we present the results of our calculation of these decay constants using our generalized NJL model.

We obtained values similar to those of Maltman, lending further support to our assignments of configurations of the $q\bar{q}$ states. It should be apparent that a study of quarkonium-glueball mixing would be most useful in increasing our understanding of the properties of the f_0 resonances.

Chapter 3

Wave Functions of the Radial Excitations of the Pion

3.1 Introduction

In Chapter 2 we found that our calculation of the wave functions of light mesons could be put into a form that is quite analogous to calculations made in the random-phase approximation (RPA) for particle-hole excitations in nuclei. The resulting wave functions provide a quite clear picture of how one passes from a highly relativistic system to more nonrelativistic system as the mass of the meson increases. (For the more massive meson states, the Tamm-Dancoff approximation may be used.)

In this chapter we wish to apply our formalism to the calculation of the wave functions of the isovector pseudoscalar mesons. As an application, we will calculate the decay constants of various states, taking into account pseudoscalar - axial-vector mixing. We obtain the wave functions and energies of the various radial excitations of the pion. We also find an additional set of states whose vertex is dominated by the Dirac matrix $\gamma_0\gamma_5$ rather than the matrix $i\gamma_5$ that dominates the vertex of the pionlike states. It is only the latter states that exhibit collective behavior, with the pion as the Goldstone boson. The pion is best studied in a Euclidean-space formulation, where we may maintain chiral symmetry in our calculation. However, our Minkowski-space study of the pion is of some interest and we present results for the pion wave function and

decay constant calculated in our Minkowski-space formalism. [In our Euclidean-space calculation, we could solve the one-body (Hartree) aspect of the problem at the same time as the two-body aspect (Bethe-Salpeter equation) and demonstrate that our model exhibits chiral symmetry. At present, we do not know how to make a corresponding calculation in Minkowski space.]

It is useful to obtain the wave functions of various mesons by first calculating vertex functions. It is possible to define several vertex functions in the study of pseudoscalar mesons. We may define functions that correspond to the use of only the confining interaction, as in Fig.2.1a and 2.1b. Here the vertex functions were denoted as $\bar{\Gamma}_5(P,k)$ and $\bar{\Gamma}^{\mu}_L(P,k)$, where the latter function was needed when we studied pseudoscalar - axial-vector mixing [Ce99c]. Note that, when we wish to construct wave functions, we solve the homogeneous equation of Fig.2.1b rather than the inhomogeneous equation of Fig.2.1a. In the present work we will solve the homogeneous equation that is given in a schematic representation in Fig.2.1c. In this case we include the NJL interaction, or the NJL interaction plus the confining interaction. The resulting vertex functions will be denoted as $\bar{\Gamma}_P(P,k)$ and $\bar{\Gamma}^{\mu}_A(P,k)$. (The bar over the vertex function is a reminder that these functions have a Dirac matrix structure.) These various vertex functions may be used to define a number of vacuum polarization integrals, as seen in Fig.3.1. Once these polarization integrals have been defined, it is a relatively simple matter to obtain equations for the vertex functions $\bar{\Gamma}_P(P,k)$ and $\bar{\Gamma}^{\mu}_A(P,k)$.

3.2 Vertex Functions for the Confining Interaction

In this Section we review various relations that serve to define the vertex functions that satisfy an equation of the form given in Fig.2.1a. We define a pseudoscalar vertex matrix [Ce99c]

$$\bar{\Gamma}_{5,ab}(P,k) = \gamma_5 - i\int \frac{d^4k'}{(2\pi)^4}\left[\gamma^\rho S_a(P/2+k')\bar{\Gamma}_{5,ab}(P,k')S_b(-P/2+k')\gamma_\rho\right] V^C(\vec{k}-\vec{k}') \ , \tag{3.2.1}$$

where $S_a(P/2+k) = [(\not{P}/2+\not{k}) - m_a + i\eta]^{-1}$, etc. We define functions Γ_5^{+-} and Γ_5^{-+}:

$$\Lambda_a^{(+)}(\vec{k})\,\bar{\Gamma}_{5,ab}(P,k)\,\Lambda_b^{(-)}(-\vec{k}) = \Gamma_{5,ab}^{+-}(P,k)\Lambda_a^{(+)}(\vec{k})\gamma_5\Lambda_b^{(-)}(-\vec{k}) \ , \tag{3.2.2}$$

and

$$\Lambda_a^{(-)}(-\vec{k})\,\bar{\Gamma}_{5,ab}(P,k)\,\Lambda_b^{(+)}(\vec{k}) = \Gamma_{5,ab}^{-+}(P,k)\Lambda_a^{(-)}(-\vec{k})\gamma_5\Lambda_b^{(+)}(\vec{k}) \ , \tag{3.2.3}$$

where

$$\Lambda_a^{(+)}(\vec{k}) = \frac{\not{k}_a + m_a}{2m_a} \ , \tag{3.2.4}$$

and

$$\Lambda_b^{(-)}(-\vec{k}) = \frac{\not{\tilde{k}}_b + m_b}{2m_b} \ , \tag{3.2.5}$$

Here, $k_a^\mu = [E_a(\vec{k}), \vec{k}]$ and $\tilde{k}_b^\mu = [-E_b(\vec{k}), \vec{k}]$.

We also define a longitudinal matrix vertex [Ce99c]

$$\bar{\Gamma}^{\mu}_{L,ab}(P,k) = \frac{P^{\mu}\not{P}}{P^2}\gamma_5 - i\int \frac{d^4k'}{(2\pi)^4}\gamma^{\rho} S_a(P/2+k')\,\bar{\Gamma}^{\mu}_{L,ab}(P,k')\,S_b(-P/2+k')\gamma_{\rho}\,V^C(\vec{k}-\vec{k}') \tag{3.2.6}$$

and introduce the function $\Gamma^{+-}_{L,ab}(P,k)$:

$$\Lambda^{(+)}_a(\vec{k})\,\bar{\Gamma}^{\mu}_{L,ab}(P,k)\,\Lambda^{(-)}_b(-\vec{k}) = \frac{P^{\mu}}{\sqrt{P^2}}\Gamma^{+-}_{L,ab}(P,k)\Lambda^{(+)}_a(\vec{k})\,\gamma_5\Lambda^{(-)}_b(-\vec{k})\ . \tag{3.2.7}$$

There is a corresponding equation defining $\bar{\Gamma}^{-+}_{L,ab}(P,k)$. It is useful to write

$$\bar{\Gamma}^{\mu}_{L,ab}(P,k) = \frac{P^{\mu}}{\sqrt{P^2}}\bar{\Gamma}_{L,ab}(P,k)\ , \tag{3.2.8}$$

so that Eq.(3.2.7) becomes

$$\Lambda^{(+)}_a(\vec{k})\,\bar{\Gamma}_{L,ab}(P,k)\,\Lambda^{(-)}_b(-\vec{k}) = \Gamma^{+-}_{L,ab}(P,k)\Lambda^{(+)}_a(\vec{k})\,\gamma_5\Lambda^{(-)}_b(-\vec{k})\ , \tag{3.2.9}$$

etc. We find that

$$\begin{aligned}\Gamma^{+-}_{L,ab}(P,k) = &\left[\frac{m_b E_a(\vec{k}) + m_a E_b(\vec{k})}{m_a m_b + E_a(\vec{k})\,E_b(\vec{k}) + \vec{k}^2}\right] \\ &- \int \frac{d^3k'}{(2\pi)^3}\,\frac{(m_a m_b)^2}{4E_a(\vec{k}')\,E_b(\vec{k}')}\,\frac{V^C(\vec{k}-\vec{k}')}{m_a m_b + E_a(\vec{k})\,E_b(\vec{k}) + \vec{k}^2} \\ &\times C(\vec{k},\vec{k}')\,\frac{\Gamma^{+-}_{L,ab}(P,k')}{P^0 - E_a(\vec{k}') - E_b(\vec{k}')},\end{aligned} \tag{3.2.10}$$

with

$$C(\vec{k},\vec{k}') = \frac{1}{m_a^2 m_b^2}$$
$$\times \{ m_b^2 (E_a(\vec{k})E_a(\vec{k}') - \vec{k}\cdot\vec{k}') + m_a^2 (E_b(\vec{k})E_b(\vec{k}') - \vec{k}\cdot\vec{k}')$$
$$+ 2m_a m_b [-E_a(\vec{k})E_b(\vec{k}) - \vec{k}^2 - E_a(\vec{k}')E_b(\vec{k}') - \vec{k}'^2 \qquad (3.2.11)$$
$$+ \frac{1}{2}E_a(\vec{k})E_b(\vec{k}') + \vec{k}\cdot\vec{k}' + \frac{1}{2}E_a(\vec{k}')E_b(\vec{k})]$$
$$-2(E_a(\vec{k})E_b(\vec{k}) + \vec{k}^2)(E_a(\vec{k}')E_b(\vec{k}') + \vec{k}'^2) - 2m_a^2 m_b^2\} .$$

We also have

$$\Gamma^{-+}_{L,ab}(P,k) = -\left[\frac{m_b E_a(\vec{k}) + m_a E_b(\vec{k})}{m_a m_b + E_a(\vec{k})E_b(\vec{k}) + \vec{k}^2}\right]$$
$$+ \int \frac{d^3k'}{(2\pi)^3} \frac{(m_a m_b)^2}{4E_a(\vec{k}')E_b(\vec{k}')} \frac{V^C(\vec{k}-\vec{k}')}{m_a m_b + E_a(\vec{k})E_b(\vec{k}) + \vec{k}^2} \qquad (3.2.12)$$
$$\times C(\vec{k},\vec{k}') \frac{\Gamma^{-+}_{L,ab}(P,k')}{P^0 + E_a(\vec{k}') + E_b(\vec{k}')} .$$

(In Eqs.(3.2.10) and (3.2.12) we have corrected a misprint that appeared in [Ce99c].) We note the relation $\Gamma^{-+}_{L,ab}(-P^0, |\vec{k}|) = -\Gamma^{+-}_{L,ab}(P^0, |\vec{k}|)$. The functions $\Gamma^{+-}_{5,ab}(P,k)$ and $\Gamma^{-+}_{5,ab}(P,k)$ satisfy equations similar to Eqs.(3.2.10)-(3.2.12), except that the inhomogeneous terms are both equal to unity [Ce99c]. Therefore, we have $\Gamma^{-+}_{5,ab}(-P^0, |\vec{k}|) = \Gamma^{+-}_{5,ab}(P^0, |\vec{k}|)$.

These vertex functions may be used to define vacuum polarization functions that are free of the singularities that would appear in a theory without confinement when the quark and antiquark go on mass shell. [See Fig.3.1] We describe various polarization functions in the next section.

3.3 Vacuum Polarization Functions

We start with a definition of the polarization functions in the absence of confinement [Ce99c]

$$-i\hat{J}^{PP}_{ab}(P) = (-1)2n_c \mathrm{Tr}\int \frac{d^4k}{(2\pi)^4}\left[i\gamma_5 iS_a(P/2+k)i\gamma_5 iS_b(-P/2+k)\right], \tag{3.3.1}$$

$$-i\hat{J}^{PA}_{\mu,ab}(P) = (-1)2n_c \mathrm{Tr}\int \frac{d^4k}{(2\pi)^4}\left[iS_a(P/2+k)i\gamma_5 iS_b(-P/2+k)\gamma_\mu\gamma_5\right], \tag{3.3.2}$$

$$-i\hat{J}^{AP}_{\mu,ab}(P) = (-1)2n_c \mathrm{Tr}\int \frac{d^4k}{(2\pi)^4}\left[iS_a(P/2+k)\gamma_\mu\gamma_5 iS_b(-P/2+k)i\gamma_5\right], \tag{3.3.3}$$

and

$$-i\hat{J}^{AA}_{\mu\nu,ab}(P) = (-1)2n_c \mathrm{Tr}\int \frac{d^4k}{(2\pi)^4}\left[iS_a(P/2+k)\gamma_\mu\gamma_5 iS_b(-P/2+k)\gamma_\nu\gamma_5\right]. \tag{3.3.4}$$

We also define [Ce99c]

$$\hat{J}^{PA}_{\mu,ab}(P) = iJ^{PA}_{ab}(P^2)\frac{P_\mu}{\sqrt{P^2}}, \tag{3.3.5}$$

$$\hat{J}^{AP}_{\mu,ab}(P) = iJ^{AP}_{ab}(P^2)\frac{P_\mu}{\sqrt{P^2}}, \tag{3.3.6}$$

and

$$\hat{J}^{AA}_{\mu\nu,ab}(P) = -\tilde{g}_{\mu\nu}(P)\hat{J}^{AA}_{T,ab}(P^2) - \frac{P_\mu P_\nu}{P^2}\hat{J}^{AA}_{L,ab}(P^2) \quad , \tag{3.3.7}$$

with $\tilde{g}_{\mu\nu} = g_{\mu\nu} - P_\mu P_\nu / P^2$. Note also that $\hat{J}^{AP}(P^2) = -\hat{J}^{PA}(P^2)$ and $P_\mu \tilde{g}^{\mu\nu} = \tilde{g}^{\mu\nu} P_\nu = 0$.

We now include the confinement vertex in the definitions of the polarization integrals. We define

$$-iJ^{PP}_{ab}(P^2) = (-1)2n_c \int \frac{d^4k}{(2\pi)^4} \mathrm{Tr}\left[i\gamma_5 iS_a(P/2+k) i\bar{\Gamma}_{5,ab}(P,k) iS_b(-P/2+k)\right]. \tag{3.3.8}$$

We find, with $\vec{P} = 0$,

$$\begin{aligned} J^{PP}_{ab}(P^2) = -2n_c \int \frac{d^3k}{(2\pi)^3} & \frac{[E_a(\vec{k})E_b(\vec{k}) + \vec{k}^2 + m_a m_b]}{E_a(\vec{k})E_b(\vec{k})} \\ & \times \left[\frac{\Gamma^{+-}_{5,ab}(P^0, |\vec{k}|)}{P^0 - E_a(\vec{k}) - E_b(\vec{k})} - \frac{\Gamma^{-+}_{5,ab}(-P^0, |\vec{k}|)}{P^0 + E_a(\vec{k}) + E_b(\vec{k})}\right] , \end{aligned} \tag{3.3.9}$$

which may be written as

$$\begin{aligned} J^{PP}_{ab}(P^2) = -2n_c \int \frac{d^3k}{(2\pi)^3} & \frac{[E_a(\vec{k})E_b(\vec{k}) + \vec{k}^2 + m_a m_b]}{E_a(\vec{k})E_b(\vec{k})} \\ & \times \Gamma^{+-}_{5,ab}(P^0, |\vec{k}|) \left[\frac{1}{P^0 - E_a(\vec{k}) - E_b(\vec{k})} - \frac{1}{P^0 + E_a(\vec{k}) + E_b(\vec{k})}\right] . \end{aligned} \tag{3.3.10}$$

We now define

$$-iJ^{PA}_{ab}(P^2) = (-1)2n_c \int \frac{d^4k}{(2\pi)^4} \mathrm{Tr}\left[iS_a(P/2+k) i\bar{\Gamma}_5(P,k) iS_b(-P/2+k)\gamma_0\gamma_5\right] \tag{3.3.11}$$

and

$$-iJ^{AP}_{\mu,ab}(P^2) = (-1)2n_c \int \frac{d^4k}{(2\pi)^4} \mathrm{Tr}\left[iS_a(P/2+k)i\bar{\Gamma}_{L,\mu}(P,k)iS_b(-P/2+k)i\gamma_5\right]. \quad (3.3.12)$$

We use Eqs.(3.2.8) and (3.2.9) to find

$$J^{PA}_{ab}(P^2) = -2n_c \int \frac{d^3k}{(2\pi)^3} \frac{[m_a E_b(\vec{k}) + m_b E_a(\vec{k})]}{E_a(\vec{k})E_b(\vec{k})} \times \left[\frac{\Gamma^{+-}_{5,ab}(P^0, |\vec{k}|)}{P^0 - E_a(\vec{k}) - E_b(\vec{k})} + \frac{\Gamma^{-+}_{5,ab}(-P^0, |\vec{k}|)}{P^0 + E_a(\vec{k}) + E_b(\vec{k})}\right]. \quad (3.3.13)$$

Using the relation $\Gamma^{-+}_{5,ab}(-P^0, |\vec{k}|) = \Gamma^{+-}_{5,ab}(P^0, |\vec{k}|)$, the last relation may be written

$$J^{PA}_{ab}(P^2) = -2n_c \int \frac{d^3k}{(2\pi)^3} \frac{[m_b(\vec{k})E_a(\vec{k}) + m_a E_b(\vec{k})]}{E_a(\vec{k})E_b(\vec{k})} \times \Gamma^{+-}_{5,ab}(P^0, |\vec{k}|)\left[\frac{1}{P^0 - E_a(\vec{k}) - E_b(\vec{k})} + \frac{1}{P^0 + E_a(\vec{k}) + E_b(\vec{k})}\right]. \quad (3.3.14)$$

We note that $J^{PA}_{ab}(0) = 0$.

In a similar fashion, we find

$$J^{AP}_{ab}(P^2) = 2n_c \int \frac{d^3k}{(2\pi)^3} \frac{[m_a m_b + \vec{k}^2 + E_a(\vec{k})E_b(\vec{k})]}{E_a(\vec{k})E_b(\vec{k})} \times \Gamma^{+-}_{L,ab}(P^0, |\vec{k}|)\left[\frac{1}{P^0 - E_a(\vec{k}) - E_b(\vec{k})} + \frac{1}{P^0 + E_a(\vec{k}) + E_b(\vec{k})}\right] \quad (3.3.15)$$

and

$$J_{ab}^{AA}(P^2) = 2n_c \int \frac{d^3k}{(2\pi)^3} \frac{[m_b E_a(\vec{k}) + m_a E_b(\vec{k})]}{E_a(\vec{k}) E_b(\vec{k})}$$
$$\times \Gamma_{L,ab}^{+-}(P^0, |\vec{k}|) \left[\frac{1}{P^0 - E_a(\vec{k}) - E_b(\vec{k})} - \frac{1}{P^0 + E_a(\vec{k}) + E_b(\vec{k})} \right], \quad (3.3.16)$$

where we have used the relation $\Gamma_L^{-+}(-P^0, |\vec{k}|) = -\Gamma_L^{+-}(P^0, |\vec{k}|)$. Relations such as those given in Eqs.(3.3.5)-(3.3.7) may also be written for the functions $J_\mu^{PA}(P)$, $J_\mu^{AP}(P)$ and $J_{\mu\nu}^{AA}(P)$.

3.4 Vertex Functions for the Sum of the NJL and the Confining Interaction

We now include the NJL interaction in addition to the confining interaction in the equation for the vertex functions, as in Fig.3.2. We define a new set of polarization intergrals by replacing $\Gamma_{S,ab}^{+-}(P^0, |\vec{k}|)$ by $\Gamma_{P,ab}^{+-}(P^0, |\vec{k}|)$ and $\Gamma_{L,ab}^{+-}(P^0, |\vec{k}|)$ by $\Gamma_{A,ab}^{+-}(P^0, |\vec{k}|)$ etc., in the expressions given in Section 3.3. With this procedure we obtain the vacuum polarization functions appearing in Fig.3.1c. We denote these new polarization functions as $\tilde{J}^{PP}$, $\tilde{J}^{PA}$, $\tilde{J}^{AA}$ *etc.* Thus,

$$\tilde{J}_{ab}^{PP}(P^2) = -2n_c \int \frac{d^3k}{(2\pi)^3} \frac{[E_a(\vec{k}) E_b(\vec{k}) + \vec{k}^2 + m_a m_b]}{E_a(\vec{k}) E_b(\vec{k})}$$
$$\times \Gamma_{P,ab}^{+-}(P^0, |\vec{k}|) \left[\frac{1}{P^0 - E_a(\vec{k}) - E_b(\vec{k})} - \frac{1}{P^0 + E_a(\vec{k}) + E_b(\vec{k})} \right] \quad (3.4.1)$$

$$= -2n_c \int \frac{d^3k}{(2\pi)^3} \frac{[E_a(\vec{k})E_b(\vec{k}) + \vec{k}^2 + m_a m_b]}{E_a(\vec{k})E_b(\vec{k})} \times \left[\tilde{\phi}_P^+(P^0, |\vec{k}|) + \tilde{\phi}_P^-(P^0, |\vec{k}|)\right], \quad (3.4.2)$$

where we have defined

$$\tilde{\phi}_P^+(P^0, |\vec{k}|) = \frac{\Gamma_{P,ab}^{+-}(P^0, |\vec{k}|)}{P^0 - E_a(\vec{k}) - E_b(\vec{k})} \quad (3.4.3)$$

and

$$\tilde{\phi}_P^-(P^0, |\vec{k}|) = -\frac{\Gamma_{P,ab}^{-+}(-P^0, |\vec{k}|)}{P^0 + E_a(\vec{k}) + E_b(\vec{k})} = -\frac{\Gamma_{P,ab}^{+-}(P^0, |\vec{k}|)}{P^0 + E_a(\vec{k}) + E_b(\vec{k})} . \quad (3.4.4)$$

Since we will be dealing with bound-state wave functions, we will write $\tilde{\phi}_P^+(P_i^0, |\vec{k}|)$ as $\tilde{\phi}_{P,i}^+(k)$ and $\tilde{\phi}_P^-(P_i^0, |\vec{k}|)$ as $\tilde{\phi}_{P,i}^-(k)$, where $k = |\vec{k}|$.

Similarly, we define $\tilde{J}_{ab}^{PA}(P^2)$ by the replacement of $\Gamma_{S,ab}^{+-}(P^0, |\vec{k}|)$ by $\Gamma_{P,ab}^{+-}(P^0, |\vec{k}|)$, etc. Thus,

$$\tilde{J}_{ab}^{PA}(P^2) = -2n_C \int \frac{d^3k}{(2\pi)^3} \frac{\left[m_b E_a(\vec{k}) + m_a E_b(\vec{k})\right]}{E_a(\vec{k})E_b(\vec{k})} \left[\tilde{\phi}_{P,i}^+(k) - \tilde{\phi}_{P,i}^-(k)\right] . \quad (3.4.5)$$

We also have

$$\tilde{J}^{AP}_{ab}(P^2) = 2n_C \int \frac{d^3k}{(2\pi)^3} \frac{\left[m_a m_b + \vec{k}^2 + E_a(\vec{k})E_b(\vec{k})\right]}{E_a(\vec{k})E_b(\vec{k})} \left[\tilde{\phi}^+_{A,i}(k) - \tilde{\phi}^-_{A,i}(k)\right] , \quad (3.4.6)$$

where

$$\tilde{\phi}^+_{A,i}(k) = \frac{\Gamma^{+-}_{A,ab}(P^0_i, |\vec{k}|)}{P^0_i - E_a(\vec{k}) - E_b(\vec{k})} \quad (3.4.7)$$

and

$$\begin{aligned} \tilde{\phi}^-_{A,i}(k) &= \frac{\Gamma^{-+}_{A,ab}(-P^0_i, |\vec{k}|)}{P^0_i + E_a(\vec{k}) + E_b(\vec{k})} \\ &= -\frac{\Gamma^{+-}_{A,ab}(P^0_i, |\vec{k}|)}{P^0_i + E_a(\vec{k}) + E_b(\vec{k})} . \end{aligned} \quad (3.4.8)$$

With these definitions we may write

$$\begin{aligned} \tilde{J}^{AA}_{ab}(P^2) &= 2n_c \int \frac{d^3k}{(2\pi)^3} \frac{[m_b E_a(\vec{k}) + m_a E_b(\vec{k})]}{E_a(\vec{k})E_b(\vec{k})} \\ &\times \Gamma^{+-}_{A,ab}(P^0, |\vec{k}|) \left[\frac{1}{P^0 - E_a(\vec{k}) - E_b(\vec{k})} - \frac{1}{P^0 + E_a(\vec{k}) + E_b(\vec{k})}\right] \end{aligned} \quad (3.4.9)$$

$$= 2n_c \int \frac{d^3k}{(2\pi)^3} \frac{[m_b E_a(\vec{k}) + m_a E_b(\vec{k})]}{E_a(\vec{k})E_b(\vec{k})} \left[\tilde{\phi}^+_{A,i}(k) + \tilde{\phi}^-_{A,i}(k)\right] . \quad (3.4.10)$$

3.5 Coupled Equations for the Wave Function Amplitudes $\phi^+_P(k)$, $\phi^-_P(k)$, $\phi^+_A(k)$ and $\phi^-_A(k)$

With the array of definitions made in the previous sections, we may easily

obtain the coupled equations relating ϕ_P^+, ϕ_P^-, ϕ_A^+ and ϕ_A^-. The equation for the vertex functions in the presence of both the NJL interaction and the confining interaction is indicated in a schematic fashion in Figs.3.2 and 3.3. For the moment, let us only consider the NJL interaction and Fig.3.2. In general, we may write $\bar{\Gamma} = \bar{\Gamma}_P + \bar{\Gamma}_A$. Taking matrix elements of $\bar{\Gamma}_P$ between the projectors $\Lambda_a^{(+)}(\vec{k})$ and $\Lambda_b^{(-)}(-\vec{k})$ and canceling a common factor of $\Lambda^{(+)}(\vec{k})\gamma_5\Lambda^{(-)}(-\vec{k})$, we obtain an equation that couples $\Gamma_P^{+-}(P^0,k)$ to $\Gamma_A^{+-}(P^0,k)$

$$\Gamma_P^{+-}(P^0,k) = e^{-k^2/2\alpha^2}\tilde{J}^{PP}(P^2)G_{88} - e^{-k^2/2\alpha^2}\tilde{J}^{AP}(P^2)G_{88} \tag{3.5.1}$$

$$\begin{aligned}
&= -2n_C G_{88} e^{-k^2/2\alpha^2}\int \frac{d^3k'}{(2\pi)^3}\frac{F(k')e^{-k'^2/2\alpha^2}}{E_a(k')E_b(k')} \\
&\times\left[\frac{\Gamma_P^{+-}(P_i^0,k')}{P^0 - E_a(k') - E_b(k')} - \frac{\Gamma_P^{+-}(P_i^0,k')}{P^0 + E_a(k') + E_b(k')}\right] \\
&-2n_C G_{88} e^{-k^2/2\alpha^2}\int \frac{d^3k'}{(2\pi)^3}\frac{F(k')e^{-k'^2/2\alpha^2}}{E_a(k')E_b(k')} \\
&\times\left[\frac{\Gamma_A^{+-}(P_i^0,k')}{P^0 - E_a(k') - E_b(k')} + \frac{\Gamma_A^{+-}(P_i^0,k')}{P^0 + E_a(k') + E_b(k')}\right] .
\end{aligned} \tag{3.5.2}$$

Since the NJL interaction requires regulation, we have replaced the coupling constant G_{88} by $\exp[-k^2/2\alpha^2]\, G_{88} \exp[-k'^2/2\alpha^2]$. This replacement corresponds to the regularization procedure we have used in our earlier work [Ce99a, Ce99c, Ce99e, Ce00]. Here, G_{88} is the interaction in octet states and is a linear combination of G_S and G_D of Eq.(2.1.1). In Eq.(3.5.1) we have introduced the function

$$F(k) = \left[E_a(\vec{k})E_b(\vec{k}) + \vec{k}^2 + m_a m_b\right] . \tag{3.5.3}$$

We also define

$$G(k) = m_a E_b(\vec{k}) + m_b E_a(\vec{k}) . \tag{3.5.4}$$

It is useful to introduce a degree of symmetry in the interaction we will derive by defining

$$\phi^+_{P,i}(k) = \frac{k\sqrt{F(k)}}{\sqrt{2E_a(\vec{k})E_b(\vec{k})}}\tilde{\phi}^+_{P,i}(k) \tag{3.5.5}$$

and

$$\phi^-_{P,i}(k) = \frac{k\sqrt{F(k)}}{\sqrt{2E_a(\vec{k})E_b(\vec{k})}}\tilde{\phi}^-_{P,i}(k), \tag{3.5.6}$$

with similar definitions for $\phi^+_A(k)$ and $\phi^-_A(k)$.

Thus, Eq.(3.5.2) may be rewritten, with $k = |\vec{k}|$ and $k' = |\vec{k}'|$, as

$$\begin{aligned}\left[P_i^0 - E_a(k) - E_b(k)\right]\phi^+_{P,i}(k) &= \int dk'\{H_N^{PP}(k,k')\phi^+_{P,i}(k') \\ &+ H_N^{PP}(k,k')\phi^-_{P,i}(k') + H_N^{PA}(k,k')\phi^+_{A,i}(k') - H_N^{PA}(k,k')\phi^-_{A,i}(k')\}.\end{aligned} \tag{3.5.7}$$

Here, $H_N^{PP}(k,k')$ is a symmetric function

$$H_N^{PP}(k,k') = -\frac{n_C}{\pi^2}\frac{G_{88}kk'\sqrt{F(k)F(k')}\,e^{-k^2/2\alpha^2}e^{-k'^2/2\alpha^2}}{\sqrt{E_a(k)E_b(k)E_a(k')E_b(k')}} , \tag{3.5.8}$$

while

$$H_N^{PA}(k,k') = -\frac{n_C}{\pi^2} G_V \sqrt{F(k)F(k')}\, \frac{kk' e^{-k^2/2\alpha^2} e^{-k'^2/2\alpha^2}}{\sqrt{E_a(k)E_b(k)E_a(k')E_b(k')}} , \qquad (3.5.9)$$

and

$$H_N^{AP}(k,k') = -\frac{n_C}{\pi^2} G_{88} \sqrt{\frac{F(k)}{F(k')}}\, \frac{G(k')kk' e^{-k^2/2\alpha^2} e^{-k'^2/2\alpha^2}}{\sqrt{E_a(k)E_b(k)E_a(k')E_b(k')}} . \qquad (3.5.10)$$

We also obtain

$$H_N^{AA}(k,k') = \frac{n_C}{\pi^2} G_V kk' \sqrt{\frac{F(k)}{F(k')}}\, G(k') \frac{e^{-k^2/2\alpha^2} e^{-k'^2/2\alpha^2}}{\sqrt{E_a(k)E_b(k)E_a(k')E_b(k')}} . \qquad (3.5.11)$$

In these equations the exponential factors are the Gaussian regulators. In the past we have used $\alpha = 0.605$ GeV, and we will continue to use that value here.

We may obtain another equation by writting

$$\Gamma_P^{+-}(P^0,k) = -\left[P^0 + E_a(\vec{k}) + E_b(\vec{k})\right] \phi_P^-(P^0,k) , \qquad (3.5.12)$$

on the left-hand side of Eq.(3.5.2).

We may also use the relation [See Fig.3.4]

$$\bar{\Gamma}_A(P,k) = -e^{-k^2/2\alpha^2} \tilde{J}^{PA}(P^2) G_V \gamma_0\gamma_5 + e^{-k'^2/2\alpha^2} \tilde{J}^{AA}(P^2) G_V \gamma_0\gamma_5 \qquad (3.5.13)$$

and form the matrix element between $\Lambda_a^{(+)}(\vec{k})$ and $\Lambda_b^{(-)}(-\vec{k})$. Thus,

$$\Gamma_A^{+-}(P^0,k) = -e^{-k^2/2\alpha^2} \tilde{J}^{PA}(P^2) G_V + e^{-k^2/2\alpha^2} \tilde{J}^{AA}(P^2) G_V . \qquad (3.5.14)$$

Here $\hat{J}^{PP}(P^2)$, $\hat{J}^{PA}(P^2)$ and $\hat{J}^{AA}(P^2)$ differ from the functions defined in Section 3.4, since they include the regulator $\exp\left[-k'^2/2\alpha^2\right]$ in the integral defining these functions.

If we put $\Gamma_A^{+-}(P^0,k) = \left[P^0 - E_a(\vec{k}) - E_b(\vec{k})\right]\phi_A^+(P^0,k)$, or

$$\Gamma_A^{+-}(P^0,k) = -\left[P^0 + E_a(\vec{k}) + E_b(\vec{k})\right]\phi_A^-(P^0,k) \ , \tag{3.5.15}$$

we obtain a total of four equations relating ϕ_P^+, ϕ_P^-, ϕ_A^+ and ϕ_A^-.

Before writting these equations, we consider the confining interaction. Our treatment of the confinement is such that we neglect pair production by the confining field in the meson rest frame so that, if we construct a matrix of the interaction terms, the confining interaction appears only in the diagonal elements. We may identify the contribution of the confining interaction by using the equations satisfied by $\Gamma_5^{+-}(P,k)$ and $\Gamma_L^{+-}(P,k)$ given previously. To that end, it is useful to write

$$C(\vec{k},\vec{k}') = C_0(k,k') + \vec{k}\cdot\vec{k}'\, C_1(k,k') \tag{3.5.16}$$

and define

$$V_l^C(k,k') = \frac{1}{2}\int dx P_l(x)\, V^C(\vec{k}-\vec{k}') \tag{3.5.17}$$

where $P_l(x)$ is a Legendre function. We find the symmetric interaction

$$H_C(k,k') = -\frac{1}{4\pi^2}\frac{(m_a m_b)^2 kk'\{C_0(k,k')V_0^C(k,k') + kk' C_1(k,k')\, V_1^C(k,k')\}}{\sqrt{F(k)F(k')}\,\sqrt{E_a(k)E_b(k)E_a(k')E_b(k')}}. \tag{3.5.18}$$

Note that the confining interaction does not require regularization.

We may then write the four coupled equations for ϕ_P^+, ϕ_P^-, ϕ_A^+ and ϕ_A^- as

$$\int dk' \{ [(E_a(k') + E_b(k')) \delta(k-k') + H_N^{PP}(k,k') + H_C(k,k')] \phi_{P,i}^+(k') + H_N^{PP}(k,k') \phi_{P,i}^-(k') + H_N^{PA}(k,k') \phi_{A,i}^+(k') - H_N^{PA}(k,k') \phi_{A,i}^-(k') \} = P_i^0 \phi_{P,i}^+(k), \tag{3.5.19}$$

$$\int dk' \{ -H_N^{PP}(k,k') \phi_{P,i}^+(k') - [(E_a(k') + E_b(k')) \delta(k-k') + H_N^{PP}(k,k') + H_C(k,k')] \phi_{P,i}^-(k') - H^{PA}(k,k') \phi_{A,i}^+(k') + H^{PA}(k,k') \phi_{A,i}^-(k') \} = P_i^0 \phi_{P,i}^-(k), \tag{3.5.20}$$

$$\int dk' \{ H_N^{AP}(k,k') \phi_{P,i}^+(k') - H_N^{AP}(k,k') \phi_{P,i}^-(k') + [(E_a(k') + E_b(k')) \delta(k-k') + H_N^{AA}(k,k') + H_C(k,k')] \phi_{A,i}^+(k') + H_N^{AA}(k,k') \phi_{A,i}^-(k') \} = P_i^0 \phi_{A,i}^+(k), \tag{3.5.21}$$

and

$$\int dk' \{ -H_N^{AP}(k,k') \phi_{P,i}^+(k') + H^{AP}(k,k') \phi_{P,i}^-(k') - H_N^{AA}(k,k') \phi_{A,i}^+(k') - [(E_a(k') + E_b(k')) \delta(k-k') + H_N^{AA}(k,k') + H_C(k,k')] \phi_{A,i}^-(k') \} = P_i^0 \phi_{A,i}^-(k). \tag{3.5.22}$$

Note that, for any solution with $P_i^0 > 0$ there is another solution with the energy $-P_i^0$. If the first solution has a wave function characterized by ϕ_P^+, ϕ_P^-, ϕ_A^+ and ϕ_A^-, the second solution is obtained by the transformation $\phi_P^+ \rightarrow \phi_P^-$, $\phi_P^- \rightarrow \phi_P^+$, $\phi_A^+ \rightarrow -\phi_A^-$, $\phi_A^- \rightarrow -\phi_A^+$ and $P_i^0 \rightarrow -P_i^0$.

3.6 Calculation of Normalized Wave Functions and the Pion Decay Constant

We may define normalized wave functions by multiplying $\phi_P^+(k)$, $\phi_P^-(k)$, $\phi_A^+(k)$ and $\phi_A^-(k)$ by a normalization factor $\sqrt{N_i}$, where

$$\frac{1}{N_i} = \frac{1}{2M_i}\frac{2n_C}{\pi^2}\int dk\{\,|\phi^+_{P,i}(k)|^2 - |\phi^-_{P,i}(k)|^2\,\}\ . \qquad (3.6.1)$$

and M_i is the mass of the meson. Here we have considered the case in which $\phi^+_A(k)$ and $\phi^-_A(k)$ are small. (The minus sign that appears in Eq.(3.6.1) is a characteristic of calculations made in the RPA.)

In the case that $\phi^+_A(k)$ and $\phi^-_A(k)$ are significant, the appropriate normalization factor is

$$\frac{1}{N_i} = \frac{1}{2M_i}\frac{2n_C}{\pi^2}\int dk\{\,|\phi^+_{P,i}(k)+\beta_{ab}(k)\phi^+_{A,i}(k)|^2 - |\phi^-_{P,i}(k)+\beta_{ab}(k)\phi^-_{A,i}(k)|^2\} \qquad (3.6.2)$$

where

$$\beta_{ab}(k) = \frac{(E_a(k)+m_a)(E_b(k)+m_b) - \vec{k}^2}{(E_a(k)+m_a)(E_b(k)+m_b) + \vec{k}^2}\ . \qquad (3.6.3)$$

When $m_a = m_b = m$, $\beta_{ab}(k) = m/E(k)$. We may define

$$\phi^+_{P,N}(k) = \sqrt{N_i}\ \phi^+_{P,i}(k)\ , \qquad (3.6.4)$$

and

$$\phi^-_{P,N}(k) = \sqrt{N_i}\ \phi^-_{P,i}(k)\ , \qquad (3.6.5)$$

etc.

A calculation of the meson decay constant yields

$$f_{\pi,i} = \frac{n_C}{\sqrt{2}\,M_i\pi^2}\int k\,dk\,\frac{[m_a E_b(k) + m_b E_a(k)]}{\sqrt{E_a(k)\,E_b(k)\,F(k)}} \qquad (3.6.6)$$
$$\times\sqrt{N_i}\,\{[\phi^+_{P,i}(k) - \phi^-_{P,i}(k)] + [\phi^+_{A,i}(k) + \phi^-_{A,i}(k)]\}\ .$$

Note that in the chiral limit ($M_i \to 0$) the bracketed term also vanishes, such that f_π remains finite. Further, in the case $m_a = m_b = m$, we have the simple form

$$f_{\pi,i} = \frac{n_C}{\pi^2 M_i}\int k\,dk\left[\frac{m}{E(k)}\right]\sqrt{N_i}\,\{[\phi^+_{P,i}(k) - \phi^-_{P,i}(k)] + [\phi^+_{A,i}(k) + \phi^-_{A,i}(k)]\}, \quad (3.6.7)$$

since $F(k) \to 2E^2(k)$ when the quark masses are equal.

The calculation of f_π for the $\pi(138)$ using Eqs.(6.6) or (6.7) yields large values of about 170 MeV. This problem is partially resolved by introducing the axial charge of the quarks. That is, we sum a series of vacuum polarization diagrams that connect the pion to the axial current. Thus, we calculate the pion decay constant to be

$$F_\pi = \frac{1}{1 - G_V J_L^{AA}(m_\pi^2)} f_\pi\ , \qquad (3.6.8)$$

where $J_L^{AA}(P^2)$ was defined earlier in this work. We define the quark axial charge to be

$$g_A = \frac{1}{1 - G_V J_L^{AA}(m_\pi^2)} \qquad (3.6.9)$$

and write Eq.(3.6.8) as $F_\pi = g_A f_\pi$. We will also evaluate Eqs.(3.6.8) and (3.6.9) using $\hat{J}^{AA}(P^2)$. If we neglect confinement, we have $G_{88} = G_V = 11.76$ GeV^{-2} and $\hat{J}_L^{AA}(m_\pi^2)$ $= -0.02416$ GeV^2, so that $g_A = 0.778$. Since we find $f_\pi = 178$ MeV in this case, we obtain $F_\pi = 138$ MeV. If we include confinement, we use $G_{88} = 13.49$ GeV^{-2} and G_V

= 12.46 GeV^{-2} and also obtain $J_L^{AA}(m_\pi^2)$ = -0.02914 GeV^2. Thus, in this case, f_π = 180 MeV, g_A = 0.745 and F_π = 134 MeV. [See Table 3.1 and Appendix B.] In this work we have not attempted to calculate g_A for other than the $\pi(138)$, since more complex techniques are needed to calculate g_A for the more massive states.

3.7 Results of Numerical Computation: Wave Functions and Mass Values

Diagonalization of the interaction matrix yields the energies shown in Fig.3.4 and Table 3.1. The figure shows the energies of the doublets in the confining field on the left-hand side. The result of including the NJL interaction produces the mass values shown in the right-hand side of the figure. In Figs. 3.5-3.10 we exhibit the wave functions of the $\pi(138)$, $\pi(1325)$, $\pi(1391)$, $\pi(1652)$, $\pi(1717)$ and $\pi(1890)$. The second, fourth and sixth of these states are "mixed" states, while the $\pi(138)$, $\pi(1391)$ and $\pi(1717)$ are "pionlike", It may be seen that $\phi_A^+(k)$ and $\phi_A^-(k)$ are small in those states we have termed "pionlike".

In Table 3.1 we also give the values of f_π, and F_π, with and without confinement, for the $\pi(138)$. We note that the values of α = 0.605 GeV and $m_u = m_d$ = 0.364 GeV were used. When we include confinement we used G_V = 12.46 GeV^{-2}, and κ = 0.055 GeV^2. The value of G_{88} = 13.49 GeV^{-2} was adjusted to yield 138 MeV for the mass of the pion. (The pion mass is very sensitive to variations of G_{88}.) When we neglected confinement, we used G_{88} = 11.76 GeV^2 and $G_V = G_{88}$. [See Table 3.1.]

3.8 Discussion

It may be seen from our presentation that, in the absence of a confining interaction, the NJL model does not allow for a description of radially-excited states.

The model leads to a separable interaction in each channel such that the vertex function is proportional to the regulator. [See Eqs.(3.5.1) and (3.5.12).] To deal with this problem, Volkov and collaborators have introduced additional separable interactions in each channel. These new terms allow for a description of radially-excited states [Vo98, Vo99, Vo00]. More closely related to our work is described in [Ri00, Ko00, Me96, Mü94]. In [Ri00, Ko00] the authors include a confinement model that has scalar, pseudoscalar and vector confining interactions. They solve the Bethe-Salpeter equation and describe a large number of light meson states. However, they do not include pseudoscalar - axial-vector coupling in their formalism. Other work related to ours may be found in [Ll00], where meson spectra are calculated using many-body techniques based upon the RPA. That work is part of a comprehensive program to investigate hadron structure using an effective Lagrangian obtained from QCD [Co00].

In the present work we have shown how to derive relativistic RPA equations that my be used to calculate the properties of radially-excited states of pseudoscalar mesons. We found that the calculated states fall into two groups. One group is composed of "pionlike" states and the other is composed of "mixed" states. The NJL interaction is strongly attractive for the pionlike states such that the state in the confining field at 1210 MeV becomes the $\pi(138)$ when the NJL interaction is included. [See Fig.3.4.] It is of interest to note that our calculations are quite similar to the RPA calculations made many years ago in the study of particle-hole excitations in nuclei [Fe71, Fe70].

We have noted earlier that the pion is best treated in Euclidean space, where

one may maintain chiral symmetry in the description of the pion [Ce97]. In our work, with the exception of [Ce97], we have used constant values for the quark masses, a feature which introduces some violation of chiral symmetry when we include the confining interaction. The effect of confinement in modifying the pion wave function is small, however, as may be seen in Fig.3.11. One might choose to neglect confinement for the pion and include confinement for all the other isovector pseudoscalar states such as those that appear in Fig.3.4. It would, of course, be desirable to produce a Minkowski-space model in which we could maintain chiral symmetry for the pion and still calculate the various radial excitations.

Our work may also be of some interest in estimating the size of the "continuum" contribution when the Borel transformation is used in the application of QCD sum rules for the calculation of the correlator of the axial-vector hadronic current [Na89].

Chapter 4

Properties of the η and η' Mesons and their Radial Excitations

4.1 Introduction

When we consider the η mesons, the wave function amplitudes, before diagonalization, could be of singlet or octet character. Therefore, for our study of the η, η' mesons and their radial excitations, we need to determine eight components for the wave function of each meson. We may also transform from the singlet-octet representation to a $n\bar{n}$ and $s\bar{s}$ basis. We will use both representations in this work.

4.2 Vacuum Polarization Functions in the Presence of a Confining Interaction

As stated in the last section, in order to derive the equations of the RPA, it is useful to first obtain expressions for the vacuum polarization functions of the NJL model. We review the expressions obtained for these functions in this section. Here we present the results in a $n\bar{n}$, $s\bar{s}$, $n\bar{s}$, or $s\bar{n}$ basis. (For our study of the η mesons we will only need the results in the $n\bar{n}-s\bar{s}$ basis.) In the following, the subscripts refer to either u, d or s quarks and antiquarks.

We now make reference to Eqs.(3.3.1)-(3.3.16). For our study we now need to construct $J^{PP}_{n\bar{n}}(P^2)$, $J^{PP}_{s\bar{s}}(P^2)$, $J^{PA}_{n\bar{n}}(P^2)$, $J^{PA}_{s\bar{s}}(P^2)$, $J^{AA}_{n\bar{n}}(P^2)$ and $J^{AA}_{s\bar{s}}(P^2)$. In Fig.4.1 and 4.2 we present values of $J^{PP}_{n\bar{n}}(P^2)$ and $J^{PP}_{s\bar{s}}(P^2)$. The singularities seen there reflect those of the confinement vertex functions $\Gamma^{+-}_{5,n\bar{n}}(P^0,k)$ and $\Gamma^{+-}_{5,s\bar{s}}(P^0,k)$, respectively. The

functions $J^{PA}_{n\bar{n}}(P^2)$ and $J^{AA}_{n\bar{n}}(P^2)$ have singularities at the same energies as $\Gamma^{+-}_{5,n\bar{n}}(P^2)$, *etc.* The positions of the singularities provide us with the energies of the bound states in the confining field. (See the first and second column of levels shown in Fig.4.3) These are the energies at which the homogeneous equations of Fig.2.1b have solutions.

To make use of the equations depicted in Figs.3.2 and 3.3, it is useful to define the vertex functions that are the solutions of these equations and then to define polarization functions, $\tilde{J}^{PP}(P^2)$, $\tilde{J}^{PA}(P^2)$ and $\tilde{J}^{AA}(P^2)$, which have the confinement vertex functions $\Gamma^{+-}_{5,ab}(P^0,k)$ and $\Gamma^{+-}_{L,ab}(P^0,k)$ replaced by $\Gamma^{+-}_{P,ab}(P^0,k)$ and $\Gamma^{+-}_{A,ab}(P^0,k)$. For the study of the η mesons we will need $\Gamma^{+-}_{P,n\bar{n}}(P^0,k)$, $\Gamma^{+-}_{P,s\bar{s}}(P^0,k)$, $\Gamma^{+-}_{A,n\bar{n}}(P^0,k)$ and $\Gamma^{+-}_{A,s\bar{s}}(P^0,k)$. We will also introduce the singlet and octet versions of these functions, $\Gamma^{+-}_{P,0}(P^0,k)$, $\Gamma^{+-}_{P,8}(P^0,k)$, $\Gamma^{+-}_{A,0}(P^0,k)$ and $\Gamma^{+-}_{A,8}(P^0,k)$. The passage between these two representations will be considered in the next section.

4.3 Wave Functions for Pseudoscalar Mesons with Singlet-Octet Mixing

In this section we will pass between a singlet-octet representation and a $n\bar{n}$, $s\bar{s}$ representation. We may use a matrix, M, to connect these representations

$$\begin{bmatrix} \lambda_{n\bar{n}} \\ \lambda_{s\bar{s}} \end{bmatrix} = M \begin{bmatrix} \lambda_8/\sqrt{2} \\ \lambda_0/\sqrt{2} \end{bmatrix}. \qquad (4.3.1)$$

Here

$$M = \frac{1}{\sqrt{3}} \begin{bmatrix} 1 & \sqrt{2} \\ -\sqrt{2} & 1 \end{bmatrix}, \qquad (4.3.2)$$

so that

$$\lambda_{n\bar{n}} = \frac{\lambda_8}{\sqrt{6}} + \frac{\lambda_0}{\sqrt{3}} \ , \tag{4.3.3}$$

$$\lambda_{s\bar{s}} = -\frac{\lambda_8}{\sqrt{3}} + \frac{\lambda_0}{\sqrt{6}} \ . \tag{4.3.4}$$

We may write a vertex for the η mesons of the form.

$$\begin{aligned} \bar{\Gamma}_{\eta}(k) &= \Gamma^{+-}_{P,n\bar{n}}(k)\gamma_5\lambda_{n\bar{n}} + \Gamma^{+-}_{P,s\bar{s}}(k)\gamma_5\lambda_{s\bar{s}} \\ &+ \Gamma^{+-}_{A,n\bar{n}}(k)\gamma_0\gamma_5\lambda_{n\bar{n}} + \Gamma^{+-}_{A,s\bar{s}}(k)\gamma_0\gamma_5\lambda_{s\bar{s}} \ , \end{aligned} \tag{4.3.5}$$

and also define a series of wave functions

$$\phi^{+}_{P,n\bar{n}}(k) = \frac{k\,\Gamma^{+-}_{P,n\bar{n}}(k)}{P^0 - 2E_u(k)} \ , \tag{4.3.6}$$

$$\phi^{-}_{P,n\bar{n}}(k) = -\frac{k\,\Gamma^{+-}_{P,n\bar{n}}(k)}{P^0 + 2E_u(k)} \ , \tag{4.3.7}$$

$$\phi^{+}_{P,s\bar{s}}(k) = \frac{k\,\Gamma^{+-}_{P,s\bar{s}}(k)}{P^0 - 2E_s(k)} \ , \tag{4.3.8}$$

$$\phi^{-}_{P,s\bar{s}}(k) = -\frac{k\,\Gamma^{+-}_{P,s\bar{s}}(k)}{P^0 + 2E_s(k)} \ , \tag{4.3.9}$$

$$\phi^{+}_{A,n\bar{n}}(k) = \frac{k\,\Gamma^{+-}_{A,n\bar{n}}(k)}{P^0 - 2E_u(k)} \ , \tag{4.3.10}$$

$$\phi^{-}_{A,n\bar{n}}(k) = -\frac{k\,\Gamma^{+-}_{A,n\bar{n}}(k)}{P^0+2E_u(k)}\ , \tag{4.3.11}$$

$$\phi^{+}_{A,s\bar{s}}(k) = \frac{k\,\Gamma^{+-}_{A,s\bar{s}}(k)}{P^0-2E_s(k)}\ , \tag{4.3.12}$$

and

$$\phi^{-}_{A,s\bar{s}}(k) = -\frac{k\,\Gamma^{+-}_{A,s\bar{s}}(k)}{P^0+2E_s(k)}\ . \tag{4.3.13}$$

Once we have defined these functions, we may introduce $\phi^{+}_{A,0}(k)$, $\phi^{+}_{P,8}(k)$, $\phi^{-}_{P,0}(k)$, $\phi^{-}_{P,8}(k)$, $\phi^{+}_{A,0}(k)$, $\phi^{+}_{A,8}(k)$, $\phi^{-}_{A,0}(k)$ and $\phi^{-}_{A,8}(k)$. We choose to solve for the functions in the singlet-octet representation. To that end, we write $E_u(k) = \left[\vec{k}^2 + m_u^2\right]^{1/2}$, $E_s(k) = \left[\vec{k}^2 + m_s^2\right]^{1/2}$, and define

$$E_{00}(k) = \frac{2}{\sqrt{3}}\left[2E_u(k) + E_s(k)\right], \tag{4.3.14}$$

$$E_{88}(k) = \frac{2}{\sqrt{3}}\left[E_u(k) + 2E_s(k)\right], \tag{4.3.15}$$

and

$$E_{08}(k) = \frac{2\sqrt{2}}{3}\left[E_u(k) - E_s(k)\right], \tag{4.3.16}$$

with $E_{80}(k) = E_{08}(k)$.

We then need to solve the following eight equations, with the functions $H^{PP}_{ij}(k,k')$, $H^{PA}_{ij}(k,k')$, $H^{AP}_{ij}(k,k')$, $H^{AA}_{ij}(k,k')$, $H^{PP(C)}_{ij}(k,k')$ and $H^{AA(C)}_{ij}(k,k')$ defined in

Appendix B. (Here, i and j are each either 0 or 8.) The equations are

$$\begin{aligned}\int dk'\{&[E_{00}(k)\delta(k-k')+G_{00}H_{00}^{PP}(k,k')+H_{00}^{PP(C)}(k,k')]\phi_{P,0}^{+}(k')\\&+[E_{08}(k)\delta(k-k')+G_{00}H_{08}^{PP}(k,k')]\phi_{P,8}^{+}(k')+G_{00}H_{00}^{PP}(k,k')\phi_{P,0}^{-}(k')\\&+G_{00}H_{08}^{PP}(k,k')\phi_{P,8}^{-}(k')-G_{00}H_{00}^{PA}(k,k')\phi_{A,0}^{+}(k')-G_{00}H_{08}^{PA}(k,k')\phi_{A,8}^{+}(k')\\&+G_{00}H_{00}^{PA}(k,k')\phi_{A,0}^{-}(k')+G_{00}H_{08}^{PA}(k,k')\phi_{A,0}^{-}(k)\}=P^{0}\phi_{P,0}^{+}(k),\end{aligned} \tag{4.3.17}$$

$$\begin{aligned}\int dk'\{&G_{88}H_{80}^{PP}(k,k')\phi_{P,0}^{+}(k')+[E_{88}(k)\delta(k-k')+G_{88}H_{88}^{PP}(k,k')\\&+H_{88}^{PP(C)}(k,k')]\phi_{P,8}^{+}(k')+G_{88}H_{80}^{PP}(k,k')]\phi_{P,0}^{-}(k')+G_{88}H_{88}^{PP}(k,k')\phi_{P,8}^{-}(k')\\&-G_{88}H_{80}^{PA}(k,k')\phi_{A,0}^{+}(k')-G_{88}H_{88}^{PA}(k,k')\phi_{A,8}^{+}(k')+G_{88}H_{80}^{PA}(k,k')\phi_{A,0}^{-}(k')\\&+G_{88}H_{88}^{PA}(k,k')\phi_{A,8}^{-}(k')\}=P^{0}\phi_{P,8}^{+}(k),\end{aligned} \tag{4.3.18}$$

$$\begin{aligned}\int dk'\{&-G_{00}H_{00}^{PP}(k,k')\phi_{P,0}^{+}(k')-G_{00}H_{08}^{PP}(k,k')\phi_{P,8}^{+}(k')-[E_{00}(k)\delta(k-k')\\&+G_{00}H_{00}^{PP}(k,k')+H_{00}^{PP(C)}(k,k')]\phi_{P,0}^{-}(k')-[E_{08}(k)\delta(k-k')+\\&G_{00}H_{08}^{PP}(k,k')]\phi_{P,8}^{-}(k')+G_{00}H_{00}^{PA}(k,k')\phi_{A,0}^{+}(k')+G_{00}H_{08}^{PA}(k,k')\phi_{A,8}^{+}(k')\\&-G_{00}H_{00}^{PA}(k,k')\phi_{A,0}^{-}(k')-G_{00}H_{08}^{PA}(k,k')\phi_{A,8}^{-}(k')\}=P^{0}\phi_{P,0}^{-}(k),\end{aligned} \tag{4.3.19}$$

$$\begin{aligned}\int dk'\{&-G_{88}H_{80}^{PP}(k,k')\phi_{P,0}^{+}(k')-G_{88}H_{88}^{PP}(k,k')\phi_{P,8}^{+}(k')\\&-G_{88}H_{80}^{PP}(k,k')\phi_{P,0}^{-}(k')-[E_{88}(k)\delta(k-k')+G_{88}H_{88}^{PP}(k,k')+\\&H_{88}^{PP(C)}(k,k')]\phi_{P,8}^{-}(k')+G_{88}H_{80}^{PA}(k,k')\phi_{A,0}^{+}(k')+G_{88}H_{88}^{PA}(k,k')\phi_{A,8}^{+}(k')\\&-G_{88}H_{80}^{PA}(k,k')\phi_{A,0}^{-}(k')-G_{88}H_{88}^{PA}(k,k')\phi_{A,8}^{-}(k')\}=P^{0}\phi_{P,8}^{-}(k)\ ,\end{aligned} \tag{4.3.20}$$

$$\int dk'\{ -G_V H_{00}^{AP}(k,k')\phi_{P,0}^{+}(k') - G_V H_{08}^{AP}(k,k')\phi_{P,8}^{+}(k') + G_V H_{00}^{AP}(k,k')\phi_{P,0}^{-}(k') + G_V H_{08}^{AP}(k,k')\phi_{P,8}^{-}(k') + [E_{00}\delta(k-k') + G_V H_{00}^{AA}(k,k') + H_{00}^{AA(C)}(k,k')]\phi_{A,0}^{+}(k') + [E_{08}(k)\delta(k-k') + G_V H_{08}^{AA}(k,k')]\phi_{A,8}^{+}(k') + G_V H_{00}^{AA}(k,k')\phi_{A,0}^{-}(k') + G_V H_{08}^{AA}(k,k')\phi_{A,8}^{-}(k')\} = P^0\phi_{A,0}^{+}(k) , \tag{4.3.21}$$

$$\int dk'\{ -G_V H_{80}^{AP}(k,k')\phi_{P,0}^{+}(k') - G_V H_{88}^{AP}(k,k')\phi_{P,8}^{+}(k') + G_V H_{80}^{AP}(k,k')\phi_{P,0}^{-}(k') + G_V H_{88}^{AP}(k,k')\phi_{P,8}^{-}(k') + [E_{80}\delta(k-k') + G_V H_{80}^{AA}(k,k')]\phi_{A,0}^{+}(k') + [E_{88}(k)\delta(k-k') + G_V H_{88}^{AA}(k,k') + H_{88}^{AA(C)}(k,k')] \times \phi_{A,8}^{+}(k') + G_V H_{80}^{AA}(k,k')\phi_{A,0}^{-}(k') + G_V H_{88}^{AA}(k,k')\phi_{A,8}^{-}(k')\} = P^0\phi_{A,8}^{+}(k), \tag{4.3.22}$$

$$\int dk'\{ G_V H_{00}^{AP}(k,k')\phi_{P,0}^{+}(k') + G_V H_{08}^{AP}(k,k')\phi_{P,8}^{+}(k') - G_V H_{00}^{AP}(k,k')\phi_{P,0}^{-}(k') - G_V H_{08}^{AP}(k,k')\phi_{P,8}^{-}(k') - G_V H_{00}^{AA}(k,k')\phi_{A,0}^{+}(k') - G_V H_{08}^{AA}(k,k')\phi_{A,8}^{+}(k') - [E_{00}(k)\delta(k-k') + G_V H_{00}^{AA}(k,k') + H_{00}^{AA(C)}(k,k')] \times \phi_{A,0}^{-}(k') - [E_{08}(k)\delta(k-k') - G_V H_{08}^{AA}(k,k')]\phi_{A,8}^{-}(k')\} = P^0\phi_{A,0}^{-}(k), \tag{4.3.23}$$

and

$$\int dk'\{ G_V H_{80}^{AP}(k,k')\phi_{P,0}^{+}(k') + G_V H_{88}^{AP}(k,k')\phi_{P,8}^{+}(k') - G_V H_{80}^{AP}(k,k')\phi_{P,0}^{-}(k') - G_V H_{88}^{AP}(k,k')\phi_{P,8}^{-}(k') - G_V H_{80}^{AA}(k,k')\phi_{A,0}^{+}(k') - G_V H_{88}^{AA}(k,k')\phi_{A,8}^{+}(k') - [E_{80}(k)\delta(k-k') + G_V H_{80}^{AA}(k,k')]\phi_{A,0}^{-}(k') - [E_{88}(k)\delta(k-k') + G_V H_{88}^{AA}(k,k') + H_{88}^{AA(C)}(k,k')]\phi_{A,8}^{-}(k')\} = P^0\phi_{A,8}^{-}(k), \tag{4.3.24}$$

The singlet and octet coupling constants depend upon the values of G_S, G_D and the $q\bar{q}$ vacuum condensates [Ce00]. For this analysis we use the values κ = 0.055 GeV^2, G_{88} = 12.46 GeV^{-2}, G_{00} = 9.10 GeV^{-2}, G_{08} = 0, G_V = 12.46 GeV^{-2}, m_u =

0.364 GeV and m_s = 0.565 GeV. These are the same parameters that were used in our earlier work, except for the fact that G_{00} has been reduced somewhat from the value of 10.46 GeV^{-2} used previously [Ce99a]. We use a Gaussian regulator which is defined in Appendix B. The Gaussian parameter α was equal to 0.605 GeV in our earlier work and we also use that value here. (In some of our earlier calculations we used a sharp cutoff of $|\vec{k}| \leq \Lambda_3$ with Λ_3 = 0.622 GeV. However, the Gaussian cutoff is preferred.)

4.4 Energy Levels and Wave Functions

The energies of states bound in the confining field are shown in Fig.4.3. The first column gives the energies of the $n\bar{n}$ states (1.216, 1.550, 1.811, 2.015, 2.200, 2.359, 2.489, 2.610 and 2.712 GeV), while the third column gives the energies of the $s\bar{s}$ states (1.559, 1.838, 2.072, 2.258, 2.423, 2.573 and 2.698 GeV). The two cross-hatched regions indicate the continuum of the model for the $n\bar{n}$ and $s\bar{s}$ states, respectively. (For example, for the $n\bar{n}$ states, the continuum threshold is $E_{n\bar{n}}^{cont} = 2m_u + \kappa/\mu e$ = 2.751 GeV.) Each of the states in columns one and three is doubly degenerated with a wave function associated with either a γ_5 or a $\gamma_0\gamma_5$ vertex in the meson rest frame.

The second column shows the results obtained upon the diagonalization of the RPA Hamiltonian. (Here we only show the positive-energy states.) The arrows give some indication of how various states are distributed into the levels of column two. [See Table 4.1] The 1 $^3S_0$ $n\bar{n}$ state bound in the confining field that has a γ_5 vertex is found with 75% probability in the lowest state of column two and with about 25% probability in the next excitation. The two lowest energy states in column two represent

the $\eta(547)$ and $\eta'(958)$. The distribution of the $1\,^3S_0\ s\bar{s}$ state has 21% probability in the $\eta(547)$ and 79% in the $\eta(958)$. The $n\bar{n}$ and $s\bar{s}$ $1\,^3S_0$ states bound in the confining field that have the $\gamma_0\gamma_5$ vertex are highly fragmented over many of the states in column two. The wave functions, $\phi^+_{P,n\bar{n}}(k)$, $\phi^-_{P,n\bar{n}}(k)$, $\phi^+_{A,n\bar{n}}(k)$ ... *etc.*, for the $\eta(547)$ are shown in Fig.4.4. Here, $\phi^-_{P,n\bar{n}}(k)$ [N2] and $\phi^-_{P,s\bar{s}}(k)$ [S2] are rather large in a state with a relatively small mass such as the $\eta(547)$. The wave function of the $\eta(547)$ has dominant components $\phi^+_{P,n\bar{n}}(k)$ [N1] and $\phi^+_{P,s\bar{s}}(k)$ [S1].

In Fig.4.5 we show the wave function of the $\eta'(958)$ which we find at 893 MeV. Here $\phi^+_{P,s\bar{s}}(k)$ [S1] and $\phi^+_{P,n\bar{n}}(k)$ [N1] are the dominant components. In Figs.4.4 and 4.5 we also see a small amplitude for the $1\,^3S_0$ $\phi^+_{A,s\bar{s}}(k)$ [N3] component, which we stated had a rather fragmented distribution. In Fig.4.6 we show the $\eta(1295)$, which we find at 1318 MeV. [See Table 4.1]. This state is dominated by the $2\,^3S_0$ $n\bar{n}$ state, with the component $\phi^+_{A,n\bar{n}}(k)$ [N3] larger than $\phi^+_{P,n\bar{n}}(k)$ [N1]. We see that the "small components" are indeed small for the more massive mesons.

In Fig.4.7 we show the wave function of the $\eta(1440)$, which we find at 1409 MeV. [See Table 4.1.] Here the state is almost entirely the $2\,^3S_0$ $n\bar{n}$ state that has the γ_5 vertex [N1]. In Fig.4.8 we show the wave function of the state at 1652 MeV. Here the $n\bar{n}$ components account for 96% of the norm, with $\phi^+_{A,n\bar{n}}(k)$ [N3] larger than $\phi^+_{P,n\bar{n}}(k)$ [N1]. These components arise from the $3\,^3S_0$ $n\bar{n}$ state bound in the confining field, as indicated in Fig.4.3. In Fig.4.9 we show the wave functions of the state found at 1659 MeV. Here the $2\,^3S_0$ $s\bar{s}$ states play an important role, with $\phi^+_{A,s\bar{s}}(k)$ [N3] being the dominant component. [See Fig.4.3.]

On the right-hand side of Fig.4.3 and in Table 4.1 we show the experimentally observed states: $\eta(547)$, $\eta'(958)$, $\eta(1295)$ and $\eta(1440)$. These are in good correspondence with the four lowest-energy states of our model.

4.5 Normalization of Wave Functions and Calculation of Decay Constants

We may define a normalization factor for each state of mass M_i

$$\frac{1}{N_i} = \frac{n_C}{2\pi^2 M_i}\int dk\{[(\phi^+_{P,n\bar{n}}(k) + \frac{m_u}{E_u(k)}\phi^+_{A,n\bar{n}}(k))^2 - (\phi^-_{P,n\bar{n}}(k) + \frac{m_u}{E_u(k)}\phi^-_{A,n\bar{n}}(k))^2] + [(\phi^+_{P,s\bar{s}}(k) + \frac{m_s}{E_s(k)}\phi^+_{A,s\bar{s}}(k))^2 - (\phi^-_{P,s\bar{s}}(k) + \frac{m_s}{E_s(k)}\phi^-_{A,s\bar{s}}(k))^2]\}, \tag{4.5.1}$$

where the various wave functions are those for the state i.

We calculate the singlet and octet decay constants in terms of the divergence of the currents

$$A^{(8)}_\mu(x) = \bar{q}(x)\gamma_\mu\gamma_5\lambda^8 q(x) \tag{4.5.2}$$

and

$$A^{(0)}_\mu(x) = \bar{q}(x)\gamma_\mu\gamma_5\lambda^0 q(x). \tag{4.5.3}$$

We find

$$f^{(8)}_{\eta,i} = \sqrt{\frac{2}{3}}\frac{n_C}{\pi^2}\frac{\sqrt{N_i}}{M_i}\int dk\, k\{(\frac{m_u}{E_u(k)})[\phi^+_{P,n\bar{n}}(k) - \phi^-_{P,n\bar{n}}(k) + \phi^+_{A,n\bar{n}}(k) + \phi^-_{A,n\bar{n}}(k)] - (\frac{m_s}{E_s(k)})[\phi^+_{P,s\bar{s}}(k) - \phi^-_{P,s\bar{s}}(k) + \phi^+_{A,s\bar{s}}(k) + \phi^-_{A,s\bar{s}}(k)]\sqrt{2}\} \tag{4.5.4}$$

and

$$f_{\eta,i}^{(0)} = \sqrt{\frac{2}{3}}\frac{n_C}{\pi^2}\frac{\sqrt{N_i}}{M_i}\int dk\,k\{(\frac{m_u}{E_u(k)})[\phi^+_{P,n\bar{n}}(k)-\phi^-_{P,n\bar{n}}(k)+\phi^+_{A,n\bar{n}}(k) \\ +\phi^-_{A,n\bar{n}}(k)]\sqrt{2}+(\frac{m_s}{E_s(k)})[\phi^+_{P,s\bar{s}}(k)-\phi^-_{P,s\bar{s}}(k)+\phi^+_{A,s\bar{s}}(k)+\phi^-_{A,s\bar{s}}(k)]\}. \tag{4.5.5}$$

For the $\eta(547)$ and $\eta'(958)$ it is useful to improve upon the results of Eqs.(4.5.4) and (4.5.5) by introducing axial charge parameters. These arise from interposing a string of vacuum polarization diagrams between the η or η' wave functions and the axial current. We define

$$g^{\eta}_{n\bar{n}} = \frac{1}{1-G_V J^{AA}_{n\bar{n}}(m^2_\eta)}\,, \tag{4.5.6}$$

$$g^{\eta}_{s\bar{s}} = \frac{1}{1-G_V J^{AA}_{s\bar{s}}(m^2_\eta)}\,, \tag{4.5.7}$$

$$g^{\eta'}_{n\bar{n}} = \frac{1}{1-G_V J^{AA}_{n\bar{n}}(m^2_{\eta'})}\,, \tag{4.5.8}$$

and

$$g^{\eta'}_{s\bar{s}} = \frac{1}{1-G_V J^{AA}_{s\bar{s}}(m^2_{\eta'})}\,. \tag{4.5.9}$$

Thus for the $\eta(547)$, we define

$$F_{\eta}^{(8)} = \sqrt{\frac{2}{3}}\frac{n_C}{\pi^2}\frac{\sqrt{N_i}}{M_i}\int dkk\{g_{n\bar{n}}^{\eta}(\frac{m_u}{E_u(k)})[\phi_{P,n\bar{n}}^{+}(k) - \phi_{P,n\bar{n}}^{-}(k) + \phi_{A,n\bar{n}}^{+}(k) + \phi_{A,n\bar{n}}^{-}(k)] - g_{s\bar{s}}^{\eta}(\frac{m_s}{E_s(k)})[\phi_{P,s\bar{s}}^{+}(k) - \phi_{P,s\bar{s}}^{-}(k) + \phi_{A,s\bar{s}}^{+}(k) + \phi_{A,s\bar{s}}^{-}(k)]\sqrt{2}\} \tag{4.5.10}$$

and

$$F_{\eta}^{(0)} = \sqrt{\frac{2}{3}}\frac{n_C}{\pi^2}\frac{\sqrt{N_i}}{M_i}\int dkk\{g_{n\bar{n}}^{\eta}(\frac{m_u}{E_u(k)})[\phi_{P,n\bar{n}}^{+}(k) - \phi_{P,n\bar{n}}^{-}(k) + \phi_{A,n\bar{n}}^{+}(k) + \phi_{A,n\bar{n}}^{-}(k)]\sqrt{2} + g_{s\bar{s}}^{\eta}(\frac{m_s}{E_s(k)})[\phi_{P,s\bar{s}}^{+}(k) - \phi_{P,s\bar{s}}^{-}(k) + \phi_{A,s\bar{s}}^{+}(k) + \phi_{A,s\bar{s}}^{-}(k)]\}, \tag{4.5.11}$$

with similar definitions of $F_{\eta'}^{(8)}$ and $F_{\eta'}^{(0)}$ for the $\eta'(958)$. We do not calculate values of the axial charge for the more highly excited states, since more complex techniques than those used here would be needed for those states. In Table 4.1 we present the values obtained for $f_{\eta}^{(0)}$ and $f_{\eta}^{(8)}$ for the twenty-eight wave functions calculated in this work, as well as values of $F_{\eta}^{(8)}$, $F_{\eta}^{(0)}$, $F_{\eta'}^{(8)}$ and $F_{\eta'}^{(0)}$.

4.6 Discussion

In this chapter we have used parameters from our earlier studies: G_{88} = 12.46 GeV^{-2}, G_V = 12.46 GeV^{-2}, κ = 0.055 GeV^2, μ = 0.010 GeV, m_u = 0.364 GeV and m_s = 0.565 GeV. The value of G_{00}, which was 10.46 GeV^{-2} in previous work, was adjusted to 9.10 GeV^{-2} so that we had 543 MeV for the mass of the $\eta(547)$. A particularly satisfactory feature of our analysis may be seen in Fig.4.3, where we see that we make a good account of the spectrum of the four experimentally determined states. The four states of lowest energy are also found to be well separated from the

large number of states found above 1.5 GeV.

The RPA representation of the wave function components is seen to be particularly well suited if one wishes to provide a physical description of the states in terms of their $n\bar{n}$ or $s\bar{s}$ components. It is also easy to see the relative importance of the γ_5 and $\gamma_0\gamma_5$ vertices. It is worth noting that the deviations from ideal mixing are due to the presence of the 't Hooft interaction. It may be seen from our results that $n\bar{n}$-$s\bar{s}$ mixing is most important for the $\eta(547)$ and $\eta'(958)$. The other states are mainly either $n\bar{n}$ or $s\bar{s}$ states. [See Table 4.1.]

Chapter 5

Decay Constants of the $a_0(980)$ and $K_0^*(1430)$

5.1 Introduction

We are motivated to calculate the decay constants of the $a_0(980)$, $a_0(1450)$ and $K_0^*(1430)$ resonances, since values have been obtained for these constants using QCD sum rules and various experimental data [Ma99, Ma00]. The calculation of these decay constants is useful in assigning the $a_0(980)$ and $K_0^*(1430)$ resonances to scalar nonets, which is a matter of some controversy. In our previous work we found that the $a_0(980)$ and $K_0^*(1430)$ should be placed in the same $1\,^3P_0$ nonet of scalar states [Ce99a, Ce00]. Maltman's work [Ma99, Ma00] supports that assignment.

5.2 Vertex Functions for Scalar Mesons

We recall that we had defined $\Gamma_S^{+-}(P,k)$ and $\Gamma_S^{-+}(P,k)$:

$$\Lambda^{(+)}(\overline{k})\,\overline{\Gamma}^S(P,k)\,\Lambda^{(-)}(-\overline{k}) = \Gamma_S^{+-}(P,k)\,\Lambda^{(+)}(\overline{k})\,\Lambda^{(-)}(-\overline{k}) \ , \tag{5.2.1}$$

and

$$\Lambda^{(-)}(-\overline{k})\,\overline{\Gamma}^S(P,k)\,\Lambda^{(+)}(\overline{k}) = \Gamma_S^{-+}(P,k)\,\Lambda^{(-)}(-\overline{k})\,\Lambda^{(+)}(\overline{k}) \ . \tag{5.2.2}$$

We also define $\Gamma_S^{++}(P,k)$ and $\Gamma_S^{--}(P,k)$:

$$\Lambda^{(+)}(\overline{k})\,\overline{\Gamma}^S(P,k)\,\Lambda^{(+)}(\overline{k}) = \Gamma_S^{++}(P,k)\,\Lambda^{(+)}(\overline{k}) \ , \tag{5.2.3}$$

and

$$\Lambda^{(-)}(-\vec{k})\bar{\Gamma}^{S}(P,k)\Lambda^{(-)}(-\vec{k}) = \Gamma_S^{--}(P,k)\Lambda^{(-)}(-\vec{k}) \ . \tag{5.2.4}$$

In our work we obtained equations for $\Gamma_S^{+-}(P,k)$ and $\Gamma_S^{-+}(P,k)$ in the frame where $\vec{P} = 0$. [See Eqs.(2.2.10) and (2.2.11).] The calculation of $\Gamma_S^{++}(P^0,k)$ and $\Gamma_S^{--}(P^0,k)$ is described in [Ce00]. This formalism may be used to obtain covariant expressions for the vertex [Ce99a, Ce00]. We write

$$\bar{\Gamma}_S(P,k) = a_1(P,k) + \hat{k}\, a_2(P,k) \ , \tag{5.2.5}$$

where $\hat{k}^{\mu}$ was defined previously in Eq.(2.2.2). We have

$$\Gamma_S^{+-}(P,k) = a_1(P,k) + m a_2(P,k) \ , \tag{5.2.6}$$

and

$$\Gamma_S^{++}(P,k) = a_1(P,k) - \frac{\vec{k}^2}{m} a_2(P,k) \ . \tag{5.2.7}$$

Note that we can write $a_1(P,k) = a_1(P^2,\sqrt{-\hat{k}^2}\,)$, and $a_2(P,k) = a_2(P^2,\sqrt{-\hat{k}^2}\,)$. The Lorentz invariants, a_1 and a_2, may be determined by relating them to the rest frame values of $\Gamma_S^{+-}(P^0,|\vec{k}|)$ and $\Gamma_S^{-+}(P^0,|\vec{k}|)$ [Ce99a, Ce00]. (The case where the quark masses are different is discussed in great detail in [Ce99a] and in Section 5.5.) Using this formalism, vacuum polarization diagrams and meson decay amplitudes may be calculated in any Lorentz frame and we have made a number of such calculations.

5.3 Vacuum Polarization Functions and Quark T Matrices

The vacuum polarization function seen in Fig.2a is given by the integral in the case we study scalar mesons. Here $n_C = 3$ is the number of colors and the factor 2 arises from the flavor trace. In Eq.(5.3.1), $S(P/2+k)$ and $S(-P/2+k)$ are

$$-iJ^S(P^2) = -2n_C \int \frac{d^4k}{(2\pi)^4} \mathrm{Tr}\left[iS(P/2+k)\bar{\Gamma}^S(P,k)iS(-P/2+k)\right] , \qquad (5.3.1)$$

propagators for constituent quarks of mass m, $S(p) = \left[\not{p} - m + i\eta\right]^{-1}$. (The case of unequal mass values for the quarks is discussed in Refs.[Ce99a] and [Ce00] and in Section 5.5.) We have

$$J^S(P^2) = -4n_C \int \frac{d^3k}{(2\pi)^3} \left[\frac{\vec{k}^2}{E^2(\vec{k})}\right] e^{-\vec{k}^2/\alpha^2} \left[\frac{\Gamma_S^{+-}(P^0,|\vec{k}|)}{P^0 - 2E(\vec{k})} - \frac{\Gamma_S^{-+}(-P^0,|\vec{k}|)}{P^0 + 2E(\vec{k})}\right] . \qquad (5.3.2)$$

In Eq.(5.3.2) we have included a Gaussian regulator $\exp[-\vec{k}^2/\alpha^2]$, which can be written in a covariant form using the four vector $\hat{k}^\mu$ of Eq.(2.2.2). (In our earlier work we have used α = 0.605 GeV.)

It is important for this work to recall that Eq.(2.3.3) allows us to write Eq.(5.3.2) as

$$J^S(P^2) = -4n_C \int \frac{d^3k}{(2\pi)^3} \left[\frac{\vec{k}^2}{E^2(\vec{k})}\right] e^{\frac{-\vec{k}^2}{\alpha^2}} \Gamma_S^{+-}(P^0,|\vec{k}|) \left[\frac{1}{P^0 - 2E(\vec{k})} - \frac{1}{P^0 + 2E(\vec{k})}\right] . \qquad (5.3.3)$$

In some of our calculations we have kept only the first term in the bracket of Eq.(5.3.3). That procedure defines the TDA, while the complete expression defines the RPA. [See Fig.2.3]

We now turn to a definition of $q\bar{q}$ T matrices [Ce99a, Ce00]. We may write, for a single-channel problem,

$$t^{\mathrm{TDA}}(P^2) = -\frac{G}{1 - GJ^S_{\mathrm{TDA}}(P^2)} \tag{5.3.4}$$

and

$$t^{\mathrm{RPA}}(P^2) = -\frac{G}{1 - GJ^S_{\mathrm{RPA}}(P^2)} \ . \tag{5.3.5}$$

We may find the meson mass values by solving the equation

$$G^{-1} - J^S(P^2) = 0 \ , \tag{5.3.6}$$

for $J^S(P^2)$ equal to $J^S_{\mathrm{RPA}}(P^2)$ or $J^S_{\mathrm{TDA}}(P^2)$. More generally, we may include $K^S(P^2)$ of Fig.2.2b as in Eqs.(2.3.8) and (2.3.9). The extension of this formalism to include singlet-octet mixing, as is appropriate in the study of the f_0 mesons, is given in [Ce00]. In that case, the coupling constants G_{88}, G_{08} and G_{00} appear. These may be related to the values of G_S, G_D and the matrix elements defining the vacuum condensates $\langle \bar{u}u \rangle$, $\langle \bar{d}d \rangle$ and $\langle \bar{s}s \rangle$ [Ce00]. We remark that the complete $q\bar{q}$ T matrix, that is defined in [Ce99d], is shown there to be represented by only $q\bar{q}$ bound-state wave functions in the case we have absolute confinement.

We use the notation $n\bar{n} = [u\bar{u} + d\bar{d}]/\sqrt{2}$. In Fig.5.2 we show values of $J^S_{n\bar{n}}(P^2)$ in both the TDA [dotted line] and the RPA [solid line]. Here $m_u = m_d = 0.364$ GeV, $\kappa = 0.055$ GeV^2 and $\alpha = 0.605$ GeV. In Fig.5.3 we show values of $J^S_{s\bar{s}}(P^2)$ for the value $m_s = 0.565$ GeV and the same value of α. It is seen that the use of the RPA rather than the TDA becomes relatively less important with increasing P^2. That may also be seen in Figs.5.4 and 5.5, where we compare the two approximations, TDA and RPA, for $J^S_{n\bar{n}}(P^2)$ and $J^S_{s\bar{s}}(P^2)$ in the range $0 < P^2 < 5$ GeV^2.

5.4 Relativistic RPA Equations

The form of the nonrelativistic RPA equations for bound states may be found in [Fe71]. The generalization to the relativistic case is straightforward. With $k = |\vec{k}|$, $k' = |\vec{k}'|$ and $E_a(k) = \left[\vec{k}^2 + m_a^2\right]^{1/2}$, we have

$$\left[E_a(k) + E_b(k)\right]\phi^+(k) + \int dk' H_{11}(k,k')\phi^+(k') + \int dk' H_{12}(k,k')\phi^-(k') = P^0\phi^+(k) \tag{5.4.1}$$

and

$$-\left[E_a(k) + E_b(k)\right]\phi^-(k) - \int dk' H_{11}(k,k')\phi^-(k') - \int dk' H_{12}(k,k')\phi^+(k') = P^0\phi^-(k) \ . \tag{5.4.2}$$

Here, we have used a form for the equations in which $H_{11}(k,k')$ and $H_{12}(k,k')$ are symmetric. We will call $\phi^+(k)$ and $\phi^-(k)$ the large and small components, respectively, although $\phi^+(k)$ and $\phi^-(k)$ are approximately of the same magnitude for the $\pi(138)$.

The contributions to H_{11} and H_{12} arise from the confining interaction and from the NJL interaction. As in all our previous works, we neglect pair creation by the confining field in the meson rest frame. Therefore, we will use

$$H_{11}(k,k') = H_C(k,k') + H_{NJL}(k,k') \tag{5.4.3}$$

and

$$H_{12}(k,k') = H_{NJL}(k,k') \ . \tag{5.4.4}$$

In the following sections we will give the form of $H_C(k,k')$ and $H_{NJL}(k,k')$ for pseudoscalar and scalar mesons. The definitions of $\phi^+(k)$ and $\phi^-(k)$ will be given in

Section 5.5 for scalar mesons, and in Section 5.6 for pseudoscalar mesons. We note that the spectrum of states obtained from solving Eqs.(5.4.1) and (5.4.2) is the same as that found when solving the equation

$$G_{88}^{-1} - J_{\mathrm{RPA}}^{S}(P^2) = 0 \tag{5.4.5}$$

for mesons in a SU(3) octet, such as those considered here.

5.5 RPA Equations for Scalar Mesons

In this section we generalize our equations for the scalar mesons to the case in which the quark and antiquark have different masses. Some of the relevant equations were given in [Ce99a]. The inhomogeneous equation for the confinement vertex of Fig.2.1a is

$$\Gamma_{S,ab}^{+-}(P^0, k) = 1 + \frac{1}{(2\pi)^2} \int k'^2\, dk' \int_{-1}^{1} dx \frac{A_1(k,k',x)}{E_a(\vec{k}')\,E_b(\vec{k}')} \frac{1}{C(\vec{k})} \times \frac{\Gamma_{S,ab}^{+-}(P^0, k')\, V^C(\vec{k}-\vec{k}')}{P^0 - E_a(\vec{k}') - E_b(\vec{k}')}\,, \tag{5.5.1}$$

with $x = \cos\theta$ and

$$C(\vec{k}) = \left[E_a(\vec{k})E_b(\vec{k}) + \vec{k}^2 - m_a m_b\right]. \tag{5.5.2}$$

The rather lengthy expression for $A_1(k,k',x)$ is given in Eq.(6.6) of [Ce99a]. The homogeneous version of Eq.(5.5.1) may be symmetrized by multiplying from the left by $k\sqrt{C(\vec{k})}/\sqrt{2E_a(\vec{k})E_b(\vec{k})}$. We define wave functions associated with the vertex of Fig.2.1c.

$$\phi^{+}_{ab}(k) = \frac{k\sqrt{C(\vec{k})}}{\sqrt{2E_a(\vec{k})E_b(\vec{k})}} \frac{\hat{\Gamma}^{+-}_{S,ab}(k)}{P^0 - E_a(\vec{k}) - E_b(\vec{k})} \ , \tag{5.5.3}$$

and

$$\phi^{-}_{ab}(k) = -\frac{k\sqrt{C(\vec{k})}}{\sqrt{2E_a(\vec{k})E_b(\vec{k})}} \frac{\hat{\Gamma}^{+-}_{S,ab}(k)}{P^0 + E_a(\vec{k}) + E_b(\vec{k})} \ . \tag{5.5.4}$$

We neglect the NJL interaction for the moment, so that we may identify $H_C(k,k')$. We have

$$\left[P^0 - E_a(\vec{k}) - E_b(\vec{k})\right]\phi^{+}_{ab}(k)$$
$$= \frac{1}{(2\pi)^2}\int kk'dk' \int_{-1}^{1} dx \frac{A_1(k,k',x)\,V^C(\vec{k}-\vec{k}')}{\sqrt{E_{al}(\vec{k})E_b(\vec{k})E_a(\vec{k}')E_b(\vec{k}')}} \frac{1}{\sqrt{C(\vec{k})C(\vec{k}')}} \phi^{+}_{ab}(k') \ . \tag{5.5.5}$$

Here P^0 is the eigenvalue equal to the mass of the bound state. If we complete the integral over x, we have

$$\left[P^0 - E_a(\vec{k}) - E_b(\vec{k})\right]\phi^{+}_{ab}(k) = \frac{1}{(2\pi)^2}\int kk'dk' \left[V_0^C(k,k')b_1(k,k') + kk'V_1^C(k,k')b_2\right]$$
$$\times \frac{1}{\sqrt{C(\vec{k})C(\vec{k}')}} \frac{1}{\sqrt{E_a(\vec{k})E_b(\vec{k})E_a(\vec{k}')E_b(\vec{k}')}} \phi^{+}_{ab}(k') \ , \tag{5.5.6}$$

with

$$b_1(k,k') = \left[E_a(\vec{k}')E_b(\vec{k}') + \vec{k}'^2\right]\left[E_a(\vec{k})E_b(\vec{k}) + \vec{k}^2\right]$$
$$- m_a m_b \{E_a(\vec{k})E_b(\vec{k}) + E_a(\vec{k}')E_b(\vec{k}') + \vec{k}^2 + \vec{k}'^2 - m_a m_b - \frac{1}{2}E_a(\vec{k})E_b(\vec{k}')$$
$$- \frac{1}{2}E_a(\vec{k}')E_b(\vec{k})\} - \frac{1}{2}m_a^2 E_b(\vec{k}')E_b(\vec{k}) - \frac{1}{2}m_b^2 E_a(\vec{k})E_a(\vec{k}') \ , \tag{5.5.7}$$

and

$$b_2 = \left[m_a m_b + \frac{1}{2}m_a^2 + \frac{1}{2}m_b^2\right] \ . \tag{5.5.8}$$

In the limit $m_a = m_b = m$, we have

$$C(\vec{k}) \to 2\vec{k}^2 \ , \tag{5.5.9}$$

$$b_1(k,k') \to 4\vec{k}^2\vec{k}'^2 \ , \tag{5.5.10}$$

and

$$b_2 \to 2m^2 \ . \tag{5.5.11}$$

Thus, Eq.(5.5.6) becomes, for $m_a = m_b = m$

$$\left[P^0 - 2E(\vec{k})\right]\phi^+(k) = \frac{1}{(2\pi)^2}\int \frac{kk'dk'}{E(\vec{k})E(\vec{k}')}\left[2kk'V_0^C(k,k') + m^2V_1^C(k,k')\right]\phi^+(k') . \tag{5.5.12}$$

[See Eq.(5.4.1).] We may identify $H_C(k,k')$ for the case $m_a \neq m_b$:

$$H_C(k,k') = -\frac{1}{(2\pi)^2}\frac{kk'}{\sqrt{E_a(\vec{k})E_b(\vec{k})E_a(\vec{k}')E_b(\vec{k}')}} \times \frac{1}{\sqrt{C(\vec{k})C(\vec{k}')}}\left[V_0^C(k,k')b_1(k,k') + kk'V_1^C(k,k')b_2\right]. \tag{5.5.13}$$

We then note that the symmetrized version of $H_{NJL}(k,k')$ is

$$H_{NJL}(k,k') = \frac{8n_C}{(2\pi)^2}\frac{\left[G_S k k' e^{-k^2/2\alpha^2} e^{-k'^2/2\alpha^2}\right]\sqrt{C(\vec{k})C(\vec{k}')}}{2\sqrt{E_a(\vec{k})E_b(\vec{k})E_a(\vec{k}')E_b(\vec{k}')}}. \tag{5.5.14}$$

In the RPA, the normalization factor may be seen to be [Fe71]

$$\frac{1}{N_i} = \frac{n_C}{(2\pi)^2}\left[\frac{1}{2M_i}\right]\int k^2 dk\left[\frac{2E_a(\vec{k})E_b(\vec{k}) - 2m_a m_b}{E_a(\vec{k})E_b(\vec{k})}\right]\left(|\tilde{\phi}_i^+(k)|^2 - |\tilde{\phi}_i^-(k)|^2\right), \tag{5.5.15}$$

where M_i is the mass of the bound state,

$$\tilde{\phi}_i^+(k) = \frac{\sqrt{2E_a(\vec{k})E_b(\vec{k})}}{k\sqrt{C(\vec{k})}}\phi_i^+(k), \tag{5.5.16}$$

and

$$\tilde{\phi}_i^-(k) = \frac{\sqrt{2E_a(\vec{k})E_b(\vec{k})}}{k\sqrt{C(\vec{k})}}\phi_i^-(k). \tag{5.5.17}$$

We now introduce the normalized functions

$$\tilde{\phi}_{i,N}^+(k) = \sqrt{N_i}\,\tilde{\phi}_i^+(k) \tag{5.5.18}$$

and

$$\tilde{\phi}^{-}_{i,N}(k) = \sqrt{N_i}\,\tilde{\phi}^{-}_{i}(k)\ , \qquad (5.5.19)$$
$$\tilde{\phi}^{-}_{i,N}(k) = \sqrt{N_i}\,\tilde{\phi}^{-}_{i}(k)\ ,$$

which may be used to define a normalized vertex function $\hat{\Gamma}^{+-}_{i,N}(k)$:

$$\tilde{\phi}^{+}_{i,N}(k) = \frac{\hat{\Gamma}^{+-}_{i,N}(k)}{P_i^0 - E_a(\vec{k}) - E_b(\vec{k})} \qquad (5.5.20)$$

and

$$\tilde{\phi}^{-}_{i,N}(k) = -\frac{\hat{\Gamma}^{+-}_{i,N}(k)}{P_i^0 + E_a(\vec{k}) + E_b(\vec{k})}\ . \qquad (5.5.21)$$

The calculation of scalar meson decay constants using these wave functions is described in Section 5.7.

5.6 RPA Equations for Pseudoscalar Mesons

Here we consider the vertex function $\bar{\Gamma}_{5,ab}(P,k)$ that describes the effects of the confining interaction for a quark of mass m_a and an antiquark of mass m_b. We have the inhomogeneous equation [Ce99a, Ce00],

$$\bar{\Gamma}_{5,ab}(P,k) = \gamma_5 - i\int \frac{d^4k'}{(2\pi)^4}\left[\gamma^\rho S_a(P/2+k')\bar{\Gamma}_{5,ab}(P,k')S_b(-P/2+k')\gamma_\rho\right]V^C(k-k')\,. \qquad (5.6.1)$$

Here $S_a(P) = \left[\not{P} - m_a + i\eta\right]^{-1}$ is the propagator of a quark of mass m_a.

It is useful to define the projection operators

$$\Lambda_a^{(+)}(\vec{k}) = \frac{\not{k}_a + m_a}{2\,m_a} \qquad (5.6.2)$$

and

$$\Lambda_b^{(-)}(-\vec{k}) = \frac{\tilde{k}_b + m_b}{2m_b} \quad , \tag{5.6.3}$$

with $k_a^\mu = [E_a(\vec{k}), \vec{k}]$ and $\tilde{k}_b^\mu = [-E_b(\vec{k}), \vec{k}]$. [Note that $\Lambda_a^{(+)}(\vec{k}) + \Lambda_a^{(-)}(\vec{k}) = 1$, while $\Lambda_a^{(+)}(\vec{k}) + \Lambda_a^{(-)}(-\vec{k}) \neq 1$.] Using these functions, we define

$$\Lambda_a^{(+)}(\vec{k})\,\bar{\Gamma}_{5,ab}(P,k)\,\Lambda_b^{(-)}(-\vec{k}) = \Gamma_{5,ab}^{+-}(P,k)\,\Lambda_a^{(+)}(\vec{k})\,\gamma_5\,\Lambda_b^{(-)}(-\vec{k}) \quad , \tag{5.6.4}$$

and

$$\Lambda_a^{(-)}(-\vec{k})\,\bar{\Gamma}_{5,ab}(P,k)\,\Lambda_b^{(+)}(\vec{k}) = \Gamma_{5,ab}^{-+}(P,k)\,\Lambda_a^{(-)}(-\vec{k})\,\gamma_5\,\Lambda_b^{(+)}(\vec{k}) \quad . \tag{5.6.5}$$

Equations for $\Gamma_{5,ab}^{+-}(P,k)$ and $\Gamma_{5,ab}^{-+}(P,k)$ were given in [Ce99a]:

$$\Gamma_{5,ab}^{+-}(P^0,|\vec{k}|) = 1 - \int \frac{d^3k'}{(2\pi)^3}\,B(\vec{k},\vec{k}') \times \frac{\Gamma_{5,ab}^{+-}(P^0,|\vec{k}'|)\,V^C(\vec{k}-\vec{k}')}{P^0 - E_a(\vec{k}') - E_b(\vec{k}')} \tag{5.6.6}$$

and

$$\Gamma_{5,ab}^{-+}(P^0,|\vec{k}|) = 1 + \int \frac{d^3k'}{(2\pi)^3}\,B(\vec{k},\vec{k}') \times \frac{\Gamma_{5,ab}^{-+}(P^0,|\vec{k}'|)\,V^C(\vec{k}-\vec{k}')}{P^0 + E_a(\vec{k}') + E_b(\vec{k}')} \quad , \tag{5.6.7}$$

(The rather lengthy expression for $B(\vec{k},\vec{k}')$ is given in Eq.(3.6) of [Ce99a].) We note that

$$\Gamma^{-+}_{5,ab}(-P^0, |\vec{k}|) = \Gamma^{-+}_{5,ab}(P^0, |\vec{k}|) \ . \tag{5.6.8}$$

Therefore, the vacuum polarization function $J^{PP}_{ab}(P^2)$, defined in Eq.(3.10) of [Ce99a], may be written as

$$J^{PP}_{ab}(P^2) = -2n_c \int \frac{d^3k'}{(2\pi)^3} \frac{[E_a(\vec{k})E_b(\vec{k}) + \vec{k}^2 + m_a m_b]}{E_a(\vec{k})E_b(\vec{k})}$$

$$\times \Gamma^{+-}_{5,ab}(P^0, |\vec{k}|) \left[\frac{1}{P^0 - E_a(\vec{k}) - E_b(\vec{k})} - \frac{1}{P^0 + E_a(\vec{k}) + E_b(\vec{k})} \right] \ . \tag{5.6.9}$$

We now write, with $k = |\vec{k}|$ and $k' = |\vec{k}'|$,

$$B(\vec{k}, \vec{k}') = \frac{1}{2E_a(k)E_b(k')F(k)} \left[d_0(k,k') + \vec{k}\cdot\vec{k}' d_1 \right], \tag{5.6.10}$$

where

$$F(k) = \left[m_a m_b + E_a(k)E_b(k) + \vec{k}^2 \right], \tag{5.6.11}$$

$$\begin{aligned} d_0(k,k') = {} & m_a m_b (E_a(k)E_b(k') + E_b(k)E_a(k') - 2E_a(k')E_b(k') \\ & - 2E_a(k)E_b(k) - 2\vec{k}^2 - 2\vec{k}'^2) + m_b^2 \left[E_a(k)E_a(k') \right] + m_a^2 \left[E_b(k)E_b(k') \right] \\ & - 2\left[(E_a(k)E_b(k) + \vec{k}^2)(E_a(k')E_b(k') + \vec{k}'^2) \right] - 2m_a^2 m_b^2 \ , \end{aligned} \tag{5.6.12}$$

and

$$d_1 = 2m_a m_b - m_a^2 - m_b^2 \ . \tag{5.6.13}$$

Thus,

$$\Gamma_5^{+-}(P,k) = -4\pi \int \frac{k'^2 dk'}{(2\pi)^3}\left[d_0(k,k')V_0^C(k,k') + d_1 kk' V_1^C(k,k')\right]$$
$$\times \frac{1}{2E_a(k)E_b(k')F(k)}\Gamma_5^{+-}(P,k')\left[\frac{1}{P^0 - E_a(k') - E_b(k')} - \frac{1}{P^0 + E_a(k') + E_b(k')}\right]. \quad (5.6.14)$$

This equation may be put into a symmetric form by multiplying from the left by $k\sqrt{F(k)}\,/\left[2E_a(k)E_b(k)\right]^{1/2}$. We then define, in analogy to Eq.(5.5.3) and (5.5.4),

$$\phi_{ab}^{+}(k) = \frac{k\sqrt{F(k)}}{\sqrt{2E_a(\vec{k})E_b(\vec{k})}} \frac{\hat{\Gamma}_{5,ab}^{+-}(k)}{P^0 - E_a(\vec{k}) - E_b(\vec{k})}, \quad (5.6.15)$$

and

$$\phi_{ab}^{-}(k) = -\frac{k\sqrt{F(k)}}{\sqrt{2E_a(\vec{k})E_b(\vec{k})}} \frac{\hat{\Gamma}_{5,ab}^{+-}(k)}{P^0 + E_a(\vec{k}) + E_b(\vec{k})}, \quad (5.6.16)$$

where $\hat{\Gamma}_{5,ab}^{+-}(k)$ describes the effect of both the confining interaction and the NJL interaction.

If we only consider the confining interaction, we have

$$\left[P_i^0 - E_a(k) - E_b(k)\right]\phi_i^{+}(k) = -\frac{1}{4\pi^2}\int dk' \frac{kk'}{\sqrt{F(k)F(k')}} \frac{1}{\sqrt{E_a(k)E_b(k)E_a(k')E_b(k')}}$$
$$\times\left[d_0(k,k')V_0^C(k,k') + d_1 kk' V_1^C(k,k')\right]\left[\phi_i^{+}(k') + \phi_i^{-}(k')\right]. \quad (5.6.17)$$

Therefore, we may identify

$$H_C(k,k') = -\frac{1}{4\pi^2}\frac{kk'}{\sqrt{F(k)F(k')}}\frac{1}{\sqrt{E_a(k)E_b(k)E_a(k')E_b(k')}} \times\left[d_0(k,k')V_0^C(k,k') + d_1 kk' V_1^C(k,k')\right]. \quad (5.6.18)$$

We may also obtain the symmetrized form of the NJL interaction for pseudoscalar mesons

$$H_{\mathrm{NJL}}(k,k') = -\frac{n_C}{\pi^2}e^{-k^2/2\alpha^2}kk'G_S e^{-k'^2/2\alpha^2}\frac{\sqrt{F(k)F(k')}}{\sqrt{E_a(k)E_b(k)E_a(k')E_b(k')}}. \quad (5.6.19)$$

5.7 Definition of Scalar Meson Decay Constants

Here we follow the definitions introduced by Maltman and use some of his notation [Ma99a, Ma00a]. Maltman studies the scalar correlator

$$\Pi(q^2) = i\int d^4x e^{iqx}\ \langle 0|\mathrm{T}(j(x)j^\dagger(0))|0\rangle\ , \quad (5.7.1)$$

with $j^{du}(x) = \partial_\mu(\bar{d}\gamma^\mu u)$ or $j^{su} = \partial_\mu(\bar{s}\gamma^\mu u)$. He then defines

$$-i\langle 0|j^{su}(0)|K_0^*(1430)\rangle = f_{K_0^*(1430)}m^2_{K_0^*(1430)}. \quad (5.7.2)$$

One might define

$$-i\langle 0|j^{du}(0)|a_0(980)\rangle = \hat{f}_{a_0(980)}m^2_{a_0(980)}. \quad (5.7.3)$$

However, Maltman introduces an alternate definition. In QCD, one has

$$\partial_\mu(\bar{q}^a\gamma^\mu q^b) = i(m_a^0 - m_b^0)S^{ab}, \quad (5.7.4)$$

with $S^{ab} = \bar{q}^a q^b$. It is then useful to define the $a_0(980)$ decay constant $f_{a_0(980)}$ using the relation

$$\left[\frac{m_s^0 - m_u^0}{m_d^0 - m_u^0}\right] \langle 0|j^{du}(0)|a_0(980)\rangle = f_{a_0(980)} m_{a_0(980)}^2 , \qquad (5.7.5)$$

so that the $a_0(980)$ and $K_0^*(1430)$ will have similar decay constants, if the wave functions are similar. If we consider mesons of positive charge, we may use

$$-ij^{su} = (m_s^0 - m_u^0)\bar{s}u \qquad (5.7.6)$$

$$= (m_s^0 - m_u^0)\frac{1}{\sqrt{2}}\bar{q}\left[\frac{\lambda_4 - i\lambda_5}{\sqrt{2}}\right]q \qquad (5.7.7)$$

and

$$-ij^{du} = (m_d^0 - m_u^0)\frac{1}{\sqrt{2}}\bar{q}\left[\frac{\lambda_1 - i\lambda_2}{\sqrt{2}}\right]q . \qquad (5.7.8)$$

We make further contact with Maltman's work by using the value of m_s^0 quoted in [Ka00]. There one finds $m_s(1\text{ GeV}) = 158.6 \pm 18.7 \pm 16.3 \pm 13.3$ MeV, where the first error is statistical, the second is due to that of V_{us}, and the third is the theoretical error. Taking $m_u^0 = m_d^0 = 5.5$ MeV, we put $m_s^0 - m_u^0 = 0.153$ GeV. Since we compare our results for the decay constants with those found by Maltman, our choice of $m_s^0 - m_u^0$ is part of a consistent procedure. The expression for the decay constant is then

$$M_i^2 f_i = \frac{2n_C}{\sqrt{2}\,\pi^2}(m_s^0 - m_u^0)\int k^2 dk \left[\frac{E_a(\vec{k})E_b(\vec{k}) + \vec{k}^2 - m_a m_b}{2E_a(\vec{k})E_b(\vec{k})}\right]\left[\tilde{\phi}_{i,N}^{+}(k) + \tilde{\phi}_{i,N}^{-}\right] , \qquad (5.7.9)$$

The functions $\tilde{\phi}_{i,N}^{+}(k)$ and $\tilde{\phi}_{i,N}^{-}(k)$ that appear in Eq.(5.7.9) were defined in

Eqs.(5.5.16) and (5.5.17).

5.8 Numerical Results: Wave Functions and Decay Constants

Values of $\phi^+(k)$ and $\phi^-(k)$ are given for the pion in Fig.5.1 We have neglected confinement for the pion. However, the confining interaction is included for all other mesons. In Fig.5.2 we show $\phi^+(k)$ and $\phi^-(k)$ for the $K(495)$. Figure 5.3 shows these functions for the $a_0(980)$, while Fig.5.4 presents $\phi^+(k)$ and $\phi^-(k)$ for the $a_0(1450)$. We show $\phi^+(k)$ and $\phi^-(k)$ for the $K_0^*(1430)$ in Fig.5.5. We show the normalized functions $\tilde{\phi}_N^+(k)$ and $\tilde{\phi}_N^-(k)$, defined in Eqs.(5.5.18) and (5.5.19), for the $a_0(980)$ and $K_0^*(1430)$ in Figs.5.6 and 5.7, respectively. It may be seen from Figs.5.6-5.10 that $\phi^-(k)$ becomes progressively smaller as we consider mesons of increasing mass. The small component is, indeed, small for the more massive mesons. The results for the decay constants, which are given in Table 1, do not differ significantly as we go from the TDA, in which we neglect $\phi^-(k)$, to the RPA. Our result for the $a_0(980)$ is about a factor of 2 larger than the value obtained by Maltman using QCD sum rules. However, the values for the $a_0(1450)$ and $K_0^*(1430)$ are in much better agreement with Maltman's values. These results may imply that the $a_0(980)$ wave function has a significant $K\bar{K}$ component, as suggested by several authors. However, further work is needed to demonstrate whether that is the case.

5.9 Discussion

In a recent work [Sh00], we have calculated the energies of the $a_0(980)$ and $f_0(980)$ resonances. In an RPA calculation we find that the $a_0(980)$ at 991 MeV, while

additional dispersive corrections move the energy down to 949 MeV. A somewhat similar calculation, which takes into account singlet-octet mixing, places the $f_0(980)$ resonance at 980 MeV [Sh00]. These calculations are parameter-free in the sense that the parameters of the model were determined in previous studies of the pseudoscalar and vector nonets of $q\bar{q}$ states. The present calculation of decay constants serves to support our conclusion that the $a_0(980)$ and $f_0(980)$ belong in the same nonet of states as the $K_0^*(1430)$.

There is no consensus as to the organization of scalar mesons into nonets. We find Maltman's efforts in this direction particularly valuable, since his analysis is based in part upon the application of QCD sum rules. His results for the decay constants of the $a_0(980)$, $a_0(1450)$ and $K_0^*(1430)$ are given in Table 5.1 along with our values for the $1\ ^3P_0$, $2\ ^3P_0$ and $3\ ^3P_0$ states of the a_0 and K_0^* resonances that were calculated in this work. It is gratifying to see that our results, calculated by an entirely different method, are in reasonable agreement with Maltman's values, although our value for the $a_0(980)$ is too large, which may suggest the presence of a significant $K\bar{K}$ component. Maltman concludes that the $a_0(980)$ is not a $K\bar{K}$ "molecule", since such a structure would lead to a very small decay constant. We have also stated that the $\sigma(500\text{-}600)$ and $\kappa(700\text{-}900)$ are "dynamically-generated" states [Sh01]. These states appear as poles of the $\pi\pi$ and πK T matrices, respectively. However, there is no corresponding $q\bar{q}$ state, since the lowest-lying poles of the $q\bar{q}$ T matrix correspond to the $a_0(980)$ and $f_0(980)$ [Ce99a, Ce00]. (In the case of absolute confinement the $q\bar{q}$ T matrix is represented by only bound states, as we have discussed in detail in [Ce99d].) The identification of the

σ(500-600) and κ(700-900) as "dynamically-generated" states is also consistent with the phenomenological model of light meson spectra introduced in [An00]. The present work, and the work of Refs.[Ce99a] and [Ce00], leads us to the conclusion that the $a_0(980)$, $K_0^*(1430)$ and $f_0(980)$ belong in the same nonet. Our work also suggests that the $f_0(1370)$ is a member of the same nonet. However, the properties of the $f_0(1370)$ are expected to be significantly modified by quarkonium-glueball mixing. Such mixing should be calculated, since it is known that the $f_0(1370)$ decays predominantly to the 4π channel.

Chapter 6

Intrinsic and Dynamically-Generated Scalar Meson States

6.1 Introduction

In the case of scalar mesons the assignment of the observed resonances to quark-model configurations is problematic. For example, one may identify either the $\sigma(500\text{-}600)$, the $f_0(980)$, or the $f_0(1370)$ with the $1\ ^3P_0\ n\bar{n}$ state. The latter choice arises if one dismisses the $f_0(980)$ as a $K\bar{K}$ molecule [We82, Ja95] or a $q\bar{q}q\bar{q}$ state [Ja77]. If one chooses the $f_0(1370)$ to be the $1\ ^3P_0\ n\bar{n}$ state, the $f_J(1710)$ could be the $1\ ^3P_0\ s\bar{s}$ state, with the $f_0(1500)$ having a large glueball component. Without an underlying dynamical model, there exist a broad range of options.

Black, Fariborz, Sannino and Schechter have made extensive studies of the scalar nonet of states [Ha96, Sa95, Bl98, Bl99, Bl00]. In their recent study of the isovector scalar states [Bl00], Black, Fariborz and Schechter place the $a_0(980)$, $\kappa(900)$, $f_0(980)$ and the $\sigma(500\text{-}600)$ in the nonet of lowest energy, with the $a_0(1450)$ in the same nonet as the $K_0^*(1430)$. The last choice creates a series of problems related to the observed energies of these resonances. (For example, one would expect the $K_0^*(1430)$ to be more massive than the $a_0(1450)$, since the $K_0^*(1430)$ contains a strange quark.) To resolve such problems, these authors introduce two additional states with the quantum numbers of the $a_0(980)$ and $K_0^*(1430)$. (These additional states could

be of $q\bar{q}q\bar{q}$ character.) The physical $a_0(980)$ and $K_0^*(1430)$ then arise upon mixing of the $q\bar{q}$ states and the $q\bar{q}q\bar{q}$ states [Bl00].

In their description of quarkonium-glueball mixing Lee and Weingarten [Le99a, Le99b, We97] and Close and Kirk [Cl00] choose the $f_0(1370)$ as the $1\ ^3P_0\ n\bar{n}$ state. Close and Kirk place the bare glueball at 1434 MeV and configuration mixing then distributes the bare state, more or less equally, in the physical $f_0(1500)$ and $f_0(1710)$ resonances. Lee and Weingarten choose a larger value for the bare glueball mass so that, upon mixing, the main glueball component is in the $f_0(1710)$, with the $f_0(1500)$ resonance having the largest component of the $1\ ^3P_0\ s\bar{s}$ state. Other attempts to understand the scalar meson spectrum may be found if one surveys the extensive references given in [Bl00].

In our study of the isovector [Ce99a] and isoscalar [Ce00] scalar $q\bar{q}$ states we obtained the nonets shown in Figs.6.1 and 6.2. In this work we introduce some evidence to support our analysis. We also show how the $\sigma(500\text{-}600)$ and $\kappa(900)$ are generated dynamically. In our model the $a_0(980)$ and $f_0(980)$ are the intrinsic scalar states of lowest energy.

In our previous work we had $G_S = 11.83\ \text{GeV}^{-2}$ and $G_D = 86.39\ \text{GeV}^{-2}$ [Ce99a]. [See Eq.(2.1.1).] The interaction strength in singlet states was $G_{00} = 10.46\ \text{GeV}^{-2}$ and the interaction strength in octet states was $G_{88} = 12.46\ \text{GeV}^{-2}$. (The nonzero value of G_D induces some small deviations from ideal mixing [Ce00].) If we go to a basis of $n\bar{n}$ and $s\bar{s}$ states, we find $G_{n\bar{n}} = 11.12\ \text{GeV}^{-2}$, $G_{s\bar{s}} = 11.84\ \text{GeV}^{-2}$ and $G_{n\bar{s}} = -0.94\ \text{GeV}^{-2}$. (See Eq.(4.28) of Ref.[Ce00].) A more recent study, using an

improved calculational scheme in the analysis of the $K(495)$, leads to the values G_{88} = 13.10 GeV^2 and G_{00} = 11.10 GeV^{-2}. Results for meson decay constants and for the spectrum of the f_0 mesons presented later in this work are based upon the most recent values of G_{88} and G_{00} that are given above.

6.2 Quark-Antiquark T Matrix

One method for studying the generalized NJL model is to consider the properties of the $q\bar{q}$ T matrix [Ce99a, Ce00]. In the case of a single channel, we obtain the form

$$t(P^2) = -\frac{G_s}{1 - G_S\left[J_S(P^2) + \mathrm{Re}K_s(P^2)\right] - iG_S \mathrm{Im}K_s(P^2)} \ . \qquad (6.2.1)$$

[See Fig.6.3] It is useful to write Eq.(6.2.1) as

$$t(P^2) = -\frac{1}{G_S^{-1} - \left[J_S(P^2) + \mathrm{Re}K_S(P^2)\right] - i\mathrm{Im}K_S(P^2)} \ . \qquad (6.2.2)$$

To find the meson masses, we solve the equation

$$G_S^{-1} - \left[J_S(P^2) + \mathrm{Re}K_S(P^2)\right] = 0 \ . \qquad (6.2.3)$$

For an isolated resonance, we may consider an expansion about the value $P^2 = m_R^2$ obtained from the solution of Eq.(6.2.3):

$$J_S(P^2) + \mathrm{Re}K_S(P^2) = J_S(m_R^2) + \mathrm{Re}K_S(m_R^2) + (P^2 - m_R^2)\left[\frac{\partial J_S(P^2)}{\partial P^2} + \frac{\partial \mathrm{Re}K_S(P^2)}{\partial P^2}\right]_{P^2 = m_R^2} + \ldots , \qquad (6.2.4)$$

With the definition

$$\frac{1}{g^2} = \left[\frac{\partial J_S(P^2)}{\partial P^2} + \frac{\partial \mathrm{Re} K_S(P^2)}{\partial P^2} \right]_{P^2 = m_R^2} + \ldots \qquad (6.2.5)$$

we write Eq.(6.2.2) as

$$t(P^2) \simeq -\frac{g^2}{P^2 - m_R^2 + i m_R \Gamma_R} , \qquad (6.2.6)$$

where

$$m_R \Gamma_R = g^2 \mathrm{Im} K_S(m_R^2) . \qquad (6.2.7)$$

We can generalize this formalism to the multichannel case, as was done in [Ce99a, Ce00]. There, we obtained the T matrix for π-π and K-$\bar{K}$ scattering in the $I = 0$ channels. In the π-π case we took into account the $\pi\pi$, $K\bar{K}$, $\eta\eta$ and $\eta\eta'$ channels. However, the $\eta\eta$ and $\eta\eta'$ channels were weakly coupled, so we presented our results for only the coupled $\pi\pi$ and $K\bar{K}$ channels. We found the values for $|T_{\pi\pi}(E)|^2$ shown in Fig.6.4. There we see resonances at P^0 = 980, 1550, 1840 and 2060 MeV. The resonance at 980 MeV is an elastic resonance for which $|T_{\pi\pi}(E)|^2$ = 1 at the peak. The resonances seen in Fig.6.4 have their origin in the $q\bar{q}$ states bound in the confining field. [See Fig.2.6.] In Fig.2.6, we see singularities at the energies of the 1 $^3P_0$, 2 $^3P_0$ and 3 $^3P_0$ $n\bar{n}$ states that are bound in the confining field. (There are bound states at the energies P^0 = 1369, 1667, 2095, 2262, 2413, 2537 and 2651 MeV, which may be seen in Fig.3 of Ref.[Ce00].) The states seen in Fig.6.4 are obtained when we include the short-range NJL interaction and the effects of $\mathrm{Re} K_S(P^2)$ and $\mathrm{Im} K_S(P^2)$ in the calculation of $|T_{\pi\pi}(E)|^2$ [Ce00]. These states are in one-to-one

correspondence with the states bound in the confining field and are therefore the *intrinsic* states that we have defined at an earlier point of our discussion. In Fig.6.4 an enhanced cross section is seen in the region $2m_\pi < E \leq$ 1200 MeV. We will return to a discussion of that enhancement in Section 6.4, where we discuss the $f_0(400\text{-}1200)$ [or $\sigma(500\text{-}600)$]. Our result for $|T_{K\bar{K}}(E)|^2$ for the $I = 0$ channel was given in Ref.[Ce00]. Those results were recalculated and are shown in Fig.6.5. In this case we have reduced the coupling to the $K\bar{K}$ channel in the calculation of $\mathrm{Im}K_S^{K\bar{K}}(P^2)$ to yield more reasonable values for the widths, which were overestimated in [Ce00]. (The large value of the width of the $f_0(1370)$ found in [Ce00] was due to an asymmetric treatment of the pion and the kaon. We had neglected confinement for the pion and included it for the kaon. A more symmetric treatment reduces the width of the $f_0(1370)$ from 192 MeV to about 50 MeV, as seen in Fig.6.5.) The states at $P^0 = 1412$, 1855 and 2105 MeV seen in Fig.6.5 are *intrinsic* states that arise from the $1\ ^3P_0$, $2\ ^3P_0$ and $3\ ^3P_0$ $s\bar{s}$ states bound in the confining field. These are among the states seen in Fig.2.7. The other (small) peaks seen in Fig.6.5 arise from deviations from ideal mixing due to the presence of the 't Hooft interaction. They correspond to the intrinsic states already seen in Fig.6.4.

A comprehensive study of the spectrum of scalar states above $P^0 = 1$ GeV requires a treatment of quarkonium-glueball mixing. A covariant treatment of such mixing is given in [Ce99f]. (We do not discuss the results of that work, since they are not important for the purposes of the present study.)

6.3 Scalar Meson Decay Constants

Maltman has argued that we can gain some information concerning the correct assignment of the $a_0(980)$ to a scalar nonet by comparing the decay constants of the $a_0(980)$ and the $K_0^*(1430)$ [Ma99, Ma00]. He remarks that it is natural to put the K meson and the pion into the same octet of Goldstone bosons, since they have decay constants which only differ by about 20%. He also notes that if the $a_0(980)$ were a $K\bar{K}$ molecule, one would expect a quite small decay constant for the $a_0(980)$ relative to the decay constant of the $K_0^*(1430)$, which is believed to be a simple $q\bar{q}$ state. Maltman studies the scalar correlator defined in Section 5.7 and the results of his and our analysis are given in Table 5.1.

We proceed by constructing the wave functions of the a_0 and K_0^* mesons. Equations may be written for the bound-state amplitudes

$$\phi_i^+(k) = \frac{\hat{\Gamma}_i^{+-}(k)}{P_i^0 - E_a(\vec{k}) - E_b(\vec{k})} \tag{6.3.1}$$

and

$$\phi_i^-(k) = -\frac{\hat{\Gamma}_i^{+-}(k)}{P^0 + E_a(\vec{k}) + E_b(\vec{k})} , \tag{6.3.2}$$

where $E_a(k) = \left[\vec{k}^2 + m_a^2\right]^{1/2}$. Here $\hat{\Gamma}_i^{+-}(k)$ is a vertex function for a bound state (i) that includes the effect of both the NJL interaction and confinement. The amplitudes $\phi_i^+(k)$ and $\phi_i^-(k)$ satisfy coupled equations which are relativistic generalizations of the nonrelativistic random-phase approximation (RPA) calculations made many years ago

in the study of particle-hole excitations in nuclei. We may also define Tamn-Dancoff-approximation (TDA) calculations by neglecting $\phi_i^-(k)$ as well as the second term in the brackets appearing in Eqs.(2.3.2) and (2.3.4). The details of such calculations are given in Section 2.3. We presented the results of our calculations in Table 5.1, where the theoretical values are compared to those obtained by Maltman, who used QCD sum rules and other methods to obtain the decay constants of the $a_0(980)$, $a_0(1450)$ and $K_0^*(1430)$. Our result for the $a_0(980)$ is about twice Maltman's value which suggests a significant $K\bar{K}$ component in the $a_0(980)$ wave function. Our results for the decay constants of the $a_0(1450)$ and $K_0^*(1430)$ are quite satisfactory when compared to Maltman's values.

As may be seen in Table 5.1, the $a_0(1450)$ and $K_0^*(1430)$ have similar decay constants which might suggest that they belong in the same nonet. However, in our model, which reproduces the experimental energies of the $a_0(980)$, $f_0(980)$, $a_0(1450)$ and $K_0^*(1430)$ quite well, the $a_0(1450)$ is a $2\ ^3P_0$ state and the $K_0^*(1430)$ is a $1\ ^3P_0$ state. Therefore, the assignment of states to nonets in our model must be that seen in Fig.6.2. We can conclude from these observations that similar values for meson decay constants is not a sufficient condition for placing meson states in the same nonet. The fact that we do rather well in reproducing Maltman's values of the decay constants serves to provide further evidence that our assignment of scalar states to nonet, based upon the results of our generalized NJL model, is correct.

6.4 Dynamically-Generated States

In this Section we wish to describe the origin of the cross section enhancements

seen in $\pi\pi$ and πK scattering that lead to the introduction of the σ(500-600) and κ(900). The results of t-channel and u-channel ρ exchange were used in [Zo94] to define a K-matrix for $\pi\pi$ scattering with the result that

$$\frac{\tan\delta_{00}(k)}{\rho} = -\frac{g^2}{16\pi}\left[2+\left[\frac{8k^2+4m_\pi^2+m_\rho^2}{2k^2}\right]\ln\left[\frac{m_\rho^2}{4k^2+m_\rho^2}\right]\right], \tag{6.4.1}$$

with $k=|\vec{k}|$. Here, $g=g_{\rho\pi\pi}\simeq 6.0$,

$$\rho = \left[1-\frac{4m_\pi^2}{P^2}\right]^{1/2}, \tag{6.4.2}$$

and

$$\vec{k}^2 = \frac{P^2}{4}-m_\pi^2 . \tag{6.4.3}$$

The phase shift generated in this manner is shown as a dotted line in Fig.6.6. We wish to combine the s-channel phase shift calculated using our generalized NJL model and the phase shift due to ρ exchange. The simplest possible scheme is just to add the phase shifts. The result of that addition is seen as the solid line in Fig.6.6. In Fig.6.7 we see that this procedure yields a total phase that fits the data quite well, although we are somewhat above the data points in the region below 600 MeV. (The small circles, which represent the values of our calculated total phase shift, are not drawn in the regions where they coincide with the data points.) Although our treatment of the unitarity constraint is oversimplified, our result does suggest that the f_0(400-1200) [or

the $\sigma(500\text{-}600)$] is a dynamically-generated state in the sense defined above.

We have also performed a similar calculation of the low-energy π-K phase shift. That phase shift is known to be elastic below 1300 MeV. The threshold for the $\eta' K$ channel is at 1453 MeV and the ηK channel is only weakly coupled to the πK channel [As88, Tö95]. Again, there are phase shifts of similar size arising from ρ and K^* exchange, and s-channel enhancements of the cross section in our $q\bar{q}$ T matrix. If we again add the phase shifts and neglect inelasticity, we obtain the dotted curve seen in Fig.6.8. We note that the experimental data [As88] for the phase shift pass through 90 degrees at about 1300 MeV which reflects the importance of the background amplitude in moving the 90 degree point to about 100 MeV below the energy of the resonance. (The model described in [Ce99a] places the $K_0^*(1430)$ at 1416 MeV.)

6.5 Discussion

Recently, Cherry and Pennington have performed a model-independent analytic continuation of the πK scattering results below 2 GeV in order to determine the number and position of the resonance poles. They find poles representing the $K_0^*(1430)$ but no pole corresponding to the $\kappa(900)$ [Ch00]. That result might appear to eliminate the model in which one places the $a_0(980)$, $f_0(980)$, $\sigma(500\text{-}600)$ and $\kappa(900)$ in an SU3 nonet of states. However, the existence of the $\kappa(900)$ is still a controversial matter. It has been suggested that the procedures used by Cherry and Pennington might not be sufficient to decide this issue. Indeed, a recent analysis of πK scattering in a chiral model with resonances finds a κ meson pole at $708 - i305$ MeV. The analysis of scalar meson decay constants made by Maltman suggests that the

$a_0(980)$ belongs in the same octet as the $K_0^*(1430)$. For the $a_0(980)$, we find that our calculated value of the decay constant is about twice the value obtained using QCD sum rules. This disagreement probably has its origin in a significant $K\bar{K}$ component of the $a_0(980)$ wave function. However, the overall agreement of the decay constants obtained by different methods suggests that the classification of scalar states shown in Fig.6.2 is correct.

We have also described the origin of the enhancements of the cross section in low-energy $\pi\pi$ and $\pi\bar{K}$ scattering that have led to the introduction of the $\sigma(500\text{-}600)$ and the $\kappa(900)$, respectively. We have considered t-channel and u-channel ρ exchange in the case of $\pi\pi$ scattering and K^* and ρ exchange in the case of πK scattering. Although our method of implementing unitarity by adding the phase shift obtained in the study of t and u-channel exchange to the s-channel phase shift calculated in our generalized NJL model might be improved upon, the results provide a satisfactory fit to the experimental data. Our model has some relation to that used in [Ja00]. In that work a chiral model with only meson degrees of freedom is used. Various resonances in the πK system are inserted in a phenomenological manner and t and u-channel exchange of vector meson nonets is considered. On the other hand, in our model, these resonances are generated dynamically when we construct the $q\bar{q}$ T matrix. That construction is supplemented by vector meson exchange in a manner similar to that used in [Ja00]. Our model has the advantage that the various resonance poles needed to fit the data in [Ja00] can be separated into three intrinsic states and a single dynamically-generated state which we identify as the $\kappa(900)$. It would be desirable to

improve our model of $\pi\pi$ and πK scattering with more attention paid to unitarity and chiral symmetry constraints.

In addition to the work of Maltman [Ma99, Ma00], there have been a number of other attempts to gain information concerning the properties of scalar mesons using QCD sum rules [El98, Sh00b]. The study of the non-strange ($n\bar{n}$) scalar sector reported in [Sh00b] suggests that both the f_0(400-1200) and the a_0(980) are not $n\bar{n}$ states. However, Maltman concludes that the a_0(980) is a $n\bar{n}$ state. He explains that the work of [Sh00b] has used a more restrictive single-resonance-plus continuum model for the input spectral function and shows that that form leads to a very poor match between the operator product expansion and the hadronic sides of the sum rule, in contrast to his results [Ma00]. (We agree with Maltman's result that the a_0(980) is a $n\bar{n}$ state, or at least, that it has a large $n\bar{n}$ component.)

There are various opinions put forth in the literature concerning the f_0(400-1200), or σ(500-600). For example, Meissner suggests that the f_0(400-1200) is not a "preexisting" resonance, but is a dynamic effect due to the strong pion-pion interaction in the L=0, I=0 wave [Me00]. He also states that the f_0(400-1200) is certainly not the chiral partner of the pion. Contrasting points of view have been put forth by Pennington [Pe99] and Hatsuda and Kunihiro [Ha94, Ku90, Ha90, Ku99].

In general, one may decide whether a meson "exists" by looking for poles in the relevant scattering matrix, as was done in [Ch00]. The conclusion reached in [Ch00] was that the κ(900) does not exist, however, that result is not conclusive. On the other hand, there does appear to be a pole associated with the σ(500-600) [Ha99,

Ol99a, Ol99b]. In our work we have stressed that, if one has an underlying dynamical model, some of these poles may be related to $q\bar{q}$ states (or more complex states) of a chiral quark model, such as our generalized NJL model. The poles that have that correspondence are associated with *intrinsic* states and other poles with *dynamically-generated* states. From this point of view, the existence of the $\kappa(900)$ is somewhat irrelevant, since it would be a dynamically-generated state in our model and, therefore, not a member of a SU3 quark-model nonet.

In Fig.2.13, we showed the relation between the states bound in the confining field and the intrinsic states of our model in the case of the f_0 mesons [Ce00]. Columns (a) and (c) show the $n\bar{n}$ and $s\bar{s}$ states bound in the confining field. The introduction of the short-range NJL interaction then generates the *intrinsic* states of column (b). (The energies of the intrinsic states are also modified somewhat by various dispersive effects described by $K_S(P^2)$ [Ce00].) The resulting intrinsic spectrum of column (b) may be compared to the experimental spectrum of f_0 states shown in column (d).

When calculating the energies shown in columns (a), (b) and (c), parameters that were previously fixed were used, so that these results may be considered predictions of the previously constructed model Lagrangian. If we assume that the spectrum of f_0 mesons may be obtained using parameters determined in the study of the pseudoscalar and vector nonets, we find that the $f_0(980)$ is the isoscalar $q\bar{q}$ state of lowest energy. It is clear from this analysis that, in our model, the $\sigma(500\text{-}600)$ must be identified as a *dynamically-generated* state, in accordance with our previous discussion.

The distinction that we have made between intrinsic and dynamically-generated states is model dependent, but has the advantage that there is an underlying quark model that in itself is related to meson spectroscopy based upon the identification of quark configurations. The identification of intrinsic and dynamically-generated states is a different matter in a theory of meson-meson scattering based upon the use of chiral Lagrangians, supplemented by a unitarization scheme. For example, in [Ol99a] it is stated that "the $a_0(980)$, σ and $\kappa(900)$ resonances are meson-meson states originating from the unitarization of the $O(P^2)$ χPT amplitude. On the other hand, the $f_0(980)$ is a combination of a strong S-wave meson-meson unitarity effect and a preexisting singlet resonance with a mass around 1 GeV." We believe further work is required to understand the relation between "dynamically-generated" states as defined in [Ol99a] and the definition we have put forth in this work.

Appendix A

In this appendix we record some of the formulas of [Ce99c], rewritten so as to make the distinction between the TDA and RPA particularly clear. In [Ce99c] we considered pseudoscalar - axial-vector mixing in a study of the kaon and its radial excitations. Here, we will consider the case of equal mass quarks for simplicity. The extension to the unequal mass case, needed for the study of the K mesons, may easily be made upon using [Ce99c].

We had defined

$$-iJ^{PP}(P) = (-1)2n_c \mathrm{Tr} \int \frac{d^4k}{(2\pi)^4} \left[i\gamma_5 iS(P/2+k) i\bar{\Gamma}_5(P,k) iS(-P/2+k) \right] , \quad \text{(A1)}$$

$$-iJ_\mu^{PA}(P) = (-1)2n_c \mathrm{Tr} \int \frac{d^4k}{(2\pi)^4} \left[iS(P/2+k) i\bar{\Gamma}_5(P,k) iS(-P/2+k)\gamma_\mu\gamma_5 \right], \quad \text{(A2)}$$

and

$$-iJ_{\mu\nu}^{AA}(P) = (-1)2n_c \mathrm{Tr} \int \frac{d^4k}{(2\pi)^4} \left[iS(P/2+k) \bar{\Gamma}_\mu(P,k) iS(-P/2+k)\gamma_\nu\gamma_5 \right] . \quad \text{(A3)}$$

We also defined

$$J_\mu^{PA}(P) = iJ^{PA}(P^2) \frac{P_\mu}{\sqrt{P^2}} \quad , \quad \text{(A4)}$$

$$J_\mu^{AP}(P) = iJ^{AP}(P^2) \frac{P_\mu}{\sqrt{P^2}} \quad , \quad \text{(A5)}$$

and

$$J^{AA}_{\mu\nu}(P) = -\tilde{g}_{\mu\nu}(P) J^{AA}_{T}(P^2) - \frac{P_\mu P_\nu}{P^2} J^{AA}_{L}(P^2) \quad , \tag{A6}$$

with $\tilde{g}_{\mu\nu} = g_{\mu\nu} - P_\mu P_\nu / P^2$. Note that $J^{AP}(P^2) = -J^{PA}(P^2)$. We found that

$$J^{PP}(P^2) = -4n_c \int \frac{d^3k}{(2\pi)^3} \Gamma_5^{+-}(P^0, |\vec{k}|) \left[\frac{1}{P^0 - 2E(\vec{k})} - \frac{1}{P^0 + 2E(\vec{k})} \right] \quad , \tag{A7}$$

where Γ_5^{+-} was found to satisfy the equation

$$\Gamma_5^{+-}(P^0, |\vec{k}|) = 1 - \int \frac{d^3k'}{(2\pi)^3} \left[\frac{m^2 - 2E(\vec{k})E(\vec{k}')}{E(\vec{k})E(\vec{k}')} \right] \frac{\Gamma_5^{+-}(P^0, |\vec{k}'|) V^C(\vec{k} - \vec{k}')}{P^0 - 2E(\vec{k}')} . \tag{A8}$$

To write Eq.(A7) we have used the fact the $\Gamma_5^{-+}(-P^0, |\vec{k}|) = \Gamma_5^{+-}(P^0, |\vec{k}|)$.

Similarly, we may write

$$J^{AA}_{L}(P^2) = 4n_c \int \frac{d^3k}{(2\pi)^3} \frac{m}{E(\vec{k})} \Gamma_L^{+-}(P^0, |\vec{k}|) \left[\frac{1}{P^0 - 2E(\vec{k})} - \frac{1}{P^0 + 2E(\vec{k})} \right] , \tag{A9}$$

where $\Gamma_L^{+-}(P^0, |\vec{k}|)$ was defined in [Ce99c]. Further,

$$J^{PA}(P^2) = -4n_c \int \frac{d^3k}{(2\pi)^3} \left[\frac{m}{E(\vec{k})} \right] \Gamma_5^{+-}(P^0, |\vec{k}|) \left[\frac{1}{P^0 - 2E(\vec{k})} + \frac{1}{P^0 + 2E(\vec{k})} \right] \tag{A10}$$

$$= -8P^0 \int \frac{d^3k}{(2\pi)^3} \left[\frac{m}{E(\vec{k})} \right] \Gamma_5^{+-}(P^0, |\vec{k}|) \frac{1}{(P^0)^2 - (2E(\vec{k}))^2} . \tag{A11}$$

We have written Eq.(A11) so that we can see that $J^{PA}(0) = 0$.

Appendix B

If we neglect confinement in the case of the pion we can solve the one-body aspect (Hartree) in conjunction with the two-body aspect (Bethe-Salpeter equation). We may relate the quark mass m, α, m_0 and G_s

$$m = m_0 + 2n_C G_s \int \frac{d^4k}{(2\pi)^4} \mathrm{Tr} \frac{i}{\not{k} - m + i\eta} e^{-k^2/\alpha^2} , \tag{B1}$$

and find

$$G_s = \frac{\pi^2 (m - m_0)}{2n_C m} \left[\int \frac{k^2 dk e^{-k^2/\alpha^2}}{\sqrt{k^2 + m^2}} \right]^{-1} . \tag{B2}$$

(Here we are neglecting the 't Hooft interaction.) This analysis leads to the choice m_0 = 0.005 MeV, α = 0.538 GeV, m = 0.364 GeV and G_S = 15.49 GeV^{-2}. If we also put G_V = 15.49 GeV^{-2}, these values yield a pion mass of 138 MeV, with f_π = 171 MeV, g_A = 0.723 and F_π = 124 MeV.

Appendix C

In this appendix we define the various interaction elements need to construct the eight equations given as Eqs.(4.3.17)-(4.3.24). We begin by working in the $n\bar{n}$-$s\bar{s}$ representation and first consider the $n\bar{n}$ space. Then we have

$$H_{n\bar{n}}^{PP}(k,k') = -\frac{2n_C}{\pi^2}kk'e^{-k^2/2\alpha^2}e^{-k'^2/2\alpha^2}, \tag{C1}$$

$$H_{n\bar{n}}^{PA}(k,k') = -\frac{2n_C}{\pi^2}kk'e^{-k^2/2\alpha^2}e^{-k'^2/2\alpha^2}, \tag{C2}$$

$$H_{n\bar{n}}^{AP}(k,k') = H_{n\bar{n}}^{PA}(k,k'), \tag{C3}$$

$$H_{n\bar{n}}^{AA}(k,k') = \frac{n_C}{\pi^2}\frac{2m_u}{E_u(k)}kk'e^{-k^2/2\alpha^2}e^{-k'^2/2\alpha^2}, \tag{C4}$$

$$H_{n\bar{n}}^{PP(C)}(k,k') = -\frac{1}{\pi^2}kk'\frac{\left[m_u^2 - E_u(k)E_u(k')\right]V_0(k,k')}{E_u(k)E_u(k')}, \tag{C5}$$

and

$$H_{n\bar{n}}^{AA(C)}(k,k') = H_{n\bar{n}}^{PP(C)}(k,k').$$

Here, with $x = \cos\theta$,

$$V_0(k,k') = \frac{1}{2}\int_{-1}^{1} dx\, V^C(\vec{k}-\vec{k}'). \tag{C7}$$

The various elements, such as $H_{s\bar{s}}^{PP}(k,k')$, are obtained by replacing m_u and $E_u(k)$ with m_s and $E_s(k)$ in the equations presented above.

We may then define

$$H_{00}^{PP}(k,k') = \frac{1}{3}\left[2H_{n\bar{n}}^{PP}(k,k') + H_{s\bar{s}}^{PP}(k,k')\right], \tag{C8}$$

$$H_{08}^{PP}(k,k') = \frac{\sqrt{2}}{3}\left[H_{n\bar{n}}^{PP}(k,k') - H_{s\bar{s}}^{PP}(k,k')\right], \tag{C9}$$

and

$$H_{88}^{PP}(k,k') = \frac{1}{3}\left[H_{n\bar{n}}^{PP}(k,k') + 2H_{s\bar{s}}^{PP}(k,k')\right], \tag{C10}$$

with $H_{80}^{PP}(k,k') = H_{08}^{PP}(k,k')$. Values for the other interaction terms in Eqs.(4.3.17)-(4.3.24) may be found by using relations of the form given in Eqs.(C8)-(C10).

Table 2.1

Theoretical mass values found for the a_0 mesons. Here $G_{88}^{RPA} = 13.10\,GeV^{-2}$, $G_{88}^{TDA} = 12.77\ GeV^{-2}$ and $\alpha = 0.605$ GeV. (Note that RPA dynamics reduces the $a_0(980)$ mass by 75 MeV relative to the TDA result.)

Meson	Configuration	Mass [expt] (MeV)	Mass (MeV)		
			$J^S_{TDA}(P^2)$	$J^S_{RPA}(P^2)$	$J^S_{RPA}(P^2)+\mathrm{Re}K^S(P^2)$
$a_0(980)$	$1\ ^3P_0$	983.5 ± 0.9	1075	991[b]	949
$a_0(1450)$	$2\ ^3P_0$	1450 ± 50	1556	1542	1542
$a_0(1830)$	$3\ ^3P_0$[a]	...	1857	1832	1832

a) This state has not been observed as yet.

b) See Fig.2.8.

Table 3.1

Properties of isovector pseudoscalar mesons calculated with $G_{88} = 13.49\ \text{GeV}^{-2}$, $G_V = 12.46\ \text{GeV}^{-2}$, $\kappa = 0.055\ \text{GeV}^2$, $\alpha = 0.605\ \text{GeV}$, $m_u = m_d = 0.364\ \text{GeV}$, and $\mu = 0.01\ \text{GeV}$. A value of $G_{88} = G_V = 11.76\ \text{GeV}^{-2}$ is used for the $\pi(138)$ when we neglect confinement.

mass (MeV)	character	f_π(MeV)	F_π(MeV)
138	Pionlike	178	136
		180 (without confinement)	134 (without confinement)
1325	Mixed	33.1	
1391	Pionlike	20.5	
1652	Mixed	30.3	
1717	Pionlike	19.7	
1890	Mixed	25.1	
1960	Pionlike	19.8	
2080	Mixed	16.1	

Table 4.1

Properties of the eta mesons. Here $G_V = 12.46\ \text{GeV}^{-2}$, $G_{00} = 9.10\ \text{GeV}^{-2}$, $G_{88} = 12.46\ \text{GeV}^{-2}$ and $\alpha = 0.605$ GeV. Using Eqs.(4.5.6)-(4.5.9), we find $g_{n\bar{n}}^{\eta} = 0.776$, $g_{s\bar{s}}^{\eta} = 0.659$, $g_{n\bar{n}}^{\eta'} = 0.742$ and $g_{s\bar{s}}^{\eta'} = 0.684$. We then use Eqs.(4.5.10) and (4.5.11) to obtain $F_{\eta}^{(8)} = 118$ MeV and $F_{\eta}^{(0)} = 50.8$ MeV. Similarly, we find $F_{\eta'}^{(8)} = 69.5$ MeV and $F_{\eta'}^{(0)} = 109$ MeV. (The absolute values of the decay constants are given.)

Meson	Mass (MeV) Expt.	Width (MeV) Expt.	Theoretical Results				
			Mass (Mev)	$f_\eta^{(0)}$ (MeV)	$f_\eta^{(8)}$ (MeV)	Percentage	
						$n\bar{n}$	$s\bar{s}$
$\eta(547)$	547.30 ± 0.12	$(1.18 \pm 0.11) \times 10^{-3}$	543	56.7	164	75.5	24.5
$\eta'(958)$	957.78 ± 0.14	0.203 ± 0.016	893	155	104	21.4	78.6
$\eta(1295)$	1297.0 ± 2.8	53 ± 6	1318	16.5	14.1	~ 10	~ 0
$\eta(1440)$	1430 ± 30	65 ± 15	1409	47.4	28.8	0	~ 0
			1652	21.0	13.4	~ 10	3.9
			1659	5.18	0.0006	0	94.7
			1717	14.0	59.4	96.1	
			1729	55.4	2.2	5.3	
			1896	29.4	19.3		
			1948	2.94	1.65		
			1966	33.5	31.0		
			1999	39.3	53.1		
			2093	42.1	28.2		

Table 4.1 (continued):

Meson	Mass (MeV) Expt.	Width (MeV) Expt.	Theoretical Results				
			Mass (Mev)	$f_\eta^{(0)}$ (MeV)	$f_\eta^{(8)}$ (MeV)	Percentage	
						$n\bar{n}$	$s\bar{s}$
			2162	30.5	30.0		
			2167	2.42	12.5		
			2213	33.5	55.6		
			2255	57.9	40.3		
			2328	33.4	29.7		
			2348	12.2	15.7		
			2392	42.5	72.9		
			2392	42.5	72.9		
			2470	32.5	28.7		
			2501	35.6	21.5		
			2511	74.0	56.1		
			2544	40.8	48.4		
			2592	31.3	27.3		
			2616	78.5	43.0		
			2633	26.4	59.7		

Table 5.1 Meson decay constants

Meson	Configuration	$m_i^2 f_i$ (GeV^3)		
		TDA	RPA	Maltman [Ma99, Ma00]
$a_0(980)$	$1\,^3P_0$	0.0649	0.0868	0.0447 ± 0.0085
$a_0(1450)$	$2\,^3P_0$	0.0357	0.0420	0.0647 ± 0.0123
$a_0(1834)$[a)]	$3\,^3P_0$	0.0377	0.0424	...
$K_0^*(1430)$	$1\,^3P_0$	0.0614	0.0508	0.0842 ± 0.0045
$K_0^*(1730)$[a)]	$2\,^3P_0$	0.0425	0.0375	...
$K_0^*(1950)$	$3\,^3P_0$	0.0414	0.0378	...

a) These states are predicted to exist in our formalism.

Figure Captions

Fig.2.1 a) Schematic representation of the equation for the confinement vertex. Here V^C denotes the confining field [Ce99a, Ce00].

b) The homogeneous version of the equation shown in a) is represented.

c) A representation of the homogeneous equation for the vertex that includes the effects of both confinement and the short-range NJL interaction is shown.

Fig.2.2 a) The diagram serves to define the function $-iJ^S(P^2)$. The triangular filled regions are the vertex functions shown in Fig. 1a). [See Eq.(2.2.3).]

b) The diagram represents the function $-iK^S(P^2)$ that describes polarization effects due to coupling to two-meson decay channels. The channels $\pi\pi$, $K\bar{K}$, $\eta\eta$ and $\eta\eta'$ were considered in [Ce00] and values for $K^S_{\pi\pi}(P^2)$ and $K^S_{K\bar{K}}(P^2)$ were presented there.

Fig.2.3 In this figure we show some Goldstone diagrams for the vacuum polarization function and T matrices. Here time increases as one moves to the right. a) The figure indicates the form of $J(P^2)$ in the TDA. b) An addtitional contribution to $J(P^2)$ in the RPA is shown. This diagram introduces $\Gamma^{-+}(-P^0, |\vec{k}|)$ in the expression for $J(P^2)$. c) The $q\bar{q}$ T matrix in the TDA is shown as a perturbation series in G (open circle). d) The $q\bar{q}$ T matrix in the RPA is shown as a perturbation series in G (open circle).

Fig.2.4 The figure shows $J^S_{n\bar{n}}(P^2)$ calculated in the TDA [dotted line] and in the RPA [solid line]. Here $m_u = m_d = 364$ MeV and $\alpha = 0.605$ GeV.

Fig.2.5 Same caption as Fig.4, but for an expanded scale.

Fig.2.6 The figure shows $J^S_{s\bar{s}}(P^2)$ calculated in the TDA [dotted line] and in the RPA [solid line]. Here $m_s = 0.565$ MeV and $\alpha = 0.605$ GeV.

Fig.2.7 Same caption as Fig.2.6, but for an expanded scale.

Fig.2.8 The figure shows $J^S_{n\bar{n}}(P^2)$, as calculated in the RPA. The horizontal line is drawn at $G_{88}^{-1} = 0.0763$ GeV^2, corresponding to $G_{88} = 13.1$ GeV^{-2}. [See Table 2.1 for the energies of the a_0 states found in this manner.] This figure may be compared to Fig.14.3 of [Ro70] or Fig.59.2 of [Fe71].

Fig.2.9 The figure shows the values of $\mathrm{Re}K^S(P^2)$ used in our study of the $a_0(980)$. The values of $K^S(P^2)$ for the individual channels, $\pi\eta$, $K\bar{K}$, and $\pi\eta'$, may be seen in [Ce99b].

Fig.2.10 The figure shows the absolute value of the T matrix, $|T_{\pi\pi}(E)|^2$, for $\pi\pi$ scattering. (For an elastic resonance $|T_{\pi\pi}(E)|^2 = \sin^2\delta(E)$.) The dotted curve is calculated using the formalism described in [Ce00] with $G_{88} = 13.10$ GeV^{-2} and $G_{00} = 11.10$ GeV^{-2} and with $\mathrm{Re}K^{\pi\pi}(P^2)$ and $\mathrm{Re}K^{K\bar{K}}(P^2)$ set equal to zero. The peak of the dotted curve is at $E = 1.060$ GeV. The solid curve is obtained when $\mathrm{Re}K^{\pi\pi}(P^2)$ and $\mathrm{Re}K^{K\bar{K}}(P^2)$ are included in the calculation. The peak of the solid curve is at $E = 980$ MeV.

Fig.2.11 The figure shows the absolute square of the T matrix for $K\bar{K}$ scattering [Ce00]. Here G_{88} = 13.10 GeV^{-2} and G_{00} = 11.1 GeV^{-2}. The 1 $^3P_0$ $s\bar{s}$ state is found at E = 1.445 GeV and is identified with the $f_0(1370)$, in a first approximation that neglects quarkonium-glueball mixing.

Fig.2.12 The values of $|T_{K\bar{K}}(E)|^2$ are shown such that the 1 $^3P_0$ $s\bar{s}$ state of Fig.2.11 is seen in more detail. (The width associated with the solid curve is 40 MeV.) The dotted curve, which has a peak at E = 1.469 GeV, shows the result of putting $\mathrm{Re}K^{\pi\pi}(P^2)$ and $\mathrm{Re}K^{K\bar{K}}(P^2)$ equal to zero. Therefore, inclusion of $\mathrm{Re}K(P^2)$ shifts the peak position downward by only 24 MeV.

Fig.2.13 Columns a) and c) show the energies of the $n\bar{n}$ and $s\bar{s}$ states bound in the confining field [Ce00]. Inclusion of the short-range NJL interaction and $K^S(P^2)$ yields the spectrum shown in column b). Since we have approximate ideal mixing [Ce00], we show the states that are mainly of $s\bar{s}$ character as dotted lines. Column d) shows some of the experimentally observed states. The anglular momentum of the $f_J(1710)$ is still uncertain; however, the $f_0(1770)$ definitely is present [Bu00]. We expect a good deal of quarkonium-glueball mixing in the region above 1 GeV, so that the experimentally observed states need not be put into one-to-one correspondence with the states of column b).

Fig.3.1 a) The functions $\hat{J}(P)$, defined in the absence of a confinement model, are shown. [See Eqs.(3.3.1)-(3.3.7).]

b) The functions $J(P)$, which include the confinement vertex functions Γ_5^{+-} and Γ_L^{+-} in their definitions. [See Eqs.(3.3.8)-(3.3.14).]

c) The functions $\tilde{J}(P)$, defined in terms of the vertex functions Γ_P^{+-} and Γ_A^{+-}. [See Eqs.(3.4.1)-(3.4.10).]

Fig.3.2 A schematic representation of the equation for $\bar{\Gamma}_P(P,k)$ is shown. [See Eqs.(3.4.16) and (3.4.17).]

Fig.3.3 A schematic representation of the equation for $\bar{\Gamma}_A(P,k)$ is shown. [See Eqs.(3.4.18) and (3.4.19).]

Fig.3.4 The first column shows the $q\bar{q}$ states bound in the confining field. The second column presents the mass values obtained when the NJL interaction is included.

Fig.3.5 The wave functions of the $\pi(138)$ are shown. The solid line represents $\phi_P^+(k)$, the dotted line represents $\phi_P^-(k)$, the dashed line represents $\phi_A^+(k)$, and the line with closely-spaced dots represents $\phi_A^-(k)$.

Fig.3.6 The wave functions of the "mixed" state $\pi(1325)$ are shown. (See caption to figure 3.5.)

Fig.3.7 The wave functions of the "pionlike" state $\pi(1391)$ are shown. (See caption to figure 3.5.)

Fig.3.8 The wave functions of the "mixed" state $\pi(1652)$ are shown. (See caption to figure 3.5.)

Fig.3.9 The wave functions of the "pionlike" state $\pi(1717)$ are shown. (See caption to figure 3.5.)

Fig.3.10 The wave functions of the "mixed" state $\pi(1890)$ are shown. (See caption to figure 3.5.)

Fig.3.11 The solid and dotted lines show the pion wave functions $\phi_P^+(k)$ and $\phi_P^-(k)$, respectively. The dashed line shows $\phi_P^+(k)$ and the line with closely-spaced dots shows $\phi_P^-(k)$ in the absence of the confinement model ($\kappa = 0$).

Fig.4.1 The function $J_{n\bar{n}}^{PP}(P^2)$ is shown. Here $\kappa = 0.055$ GeV^2 and $m_u = 0.364$ GeV.

Fig.4.2 The function $J_{s\bar{s}}^{PP}(P^2)$ is shown. Here $\kappa = 0.055$ GeV^2 and $m_s = 0.565$ GeV.

Fig.4.3 The first and third column of levels show the $n\bar{n}$ and $s\bar{s}$ states bound in the confining field, respectively. The second column shows the 28 levels found when the RPA Hamiltonian is brought to diagonal form. The various arrows show the parentage of the resulting states. The $\eta(547)$ has 75% of the $1\ ^1S_0\, n\bar{n}$ state that has the γ_5 vertex and 25% of the $1\ ^1S_0\ s\bar{s}$ state that has the γ_5 vertex. These percentages are reversed for the $\eta'(958)$. [See Table 4.1.] The $1\ ^1S_0 n\bar{n}$ and $s\bar{s}$ states with the $\gamma_0\gamma_5$ vertex are fragmented over many states. The $\eta(1295)$ and $\eta(1440)$ are almost entirely of $2\ ^1S_0\ n\bar{n}$ character. [See the text and Table 4.1.]

Fig.4.4 The wave function for the $\eta(547)$ found at 543 MeV is shown. The various components are $\phi_{P,n\bar{n}}^+(k)$ [solid, N1], $\phi_{P,n\bar{n}}^-(k)$ [dash, N2], $\phi_{A,n\bar{n}}^+(k)$ [dot, N3], $\phi_{A,n\bar{n}}^-(k)$ [dash-dot, N4], $\phi_{P,s\bar{s}}^+(k)$ [dash-dot-dot, S1], $\phi_{P,s\bar{s}}^-(k)$ [short dash, S2], $\phi_{A,s\bar{s}}^+(k)$ [short dot, S3], $\phi_{A,s\bar{s}}^-(k)$ [short dash-dot, S4].

Fig.4.5 The wave function of the $\eta'(958)$ found at 893 MeV is shown. (Same caption as Fig.4.4.)

Fig.4.6 The wave function of the $\eta(1295)$ found at 1318 MeV is shown. (Same caption as Fig.4.4.)

Fig.4.7 The wave function of the $\eta(1440)$ found at 1409 MeV is shown. (Same caption as Fig.4.4.)

Fig.4.8 The wave function of the state found at 1652 MeV in our calculation is shown. (Same caption as Fig.4.4.)

Fig.4.9 The wave function of the state found at 1659 MeV in our calculation is shown. (Same caption as Fig.4.4.)

Fig.5.1 The $\phi^+(k)$ [solid line] and $\phi^-(k)$ [dotted line] components are shown for the $\pi(138)$. Here we have neglected confinement and used $G_{88} = 11.81$ GeV^{-2} and $m_u = m_d = 0.364$ GeV. (The normalization is arbitrary and only the relative sign of the components is meaningful.)

Fig.5.2 The $\phi^+(k)$ [solid line] and $\phi^-(k)$ [dotted line] components are shown for the $K(495)$. Here we have used $G_{88} = 13.35$ GeV^{-2}, $\kappa = 0.055$ GeV^2, $m_u = 0.364$ GeV and $m_s = 0.565$ GeV. (If pseudoscalar-axial-vector mixing were taken into account, we would use $G_{88} = 13.1$ GeV^{-2} and $G_V = 12.46$ GeV^{-2} to obtain 495 MeV for the mass of the kaon. (See the caption to Fig.5.1.)

Fig.5.3 The $\phi^+(k)$ [solid line] and $\phi^-(k)$ [dotted line] components are shown for the $a_0(980)$. Here we use $G_{88} = 13.1$ GeV^{-2} as determined in our study of the kaon in which pseudoscalar-axial-vector mixing was taken into account in an RPA

calculation.

Fig.5.4 The $\phi^+(k)$ [solid line] and $\phi^-(k)$ [dotted line] components are shown for the $a_0(1450)$, which is a $2\ ^3P_0$ state in our model. Here we have used $G_{88} = 13.1$ GeV^{-2}, $\kappa = 0.055$ GeV^2 and $m_u = m_d = 0.364$ GeV. (See caption of Fig.5.3.)

Fig.5.5 The $\phi^+(k)$ [solid line] and $\phi^-(k)$ [dotted line] components for the $K_0^*(1430)$ resonance are shown. (Here we have put $G_{88} = 10.0$ GeV^{-2} to place the $K_0^*(1430)$ at 1350 MeV, since the value of $G_{88} = 13.1$ GeV^{-2} leads to some degree of overbinding.)

Fig.5.6 The normalized functions $\tilde{\phi}_N^+(k)$ [solid line] and $\tilde{\phi}_N^-(k)$ [dotted line] are shown for the $a_0(980)$ resonance. These functions were defined in Eqs.(5.5.18) and (5.5.19).

Fig.5.7 The normalized functions $\tilde{\phi}_N^+(k)$ [solid line] and $\tilde{\phi}_N^-(k)$ [dotted line] are shown for the $K_0^*(1430)$ resonance. These functions were defined in Eqs.(5.5.18) and (5.5.19).

Fig.6.1 The nonets of $1\ ^3S_1$ and $2\ ^3S_1$ vector meson states obtained in [Ce99a] are shown.

Fig.6.2 The nonets of $1\ ^3P_0$ and $2\ ^3P_0$ scalar meson states obtained in [Ce99a] and [Ce00] are shown. The $f_0(1864)$ and $K_0^*(1738)$ are predictions of our analysis with the $f_0(1864)$ being the $2\ ^3P_0\ s\bar{s}$ state. (The properties of the scalar-isoscalar states are modified when we consider quarkonium-glueball mixing. In [Ce00] we identified the $f_0(1770)$ as the state with the maximum glueball component after such mixing. A covariant model of quarkonium-glueball mixing is

presented in Ref.[Ce99f].)

Fig.6.3 A perturbation expansion of a $q\bar{q}$ T matrix of our model is shown. Here we have not shown the vertex functions that implement confinement for the initial and final $q\bar{q}$ states. That matter is discussed in detail in [O199], where it is shown that the T matrix is represented only in terms of bound states in a theory with absolute confinement.

Fig.6.4 The values of the squared T matrix for $\pi\pi$ scattering obtained in [Ce00] are shown. In the absence of inelastic events, the quantity shown is equal to $\sin^2\delta_{00}(E)$. The first peak represents the $f_0(980)$ resonance and the second is the $f_0(1500)$ resonance, which we found at 1550 MeV [Ce00]. (In the case of the $f_0(1500)$, the width is greatly enhanced when we consider the decay to the 4π channel. A discussion of the $\pi\pi$ and $K\bar{K}$ decay widths of the $f_0(1500)$ is given in [Ce99f], where quarkonium-glueball mixing is taken into account in a covariant model.)

Fig.6.5 Values of $|T_{K\bar{K}}(E)|^2$ are shown. These results may be compared to those of Fig.16 of [Ce00]. Here we have reduced the values of $\mathrm{Im}K_S^{K\bar{K}}(P^2)$ by a factor of four to obtain a reasonable value for the $K\bar{K}$ decay width of the $f_0(1370)$ of 50 MeV. (We believe that the value of g_{Kqq} used in [Ce00] was about 40% too large due to an asymmetric treatment of the pion and the kaon in that work. [See the text.] The three small peaks above 1.5 GeV correspond to the three peaks above 1.5 GeV seen in Fig.6.4. Their presence represents deviations from ideal mixing.

Fig.6.6 The phase shift $\delta_{00}(E)$ is shown for the case of t-channel and u-channel ρ exchange (dotted line) [Zo94]. The solid line is the result obtained when the phase shift of our model is added to the phase shift for ρ exchange as calculated in [Zo94].

Fig.6.7 Experimental values of the δ_{00} phase shift for $\pi\pi$ scattering as complied in [Ha96] are shown. The small circles represent the values given by the solid curve in Fig.6.6.

Fig.6.8 The experimental values of the π-K scattering phase shift is shown in the region below the $\eta' K$ threshold at 1453 MeV [As88]. The dotted line represents the sum of the phase shift calculated for ρ and K^* exchange and the s-channel phase shift of our generalized NJL model. These effects give rise to an enhanced cross section from threshold to the energy of the K_0^* (1430) resonance.

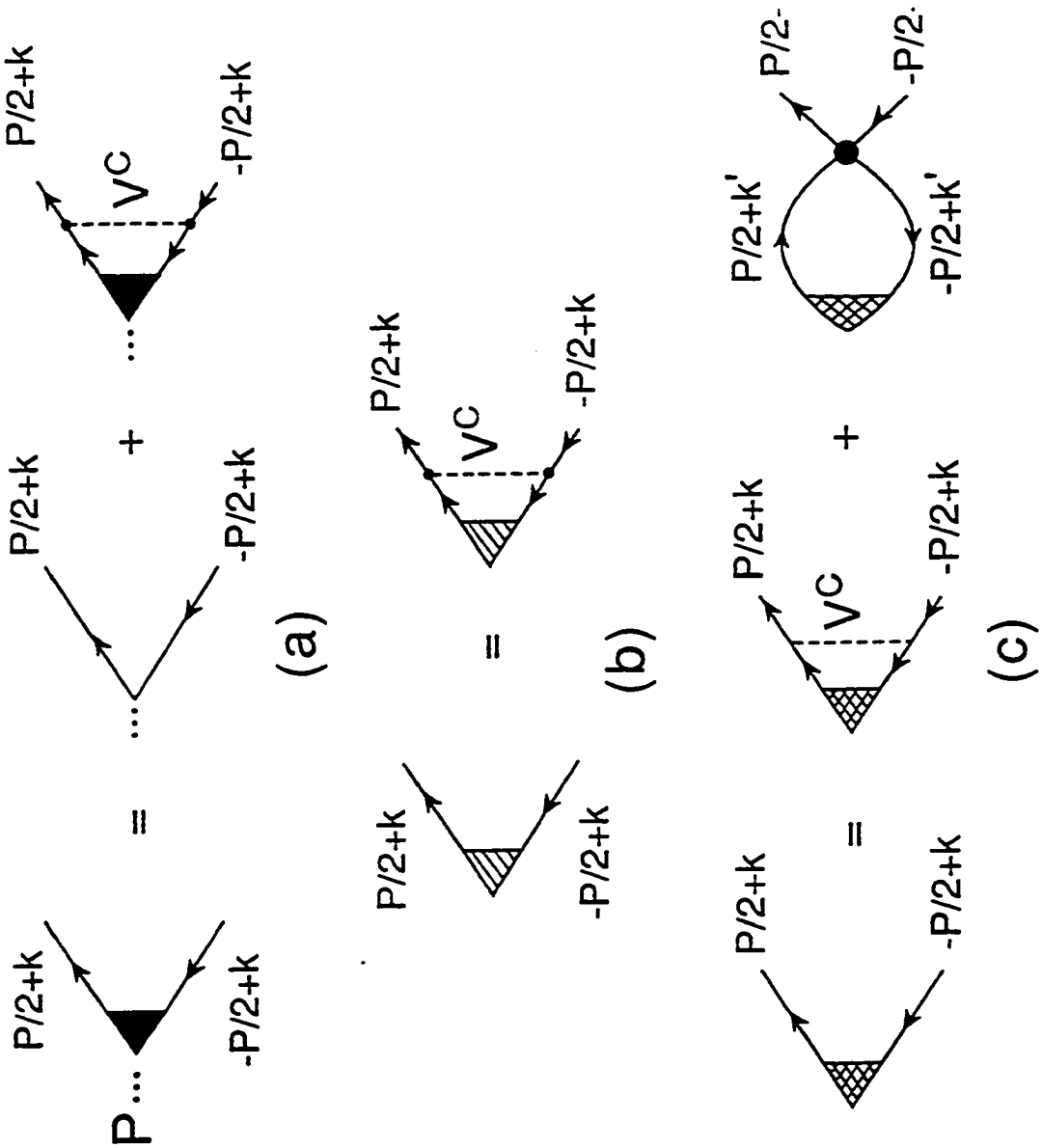

Fig. 2.1

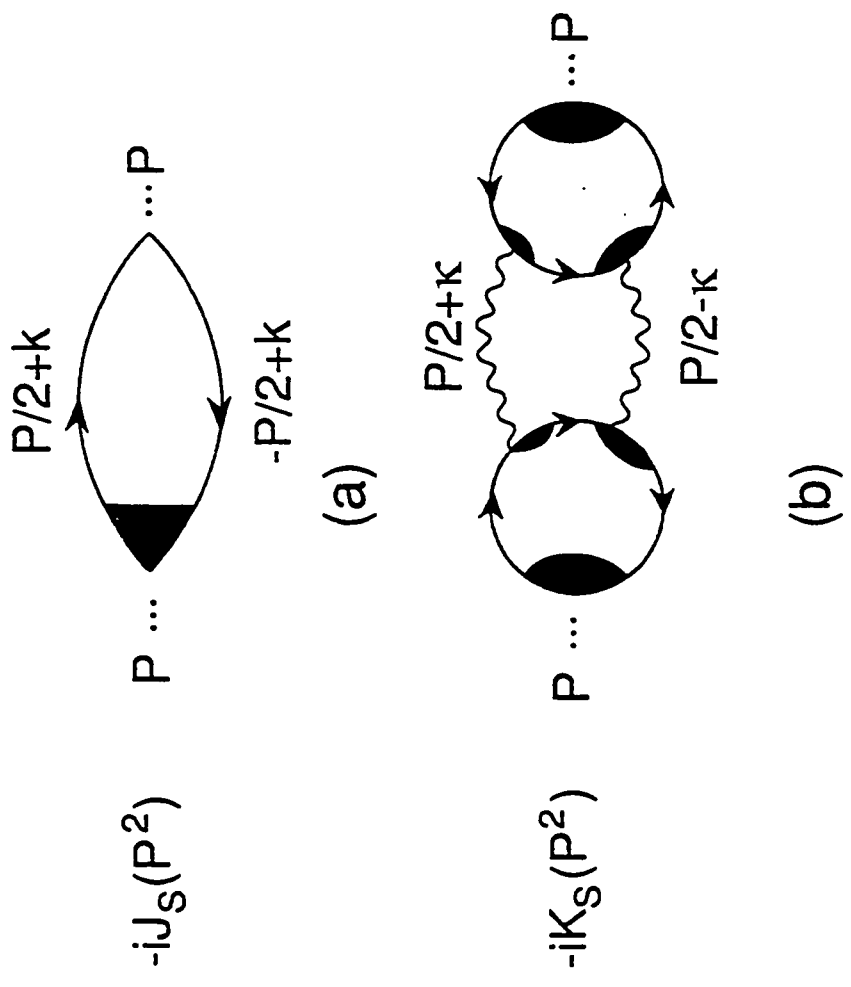

Fig. 2.2

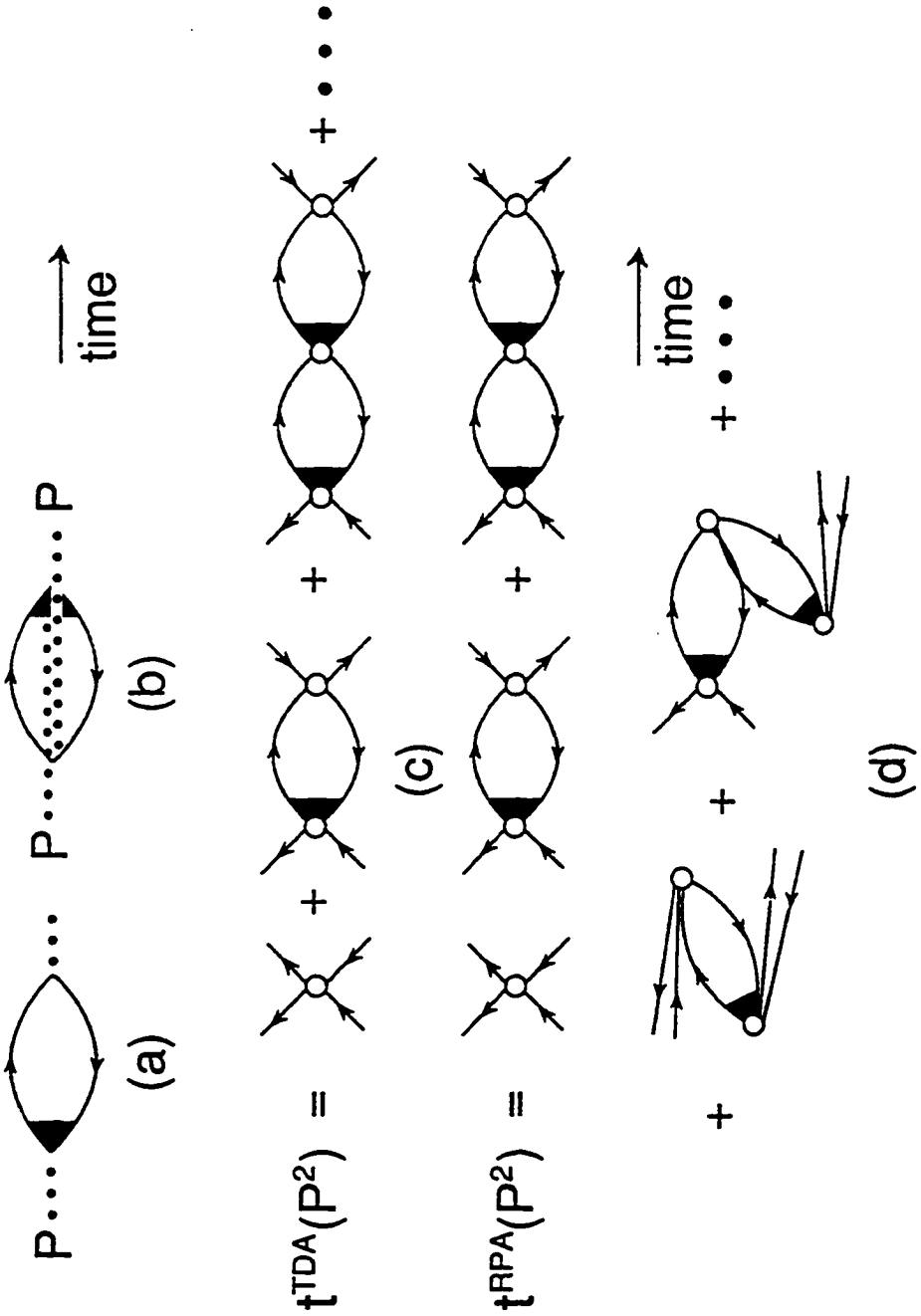

Fig. 2.3

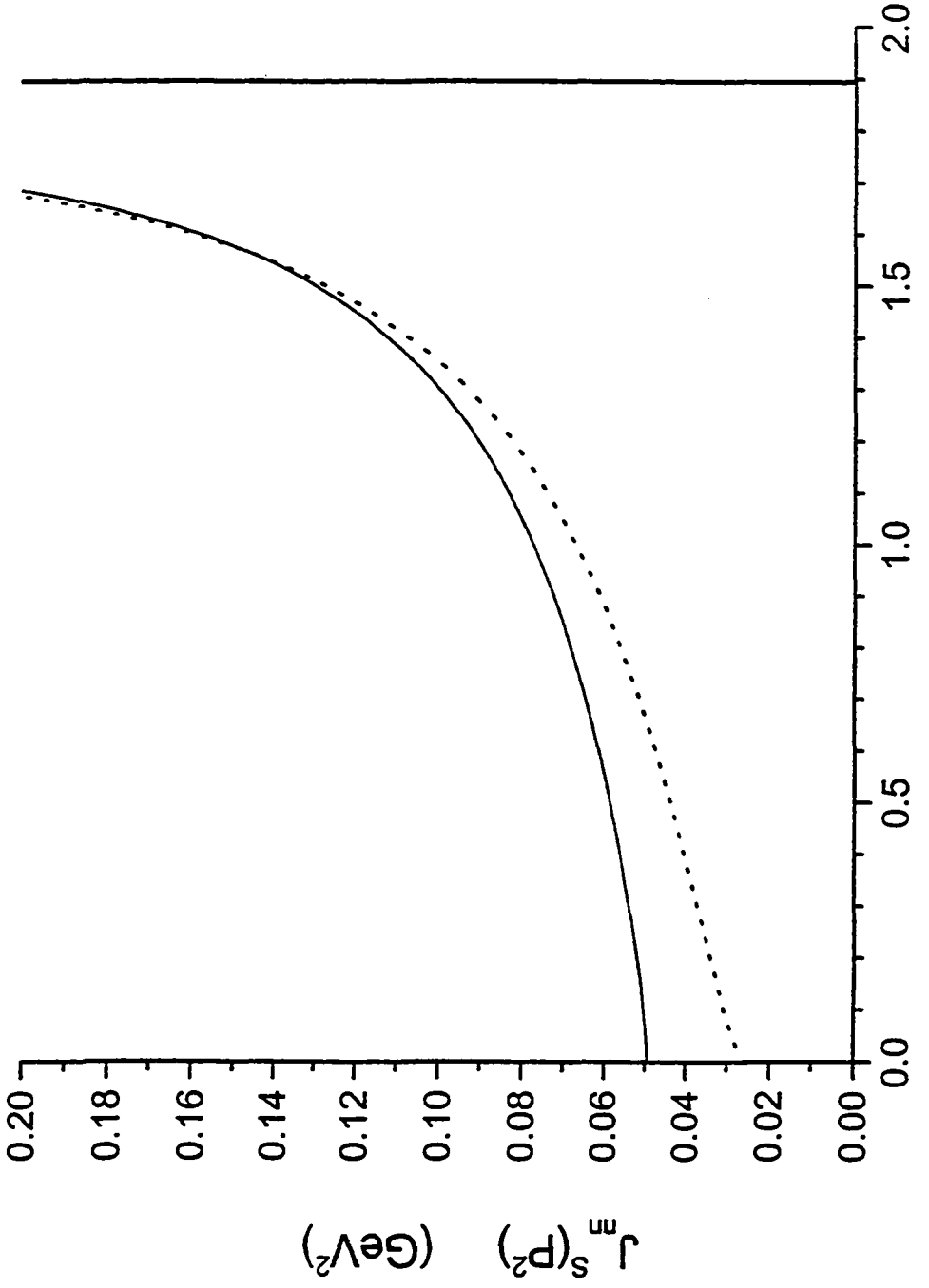

Fig. 2.4

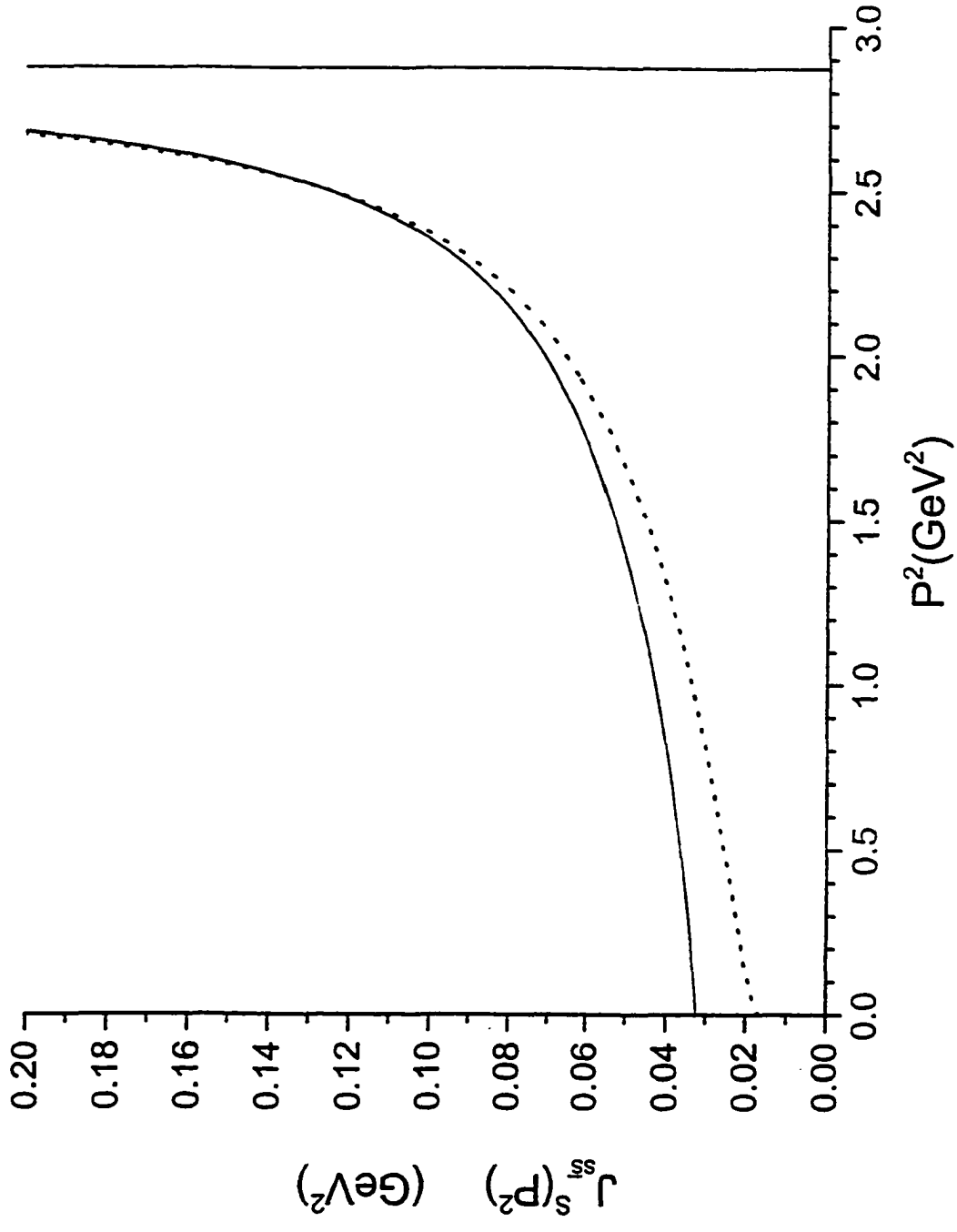

Fig .2.5

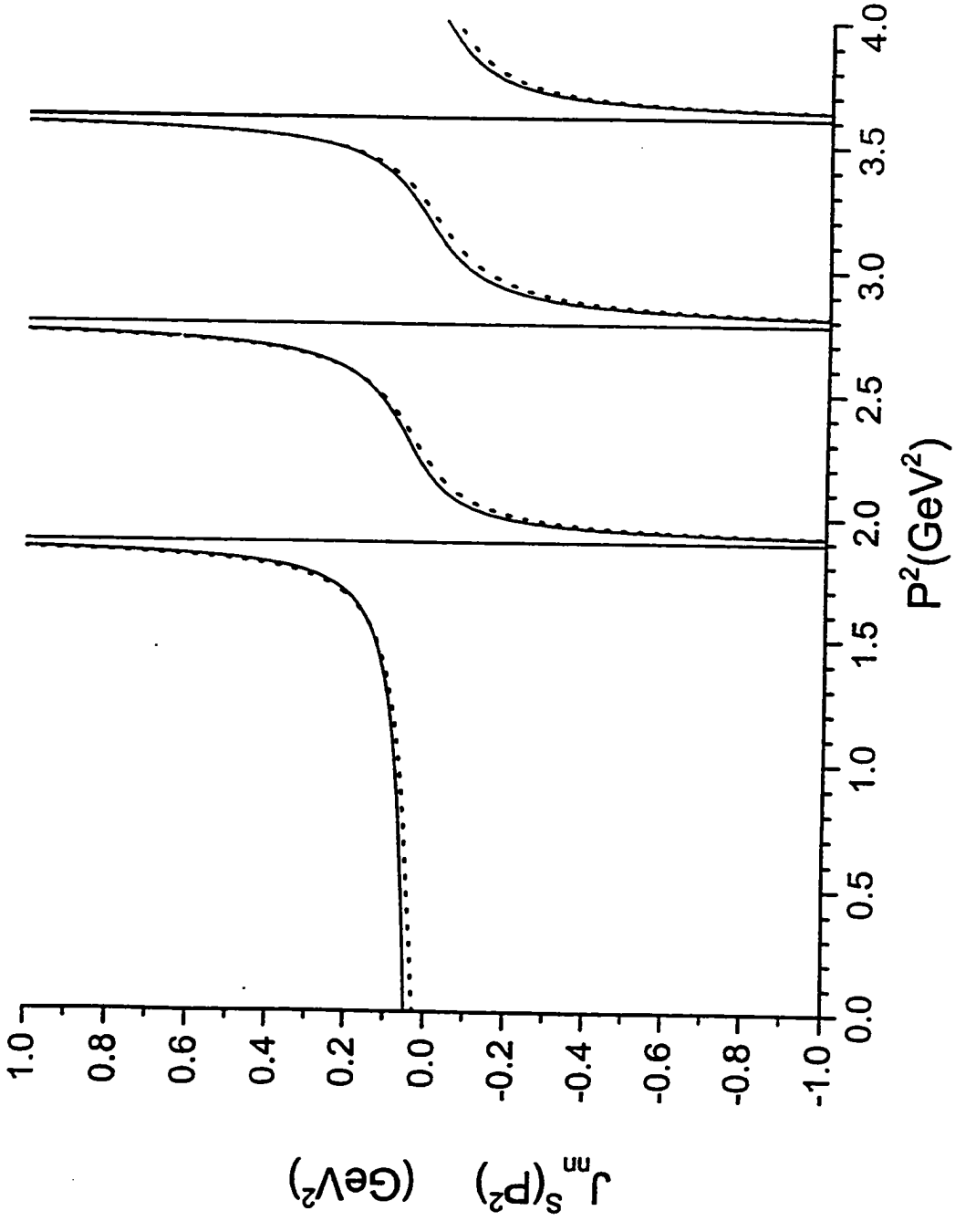

Fig. 2.6

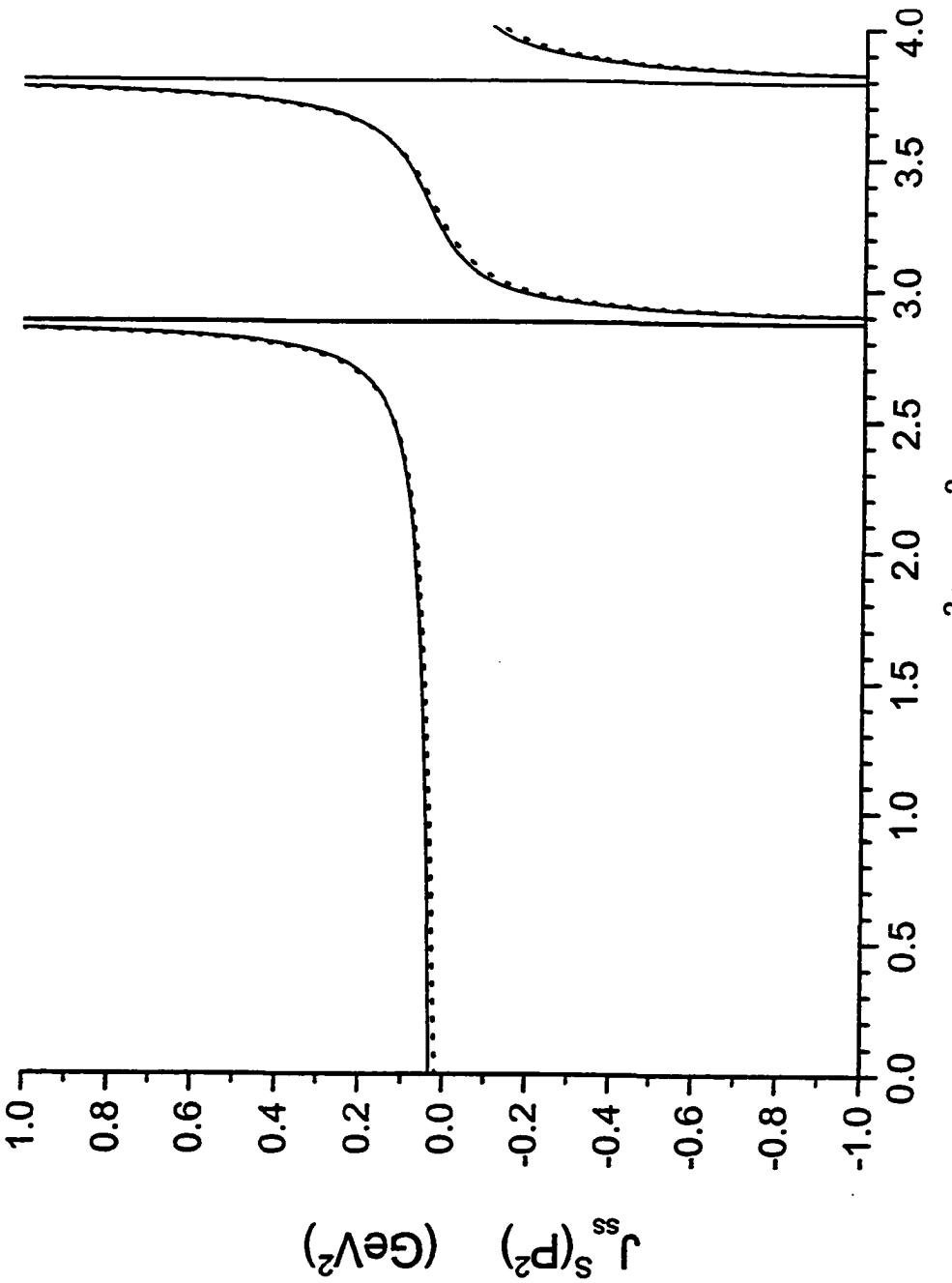

Fig. 2.7

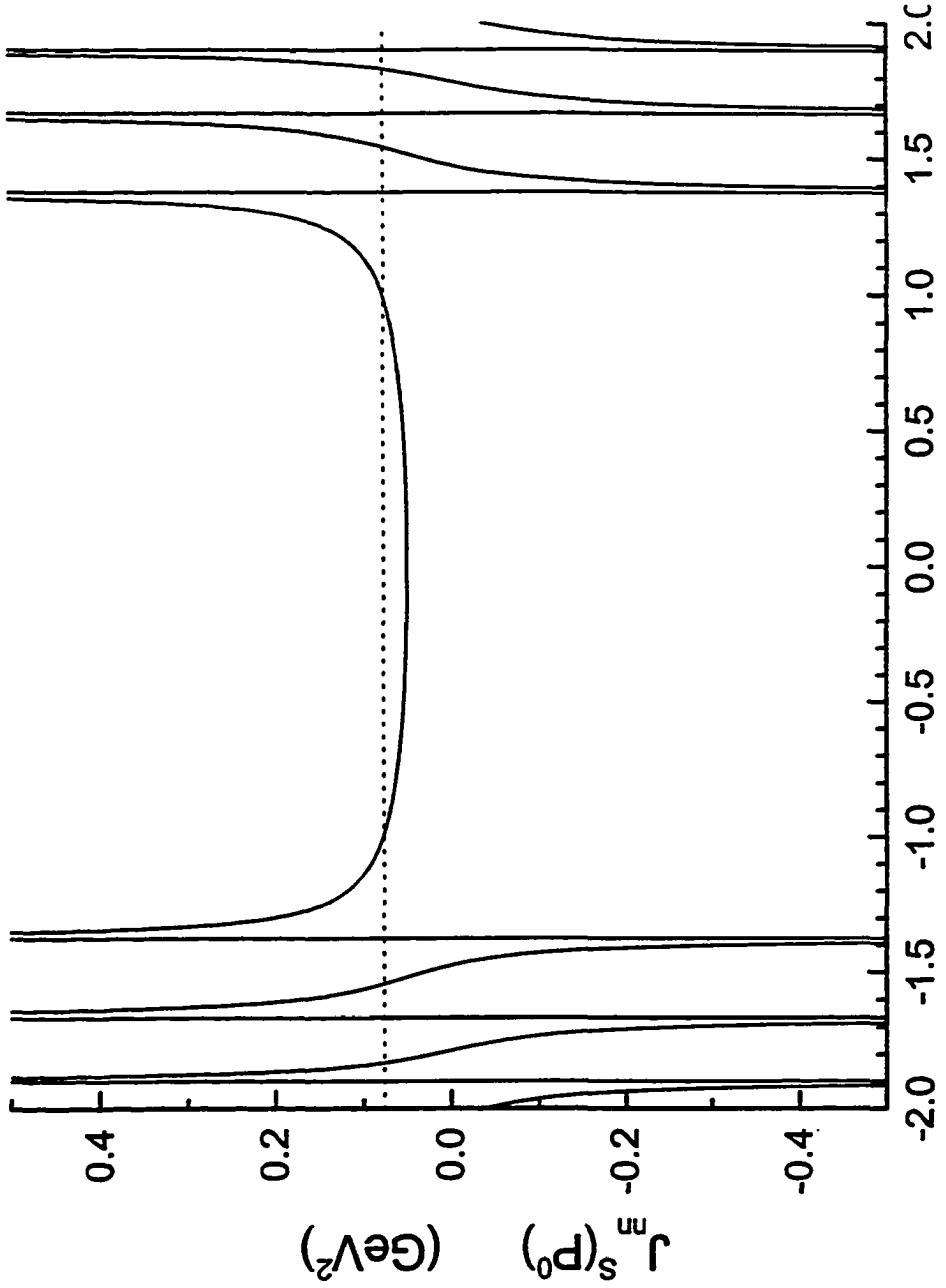

Fig. 2.8

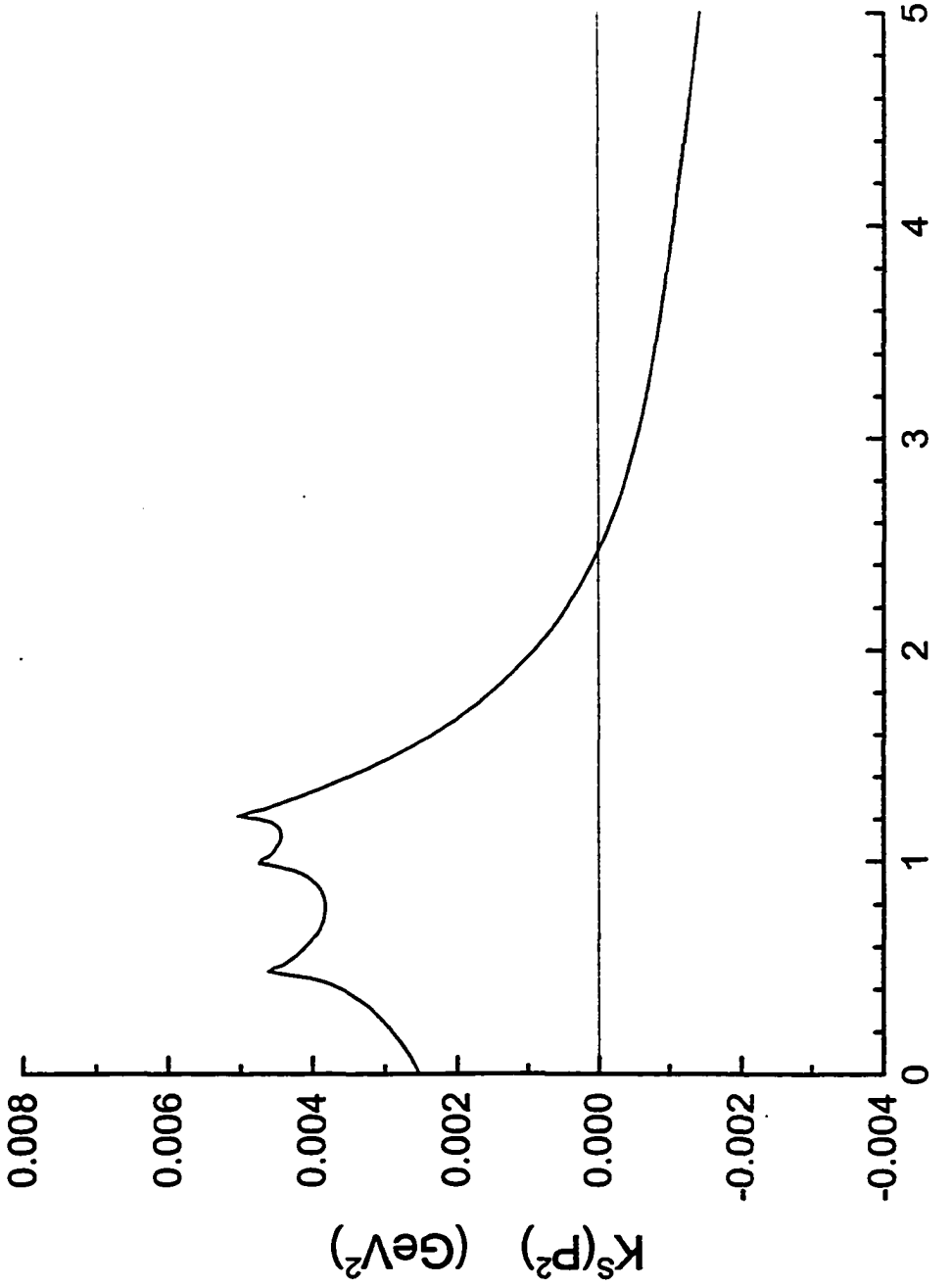

Fig. 2.9

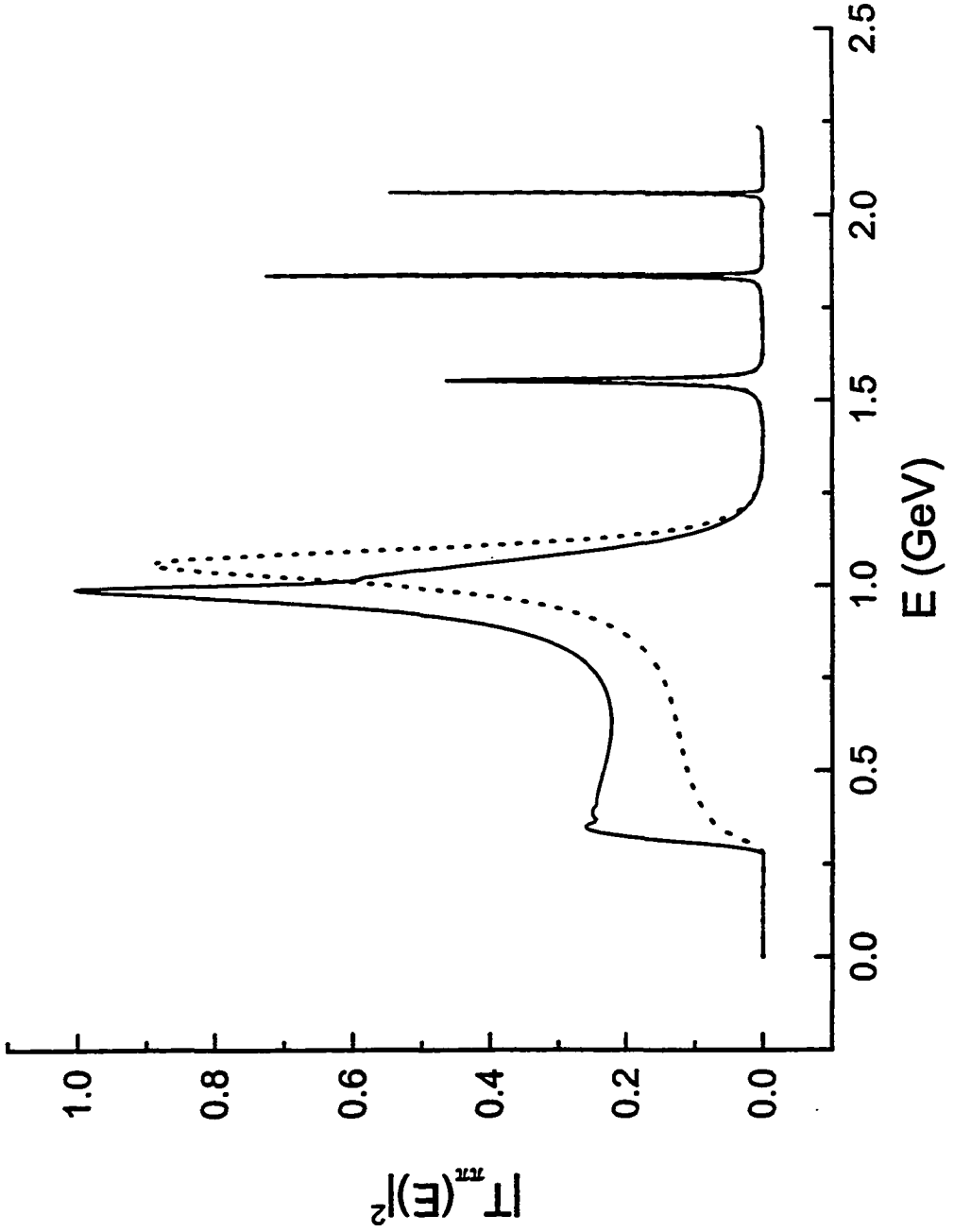

Fig. 2.10

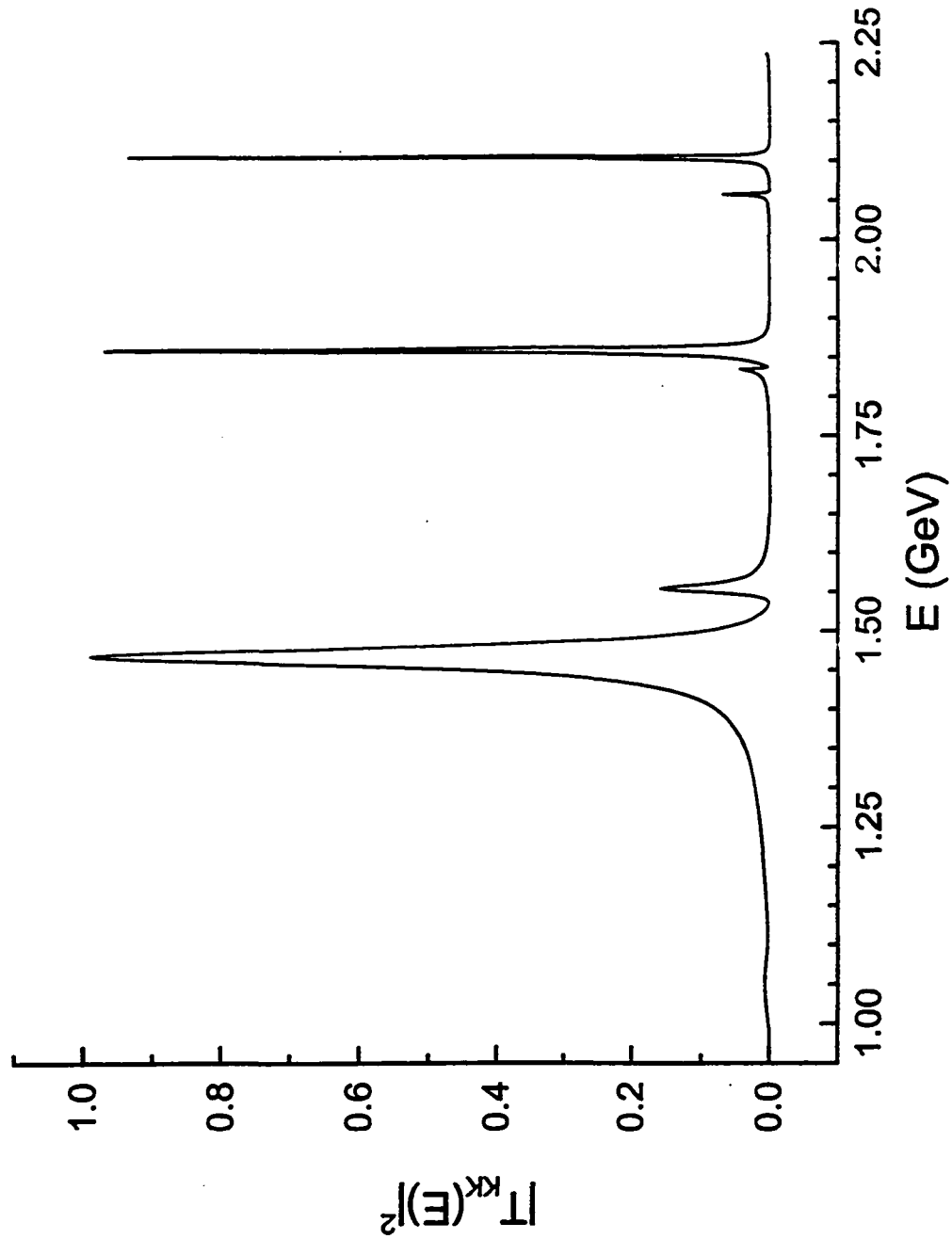

Fig. 2.11

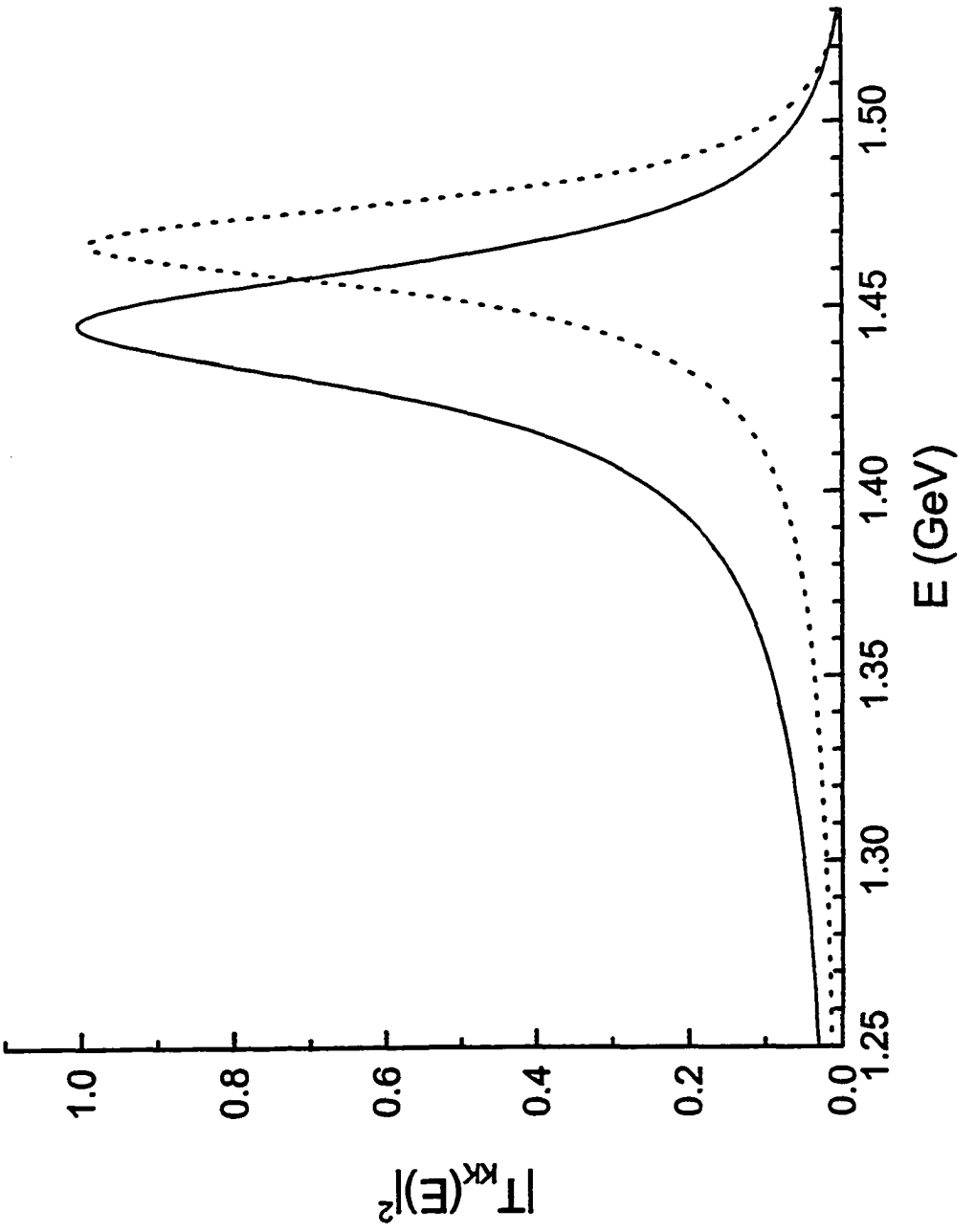

Fig. 2.12

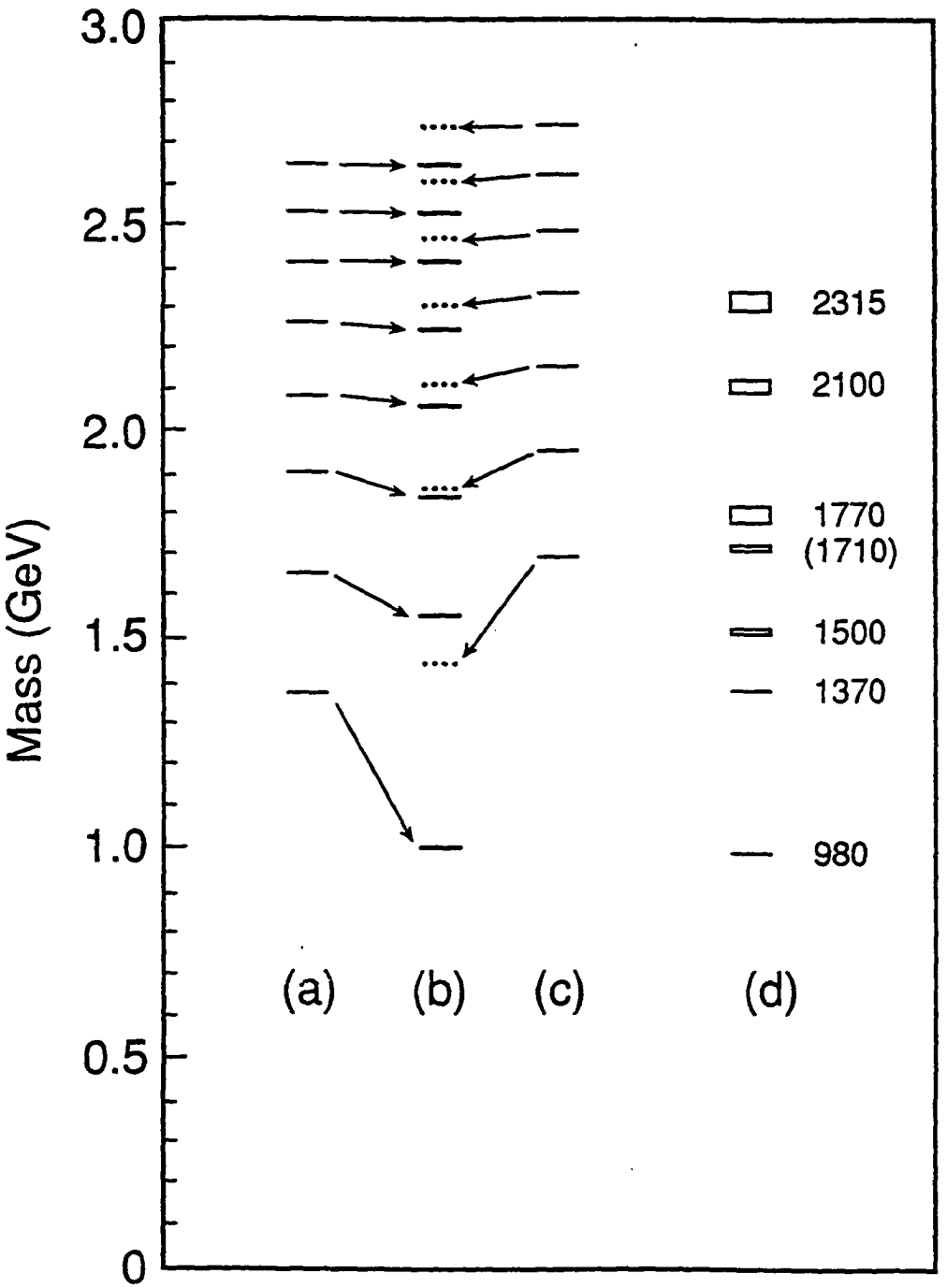

Fig. 2.13

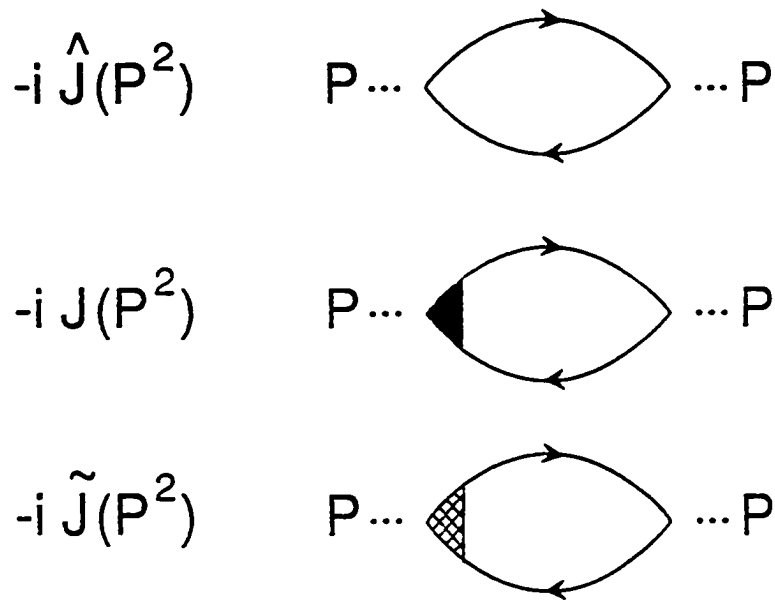

Fig. 3.1

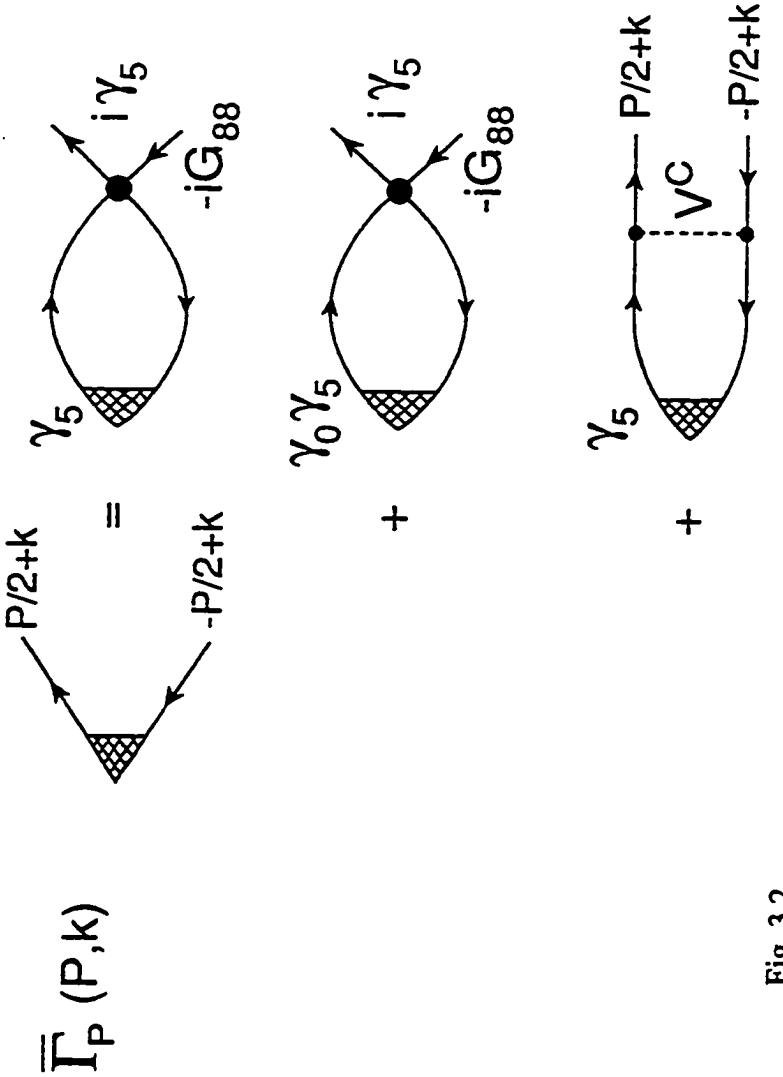

Fig. 3.2

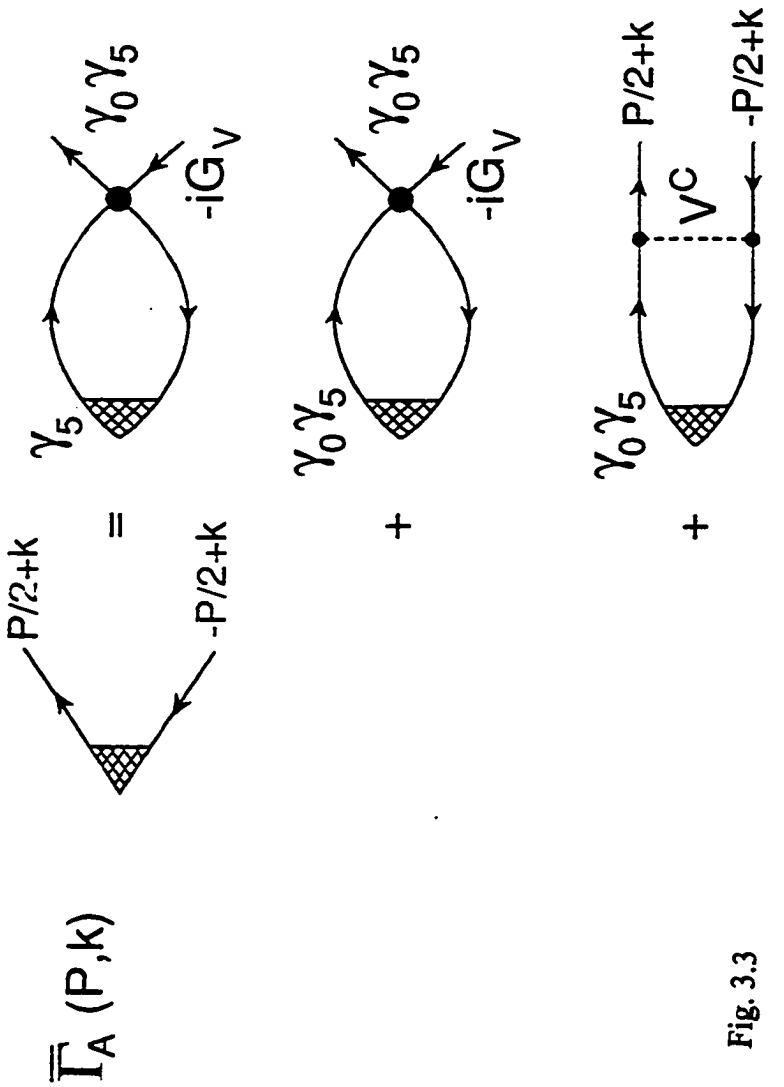

Fig. 3.3

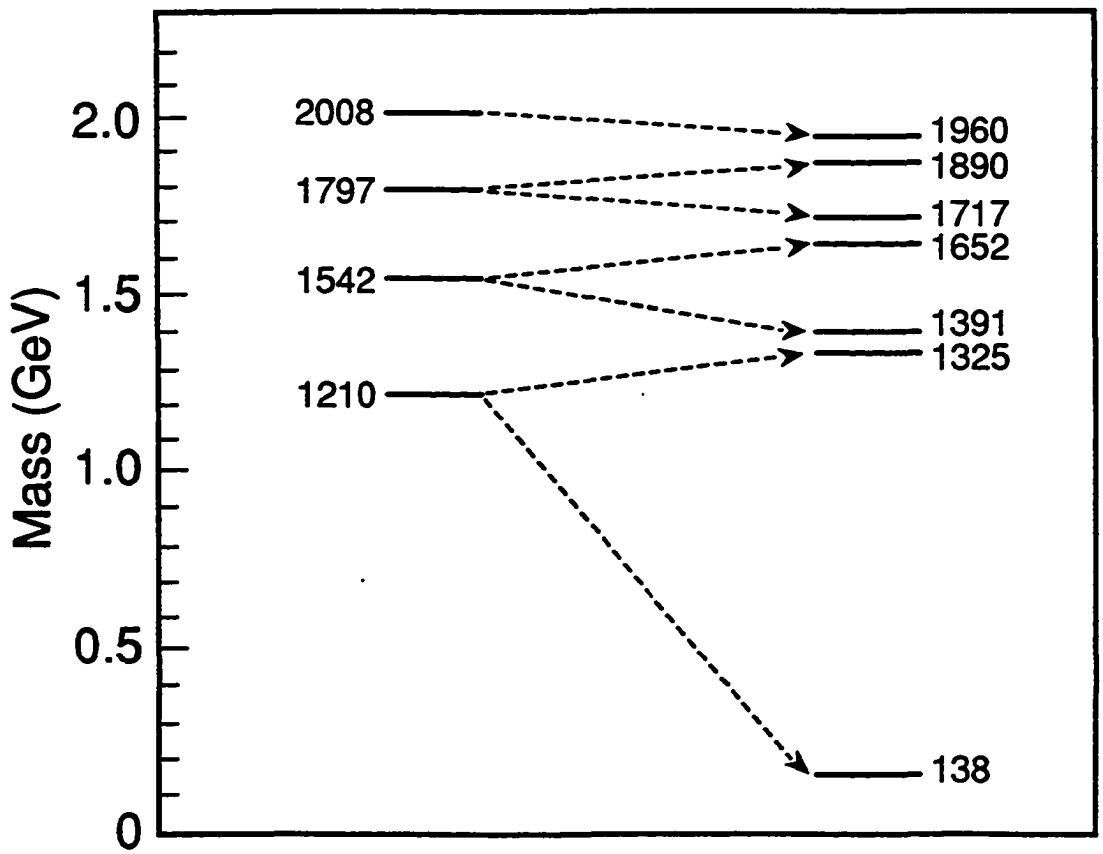

Fig. 3.4

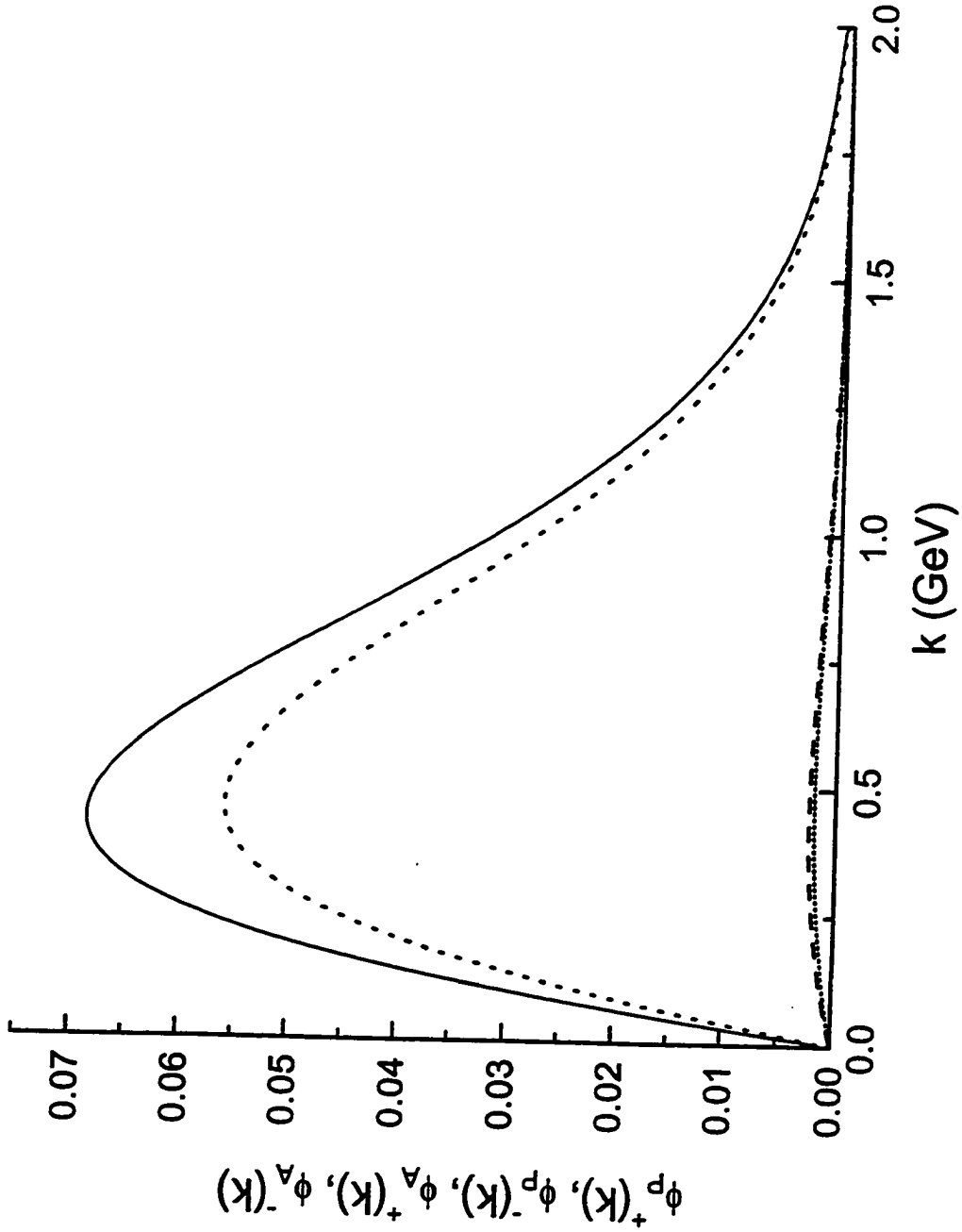

Fig. 3.5

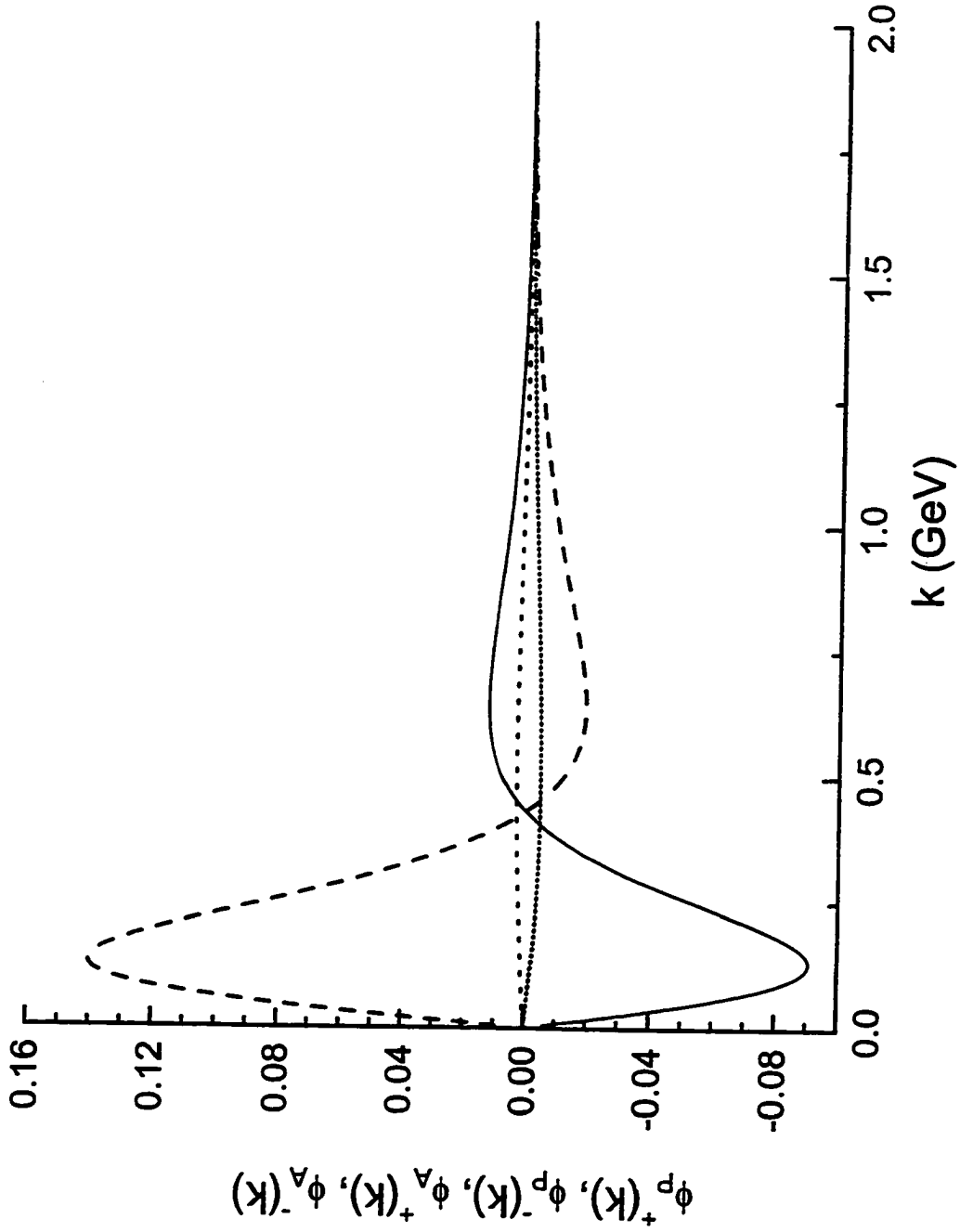

Fig. 3.6

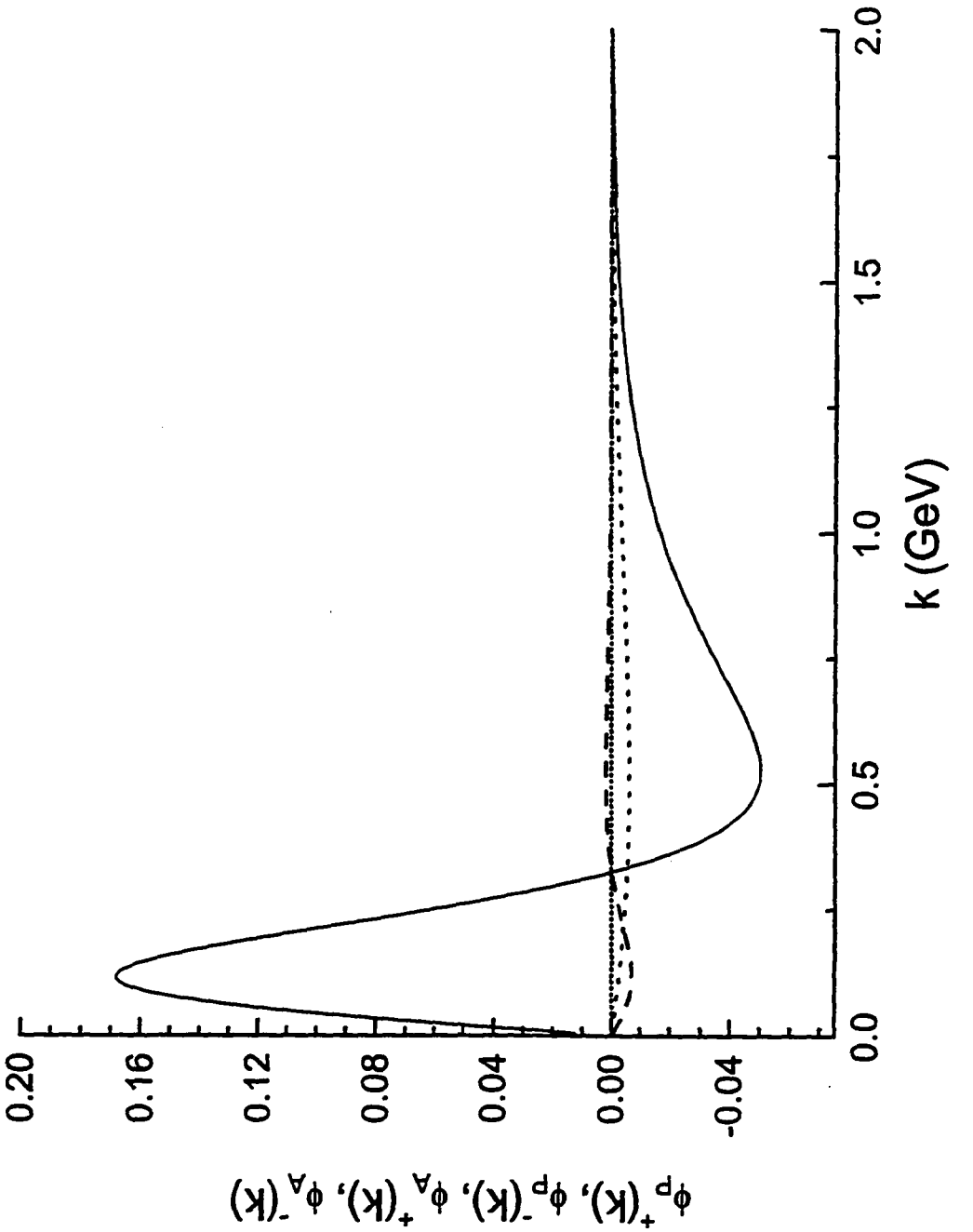

Fig. 3.7

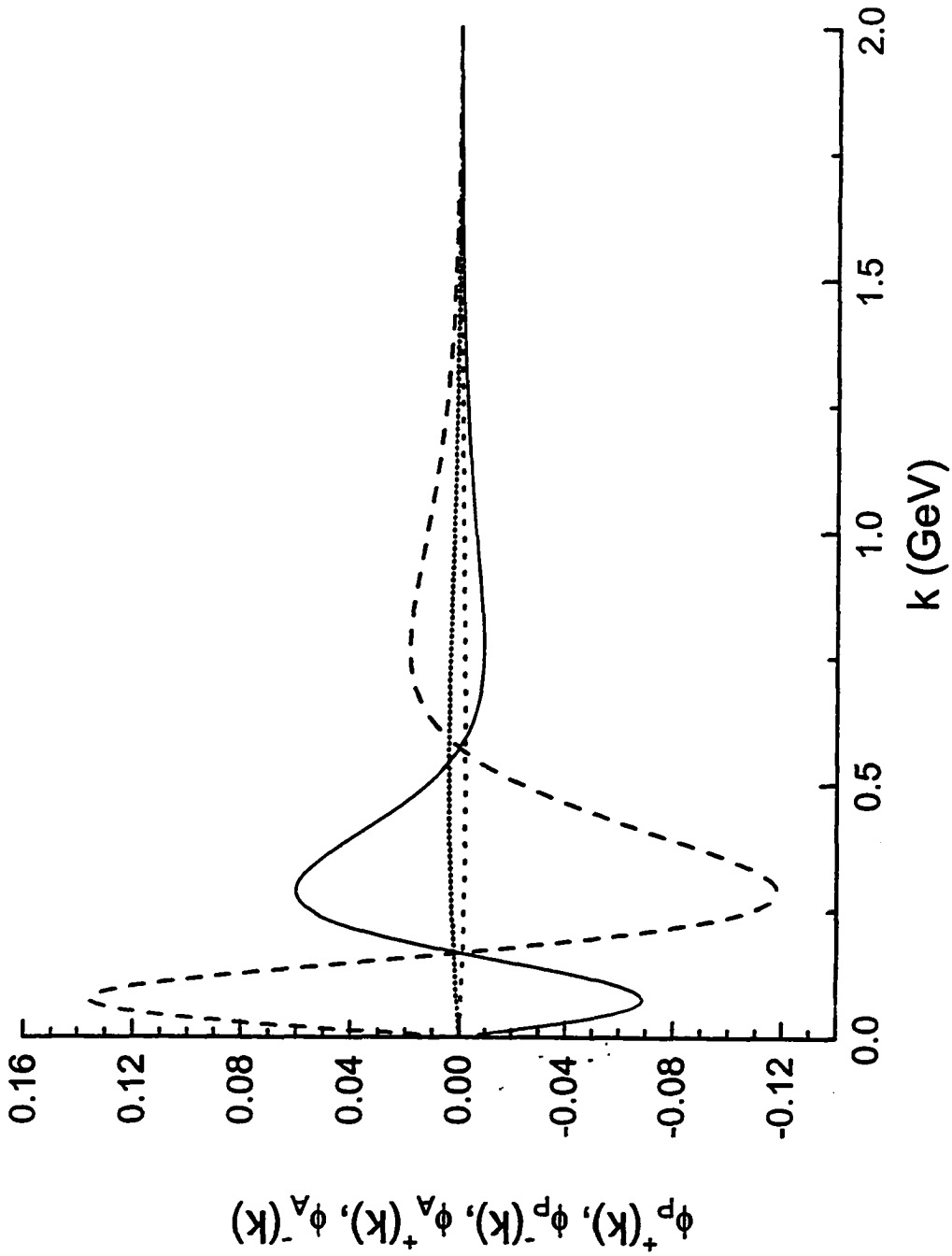

Fig. 3.8

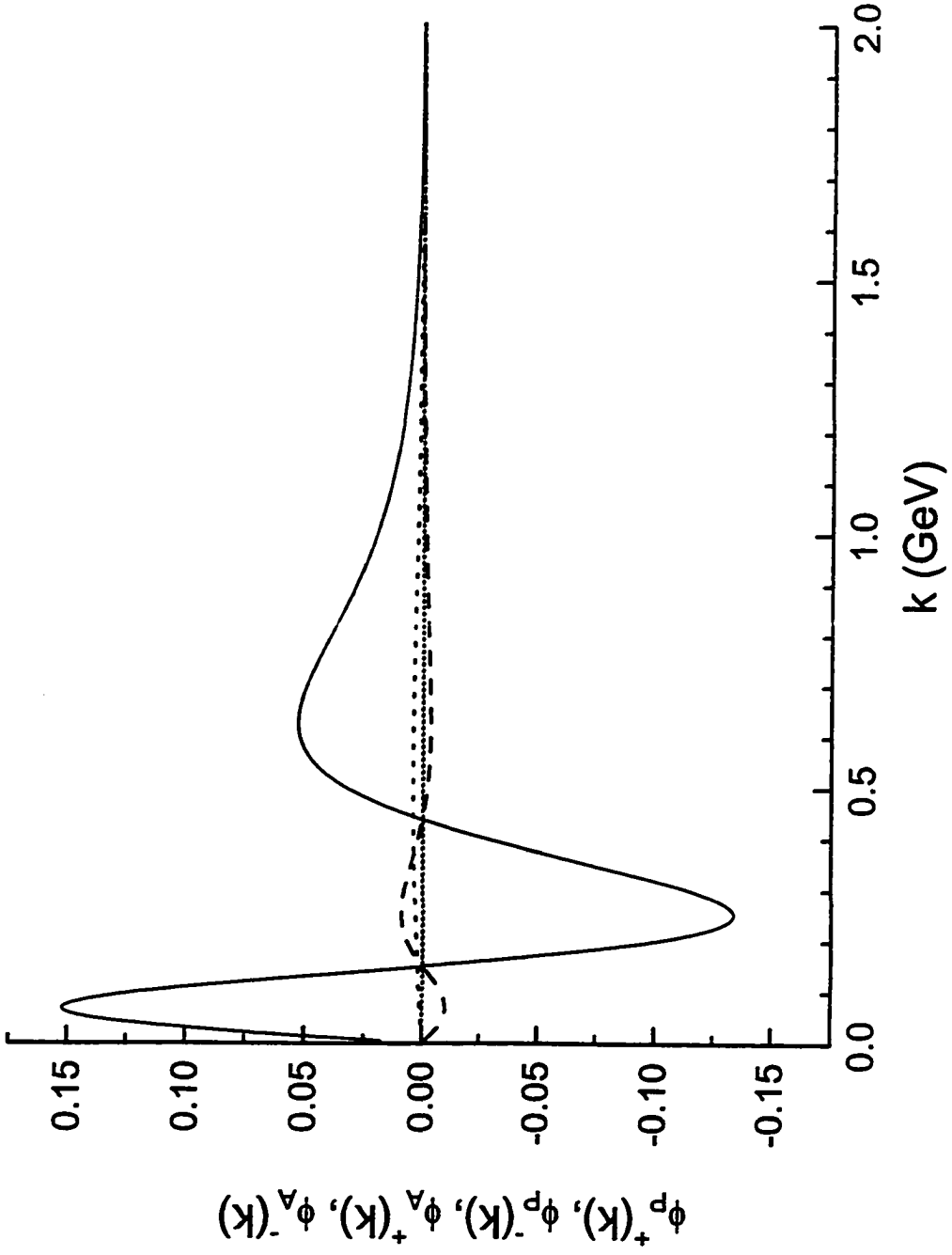

Fig. 3.9

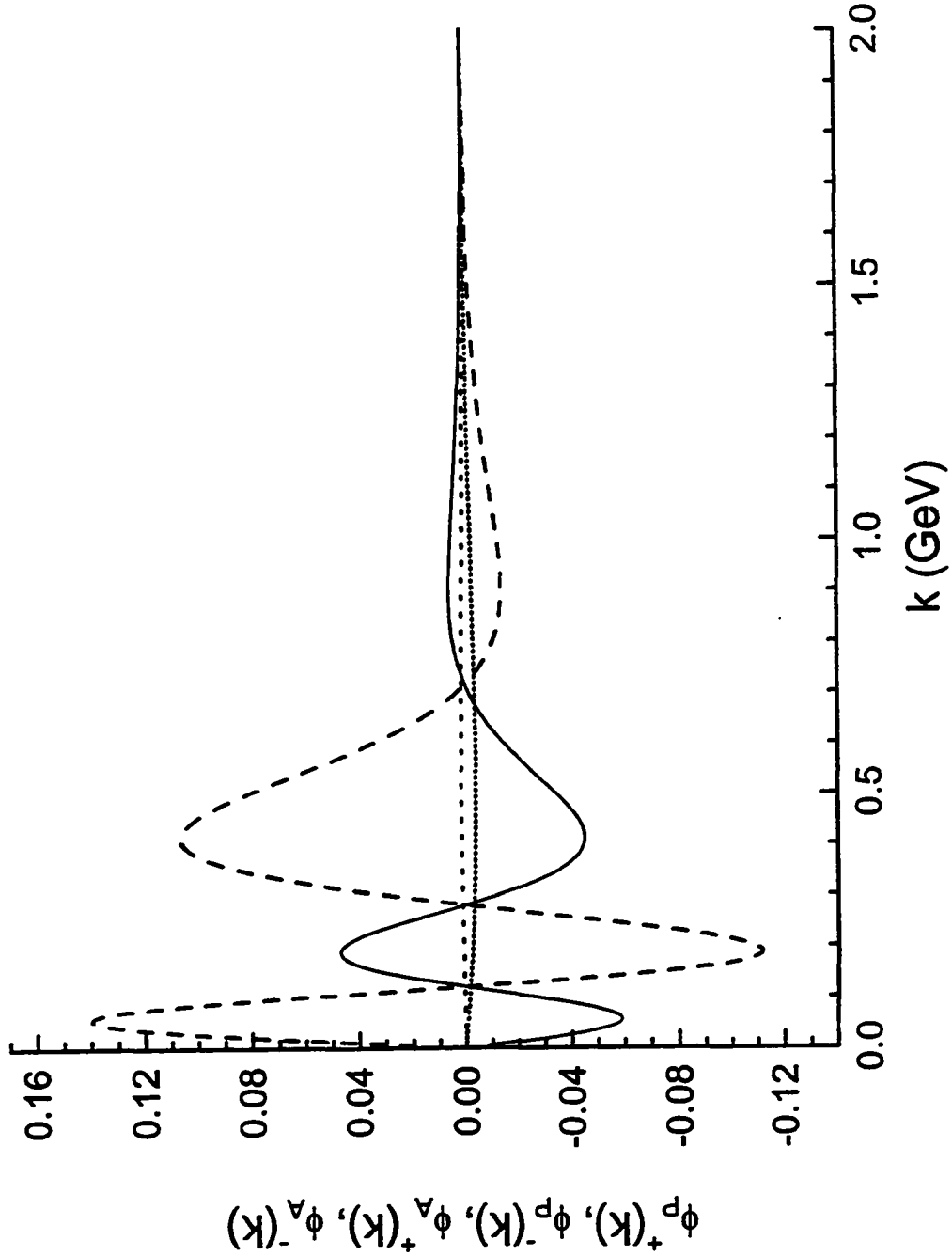

Fig. 3.10

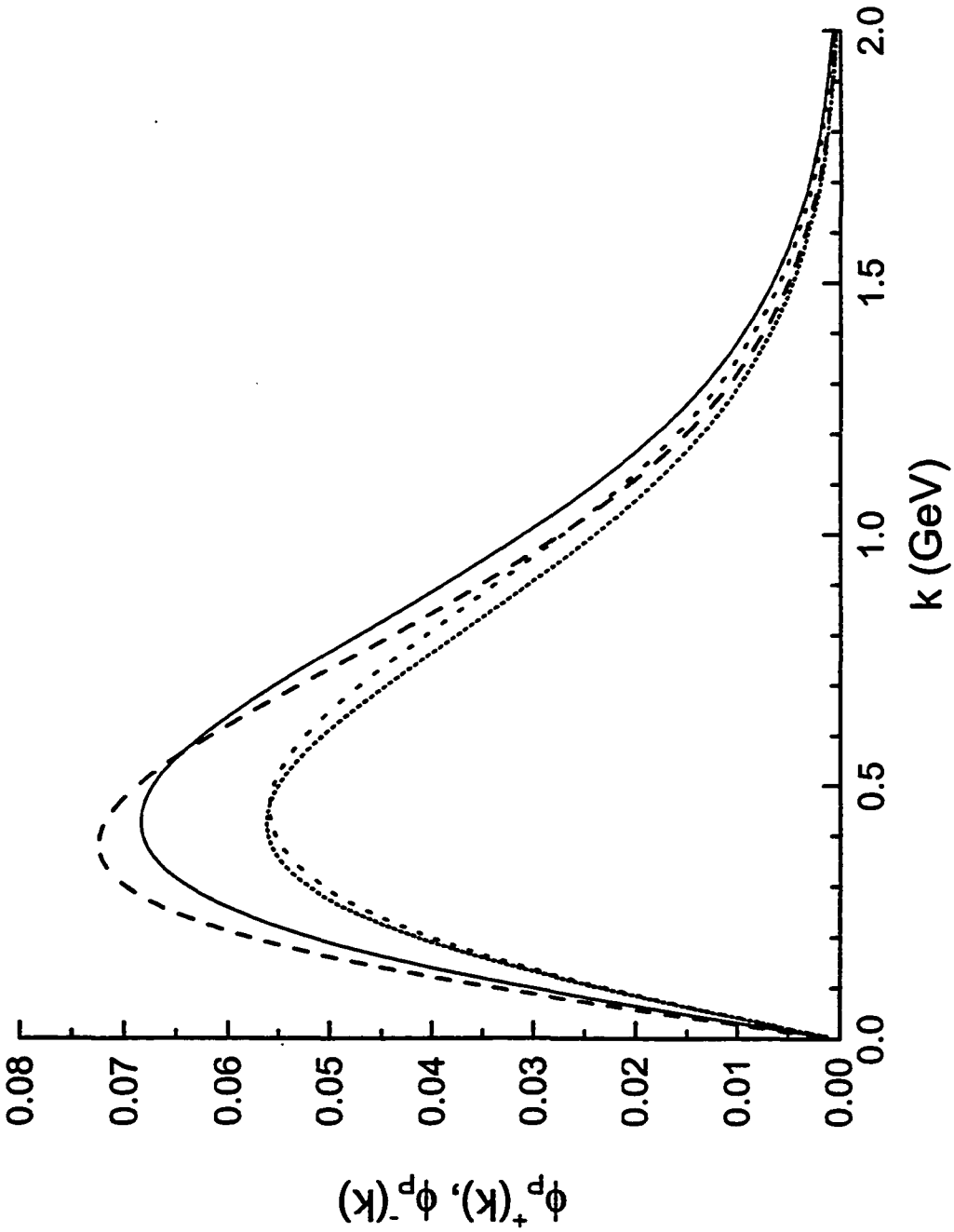

Fig. 3.11

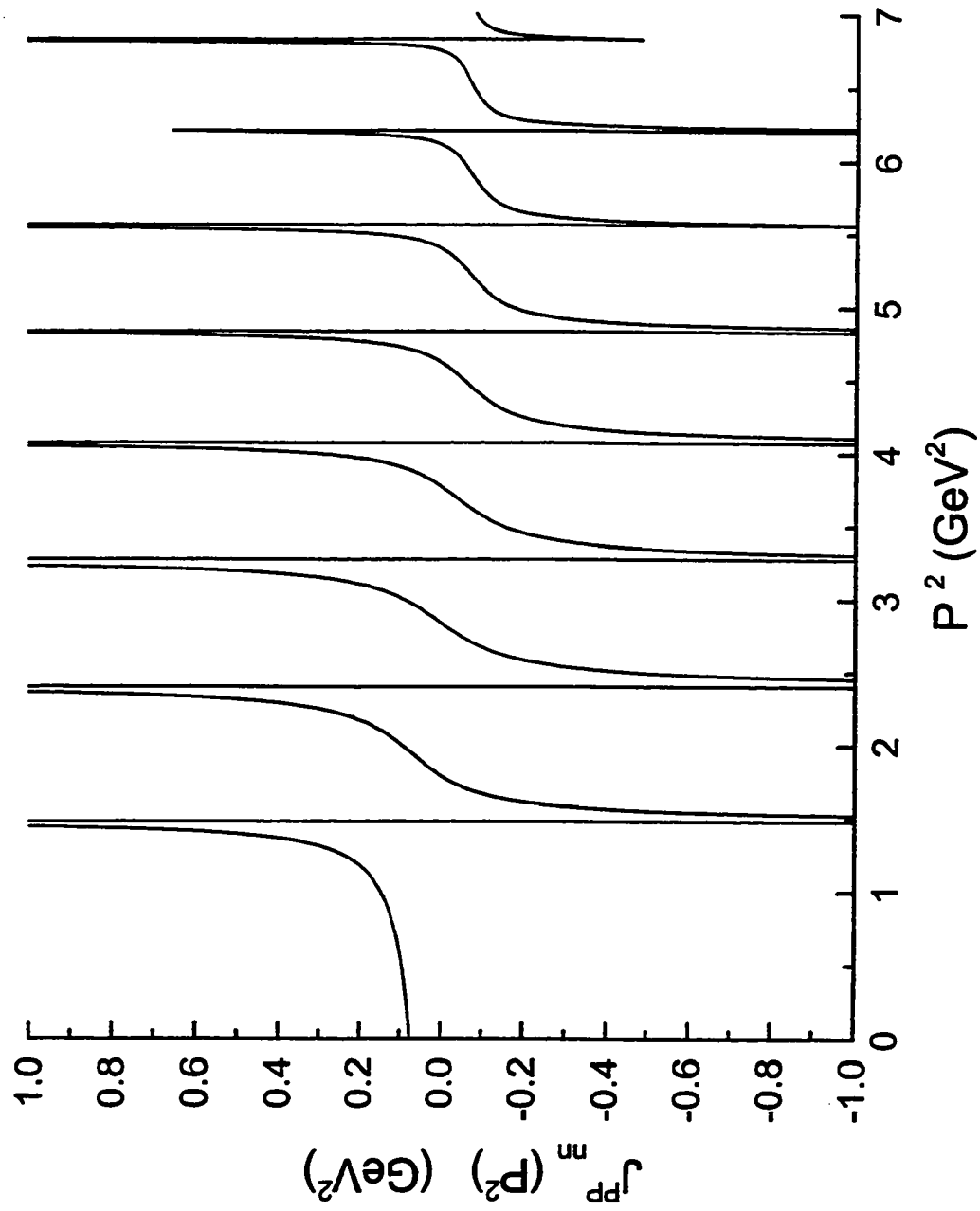

Fig. 4.1

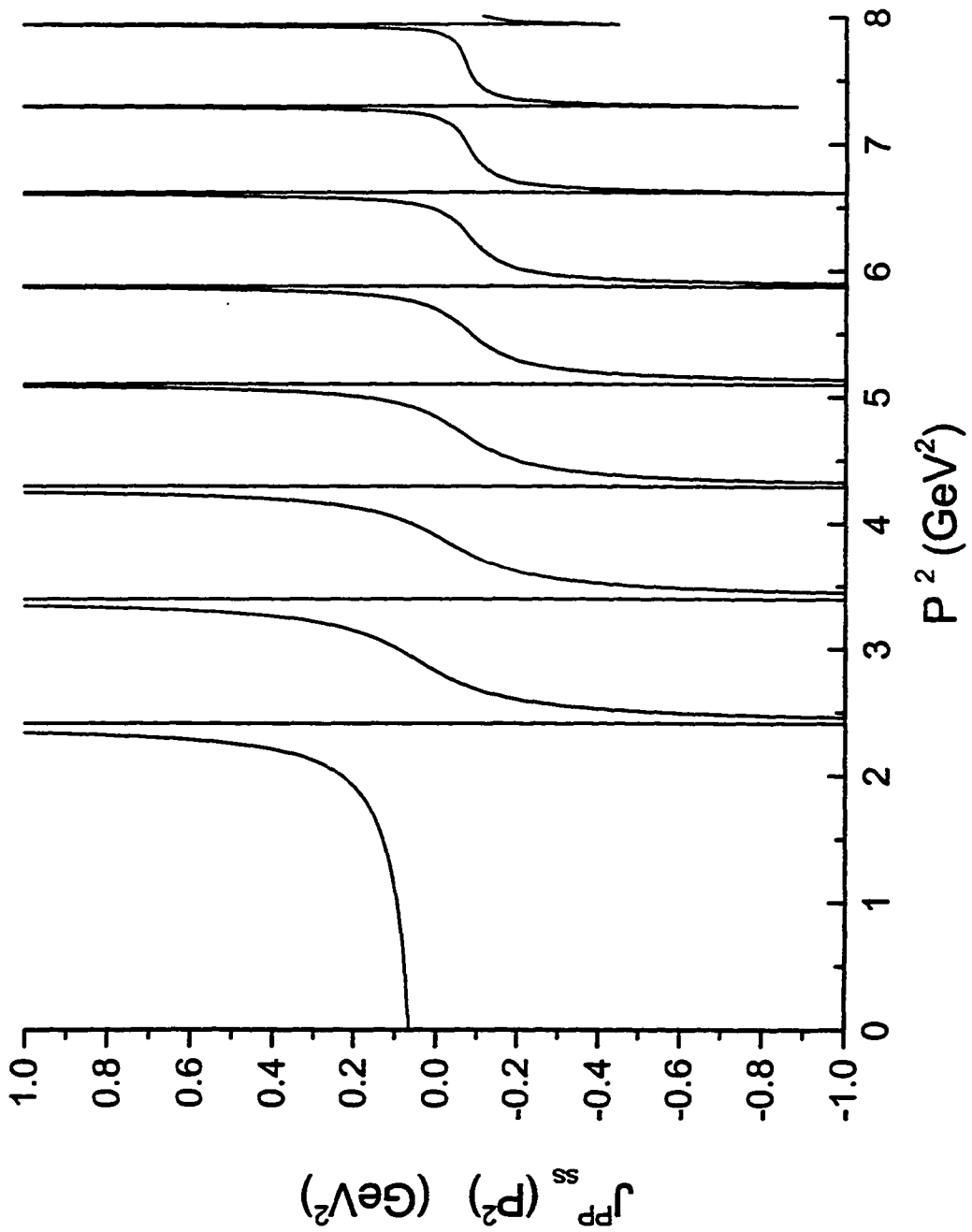

Fig. 4.2

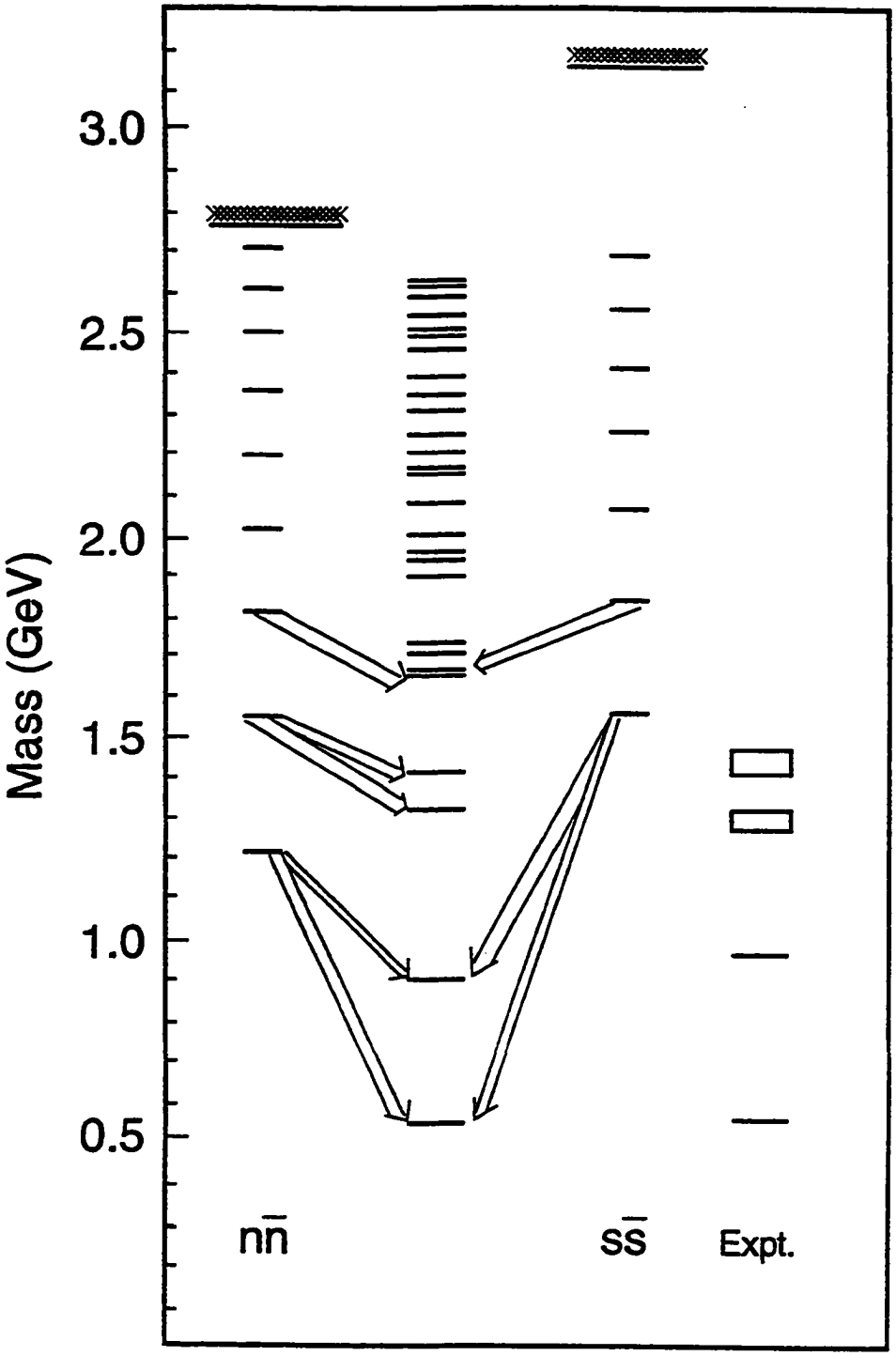

Fig. 4.3

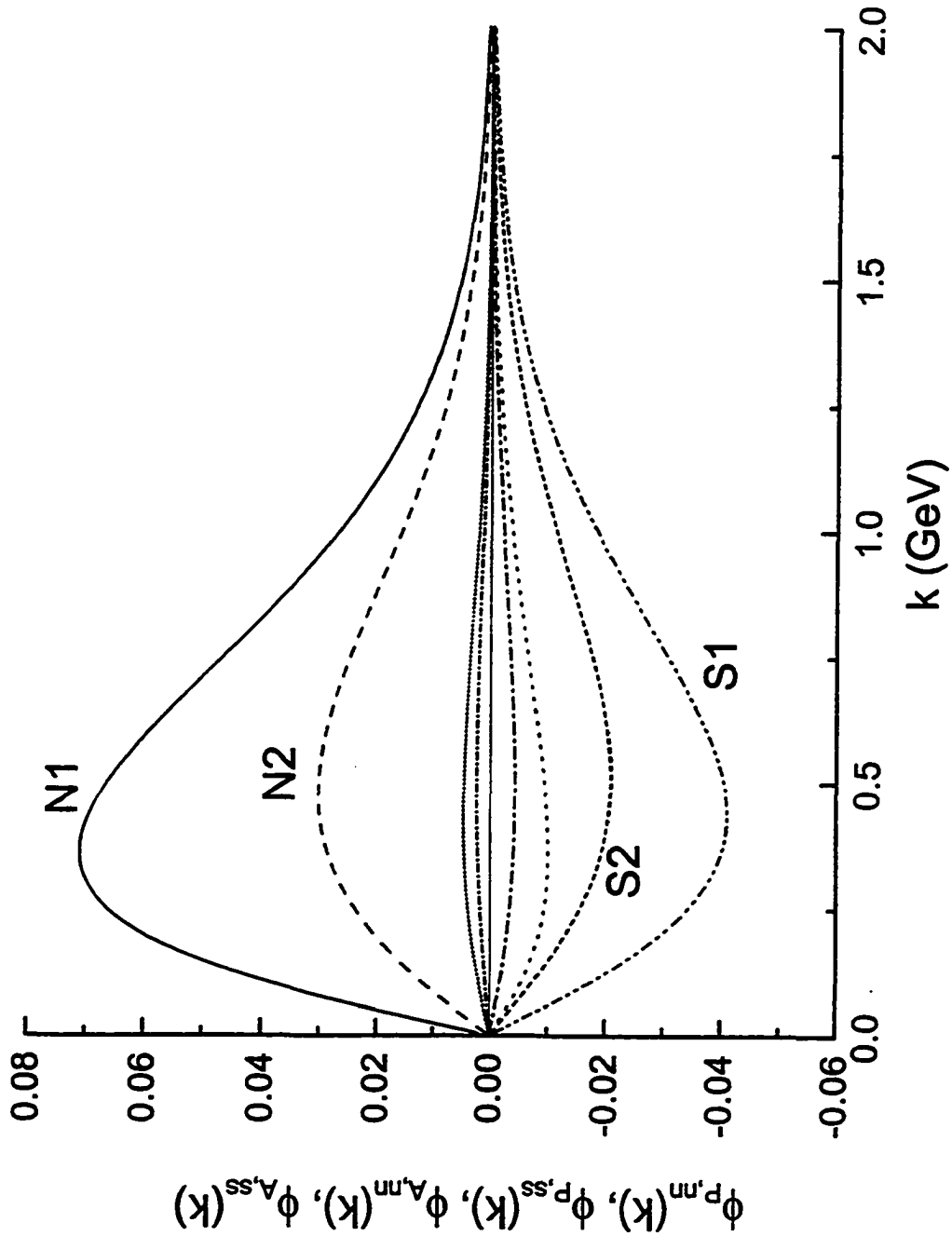

Fig. 4.4

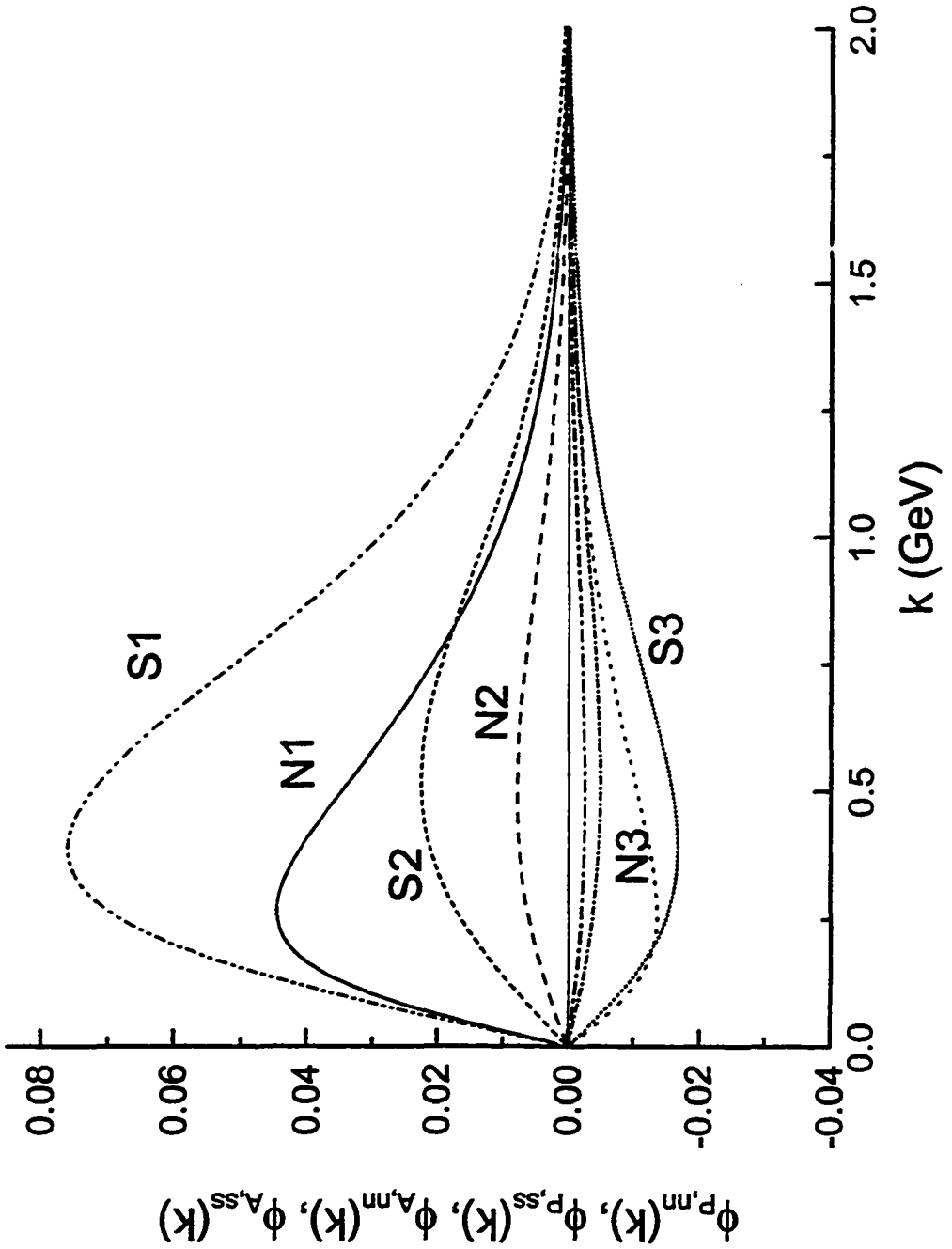

Fig. 4.5

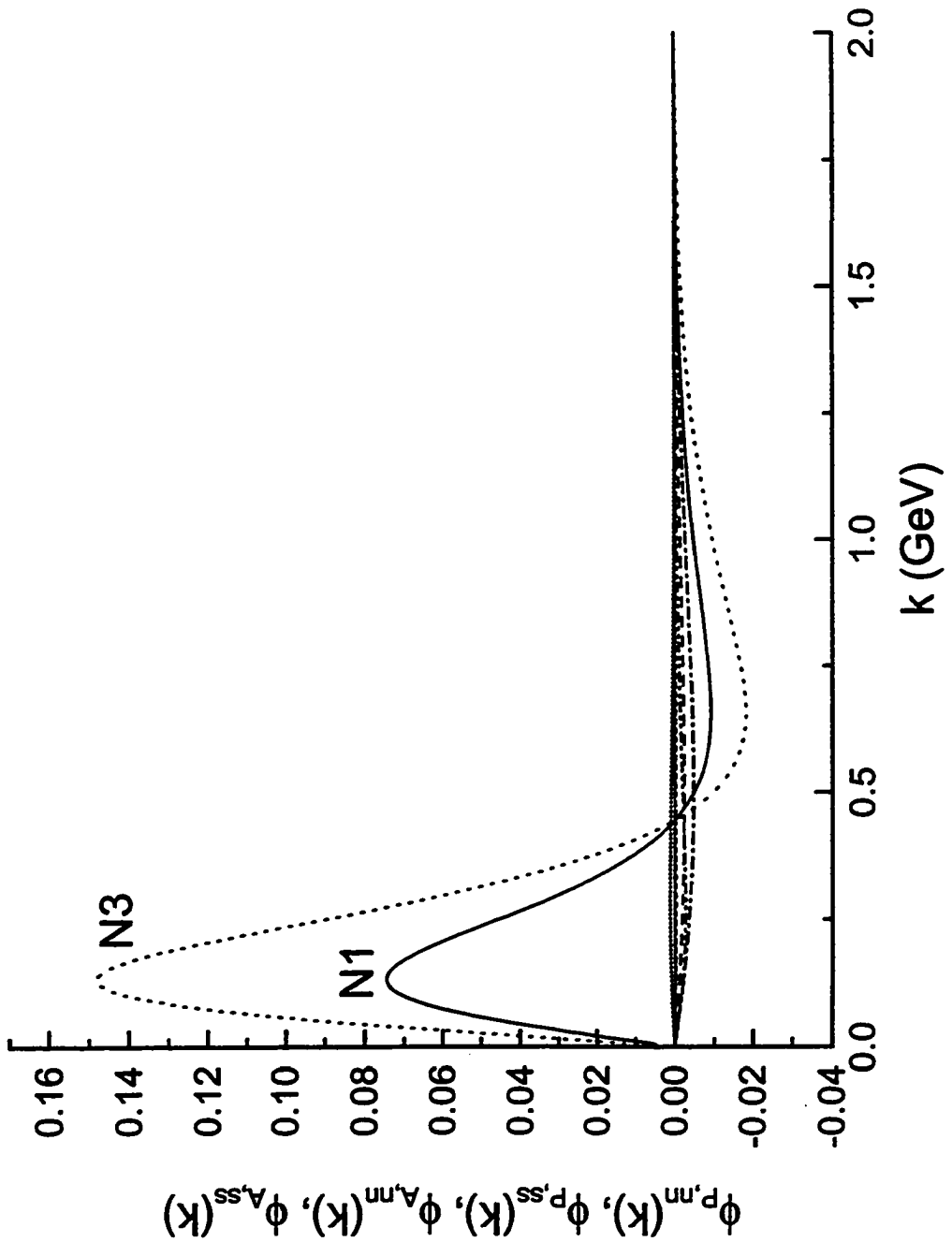

Fig. 4.6

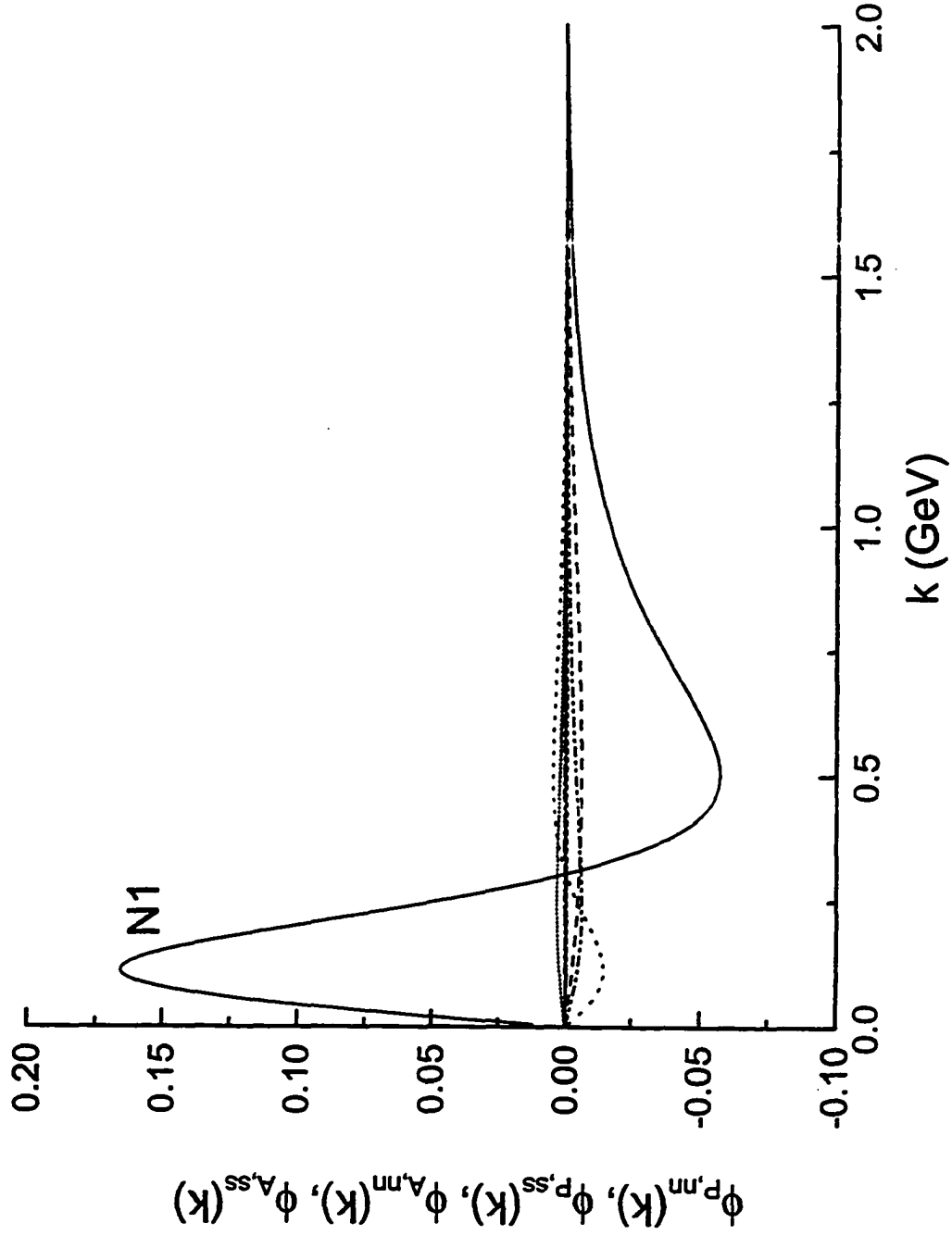

Fig. 4.7

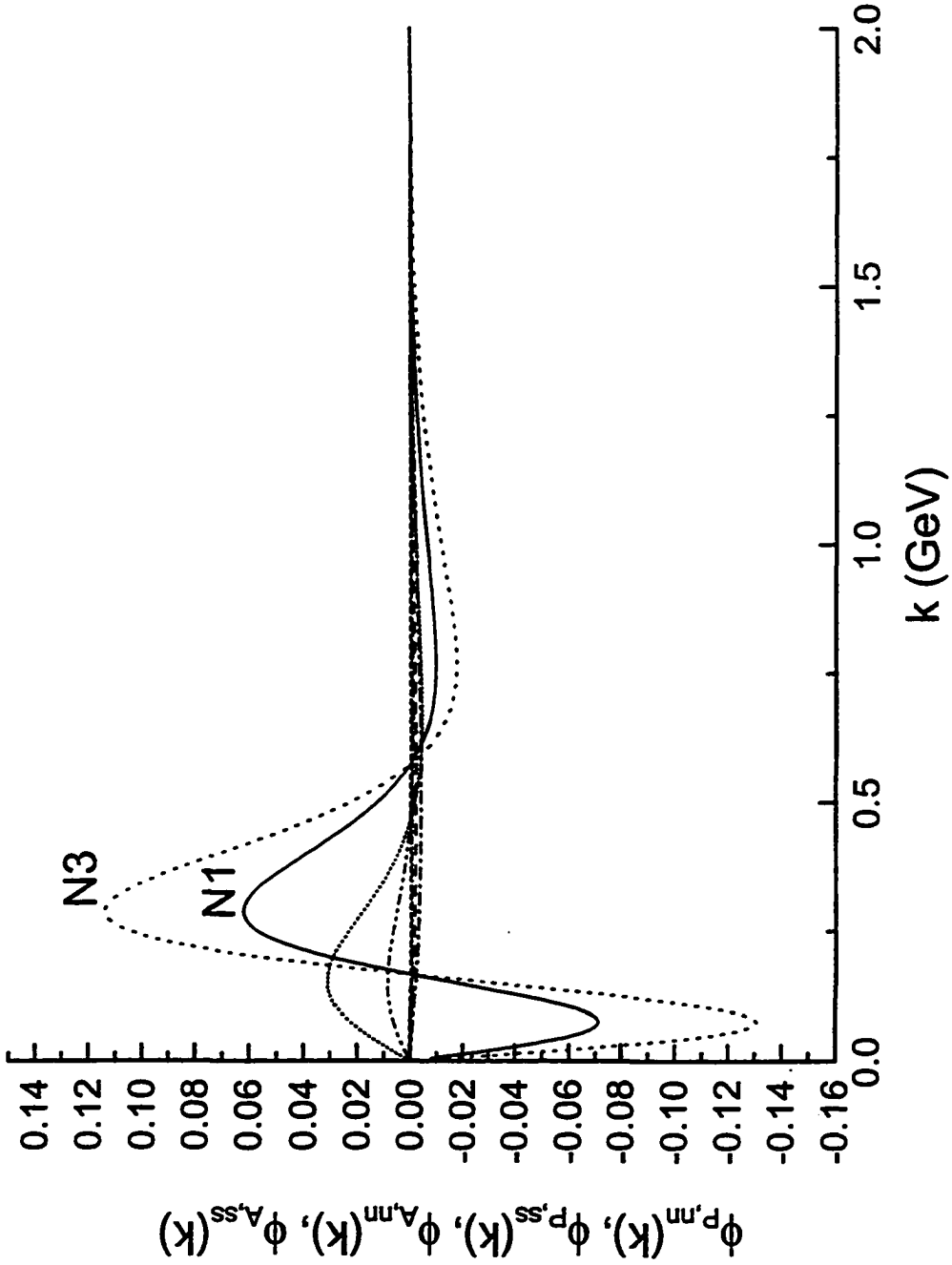

Fig. 4.8

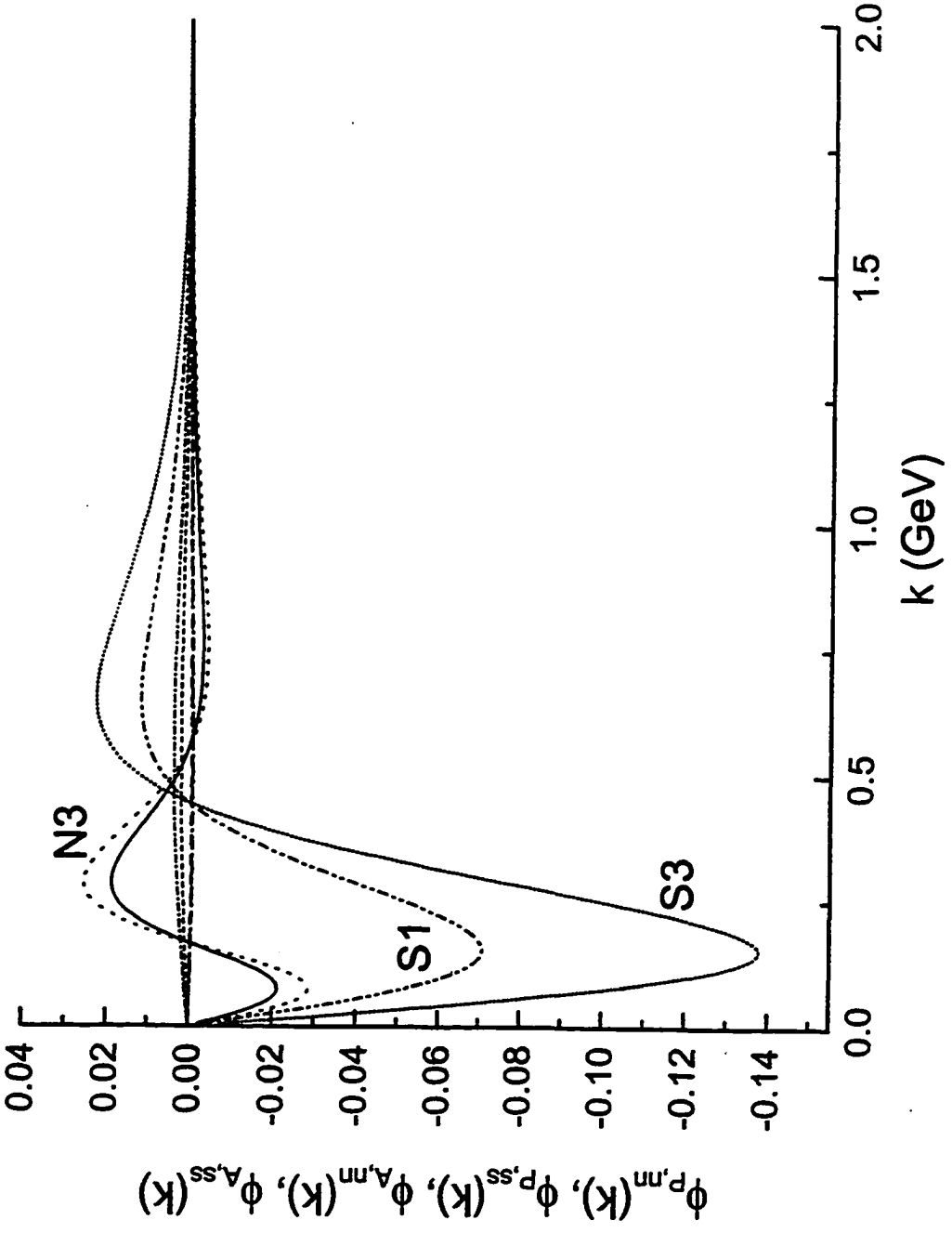

Fig. 4.9

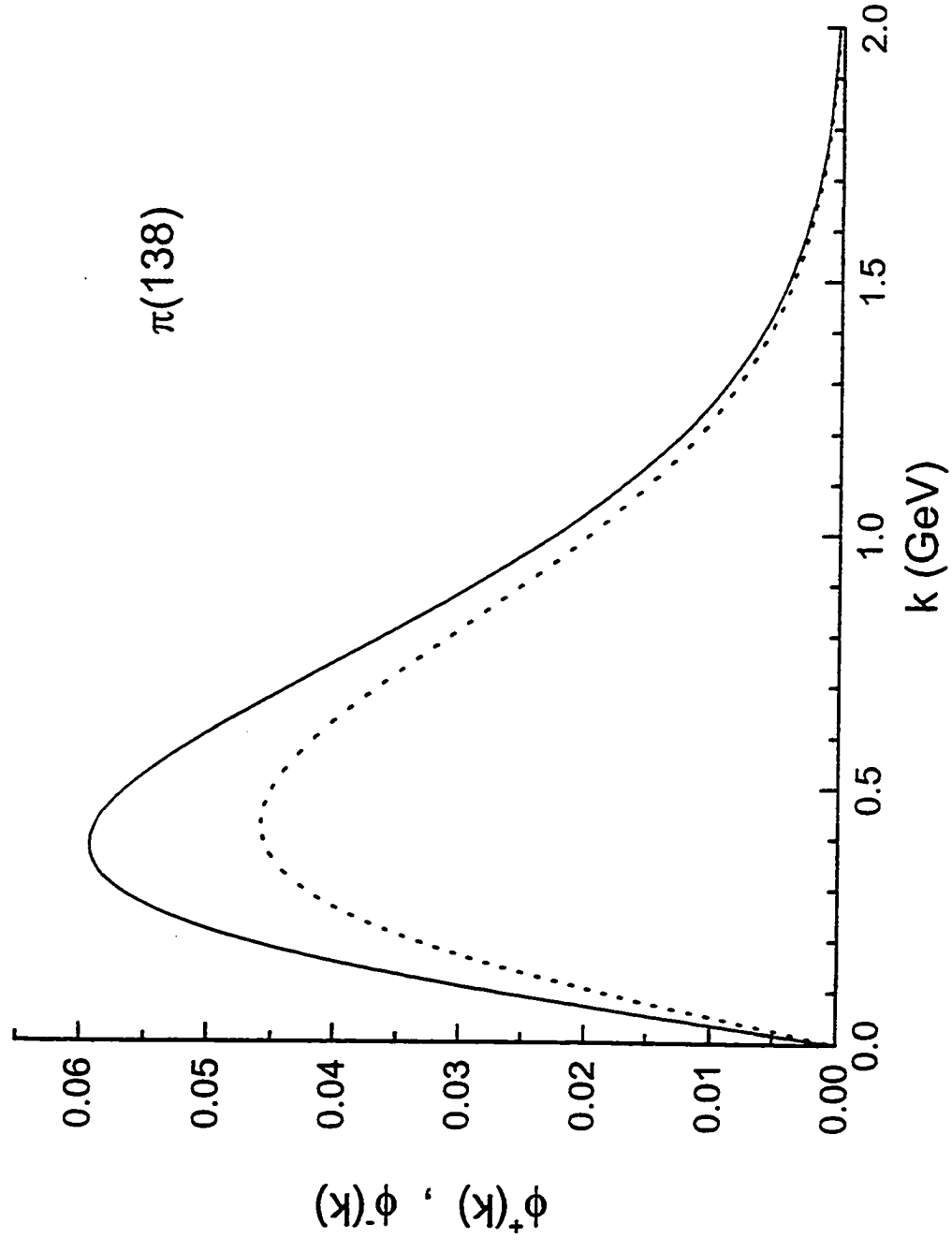

Fig. 5.1

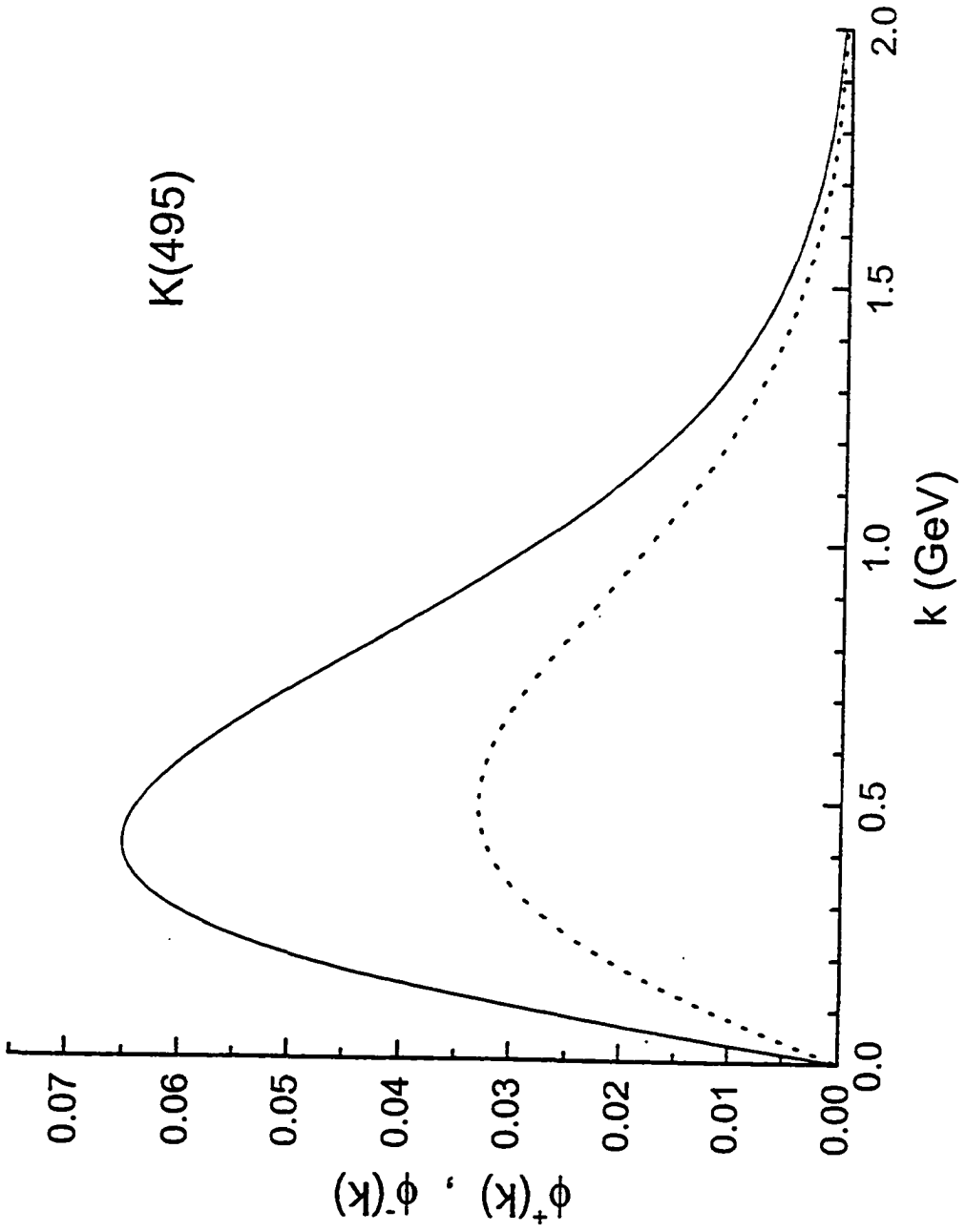

Fig. 5.2

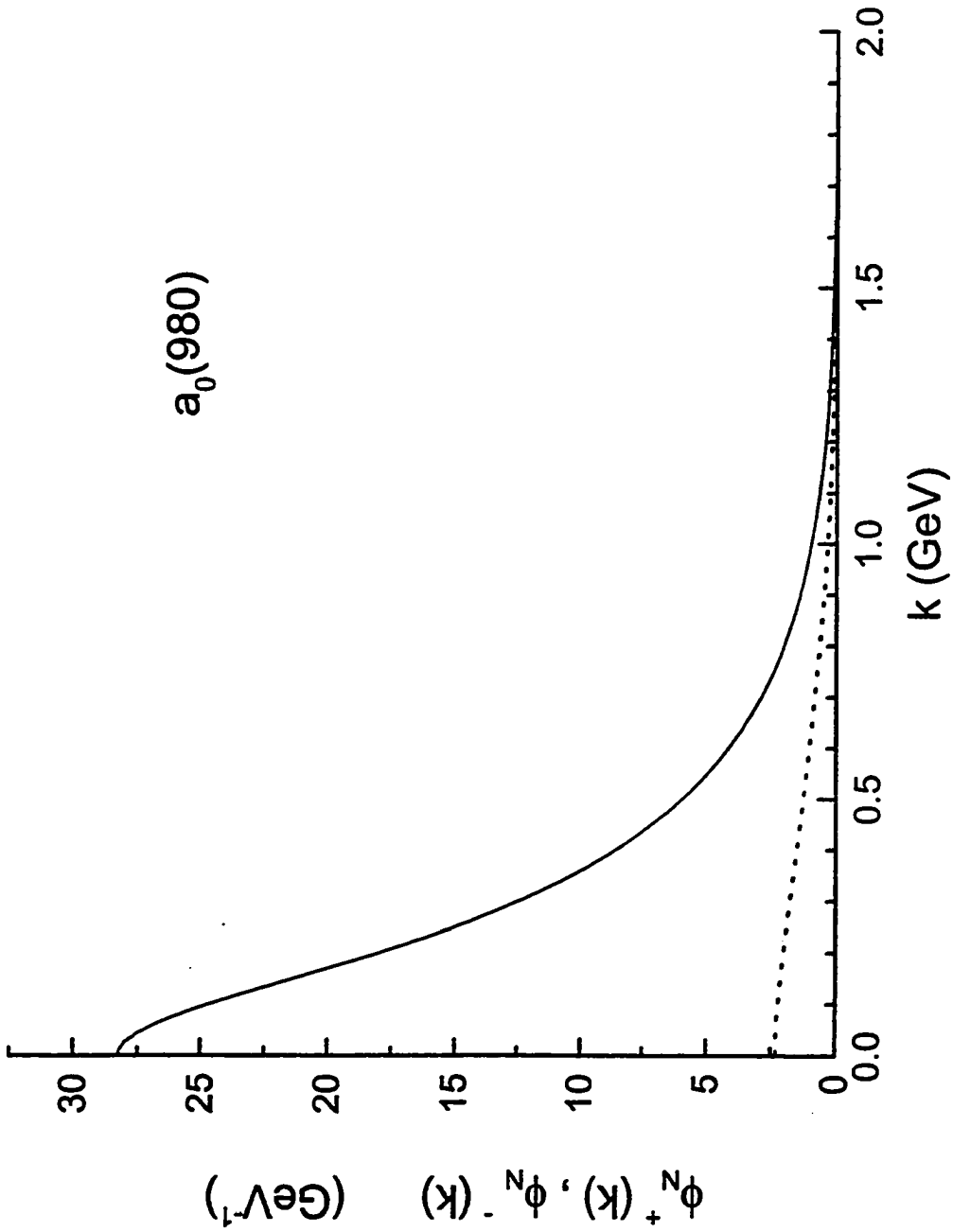

Fig. 5.3

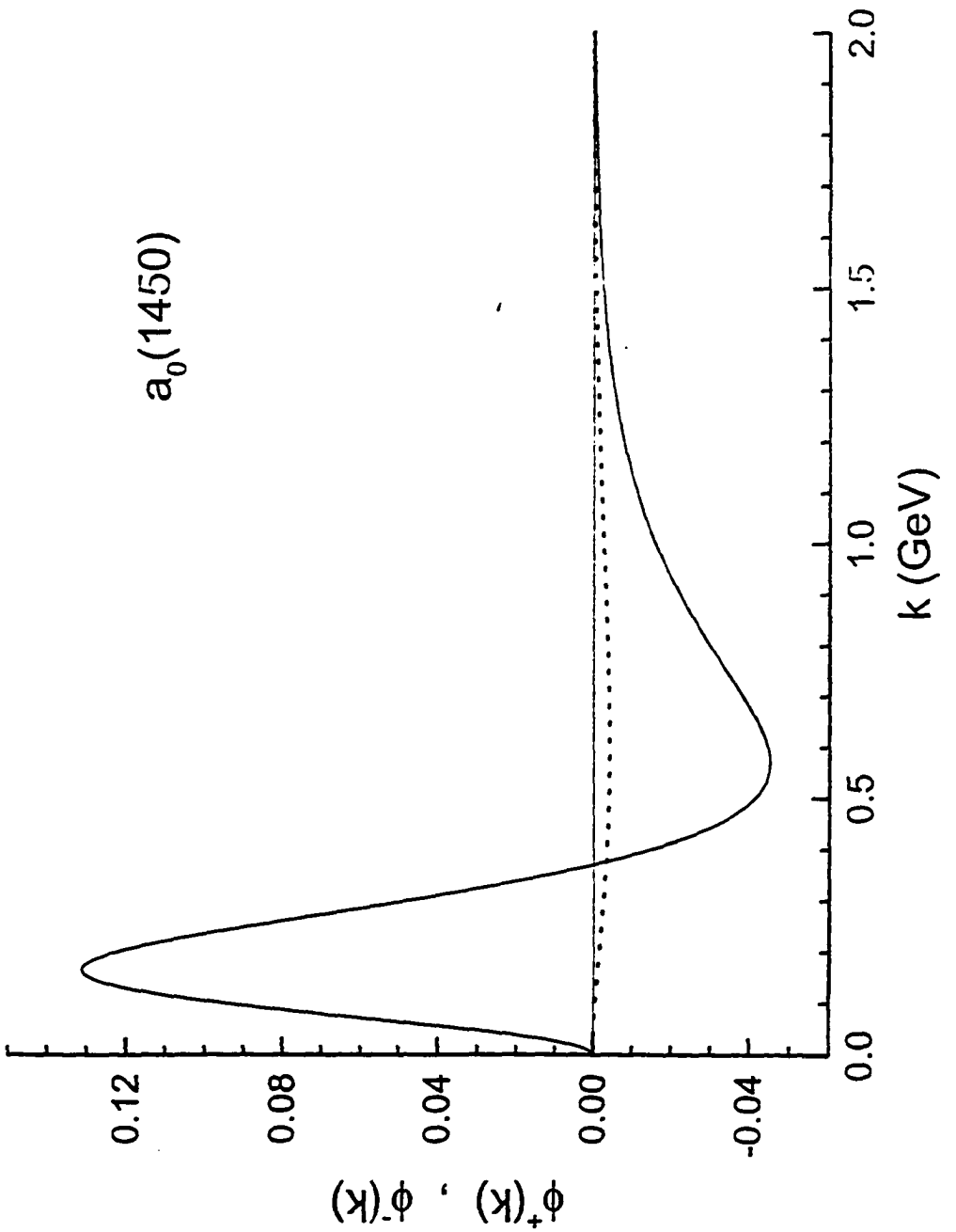

Fig. 5.4

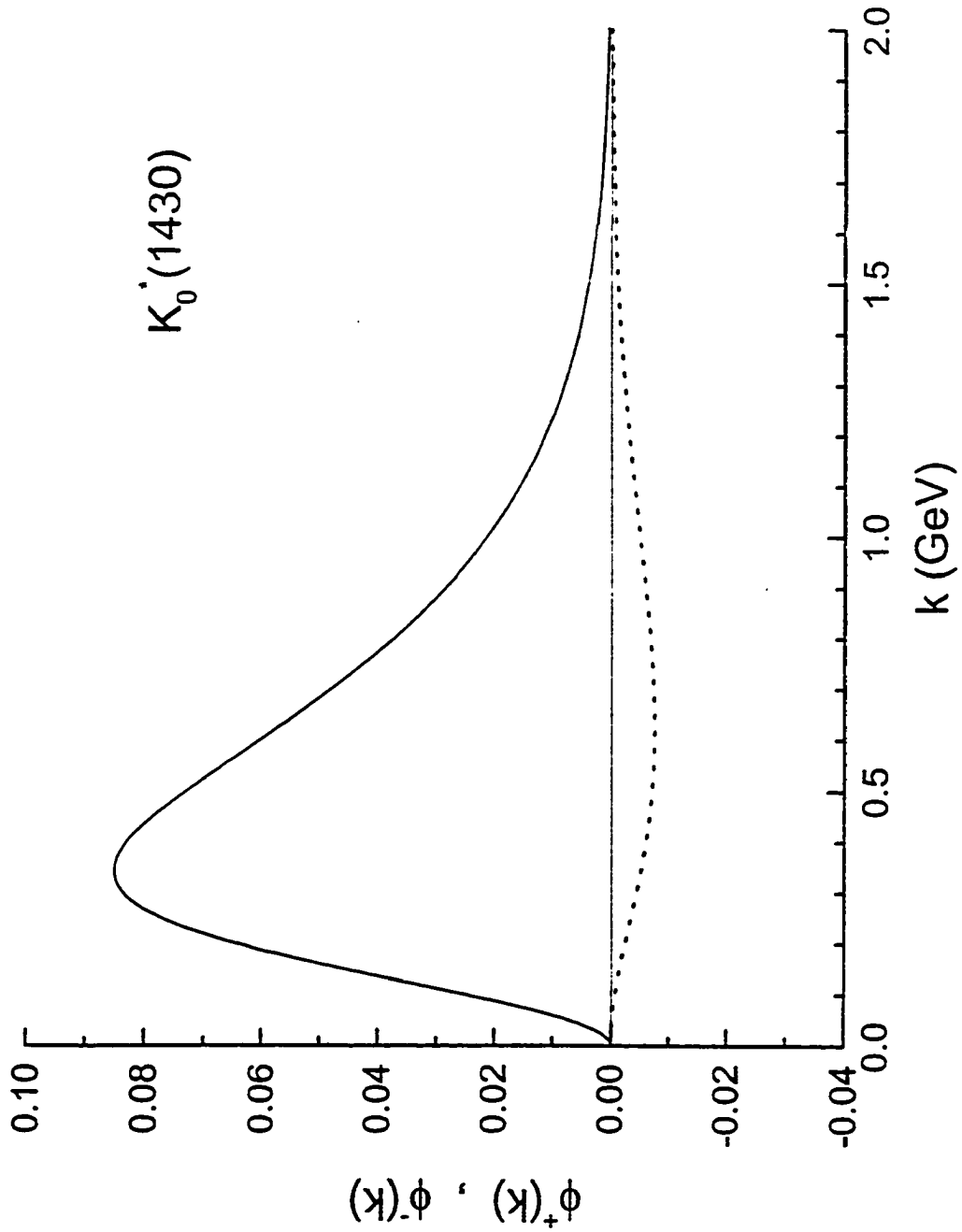

Fig. 5.5

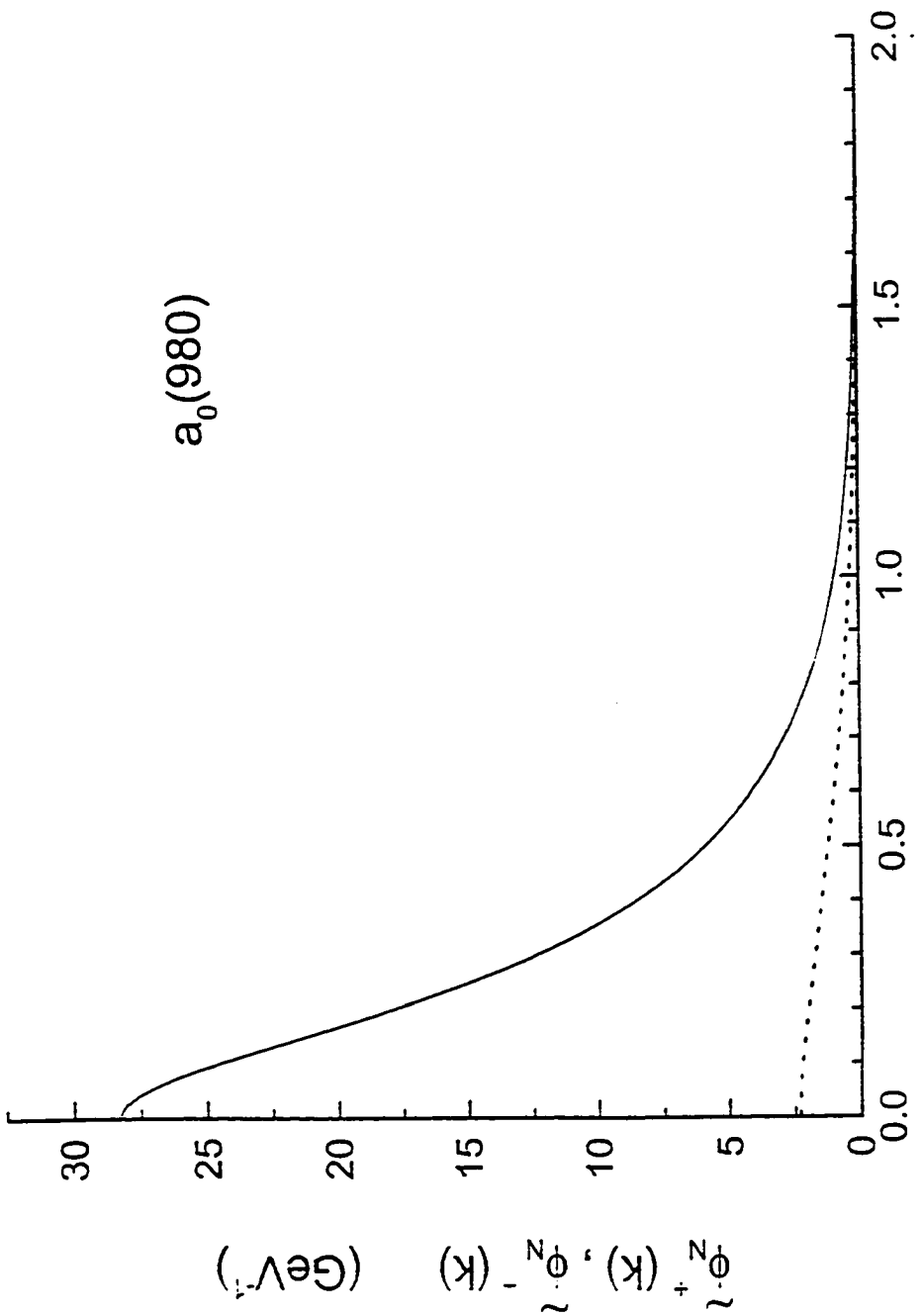

Fig. 5.6

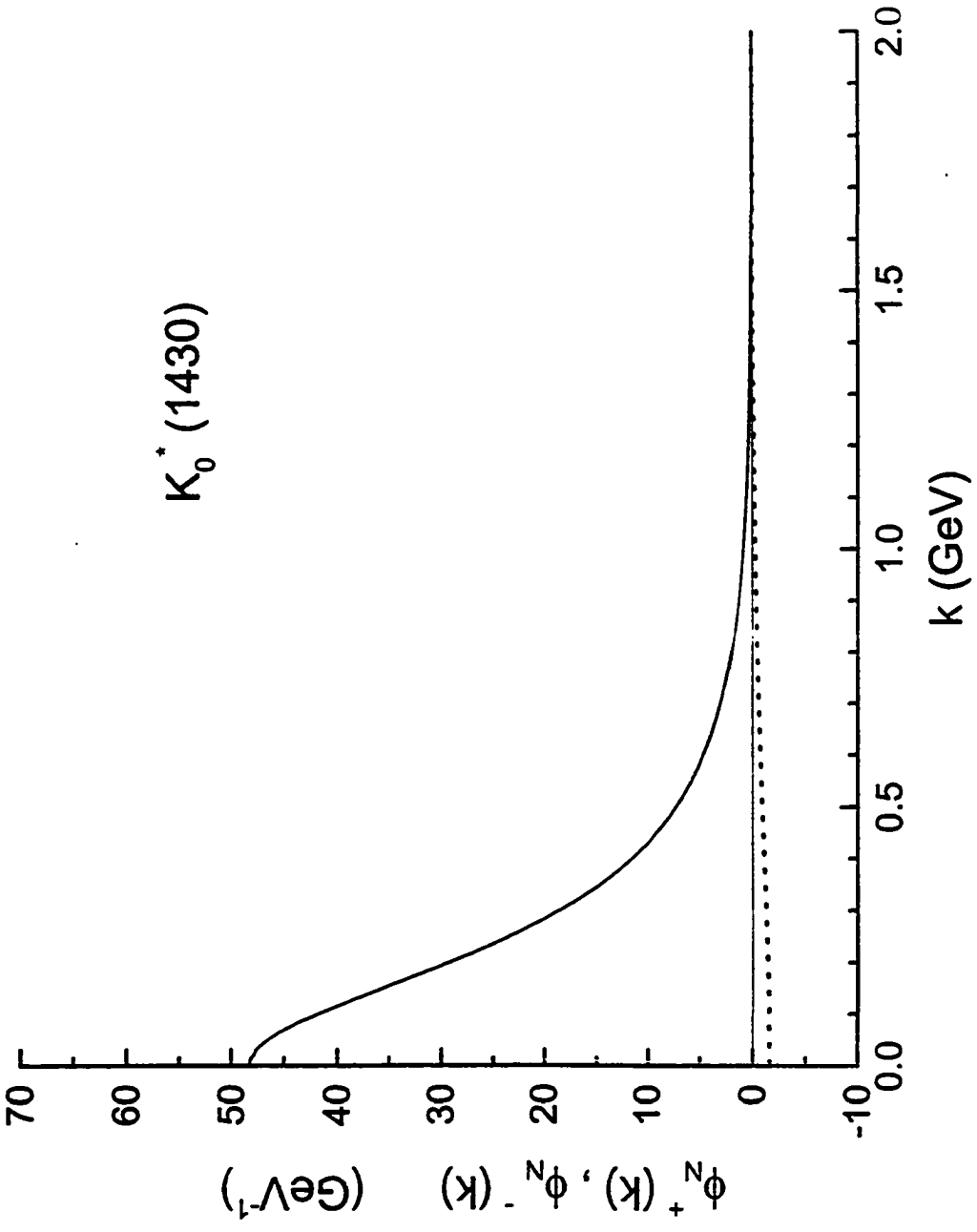

Fig. 5.7

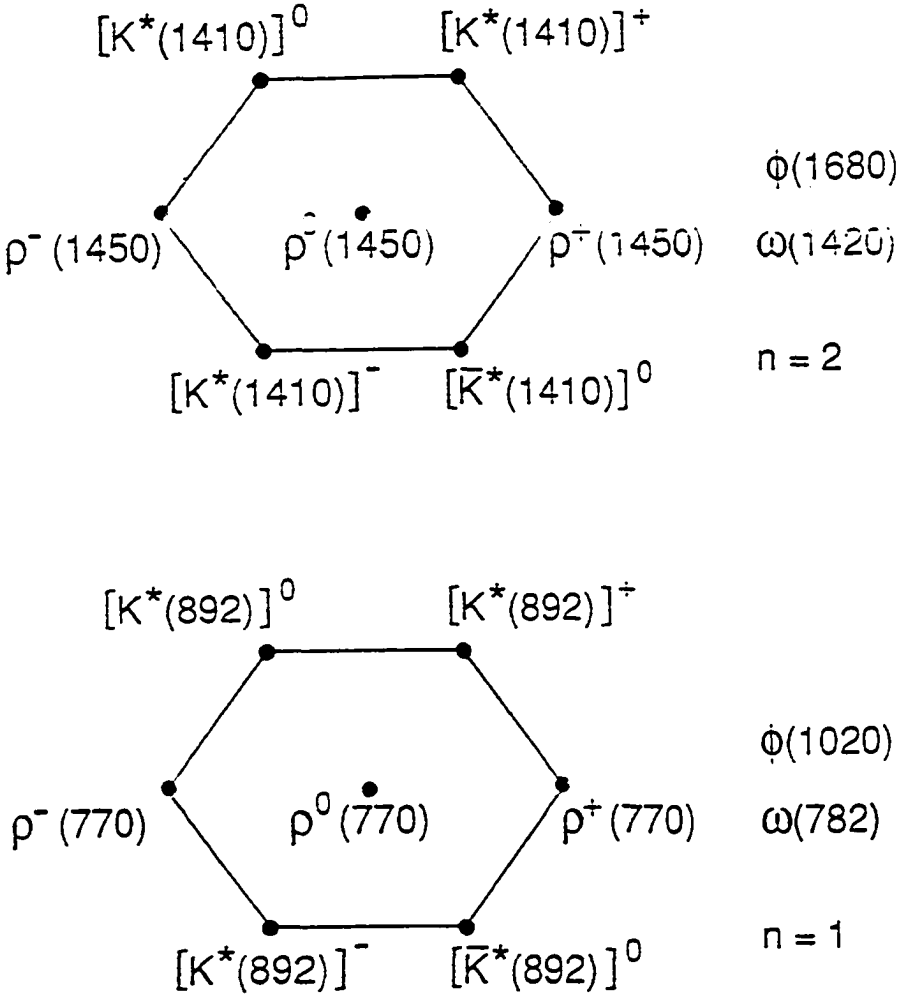

Fig. 6.1

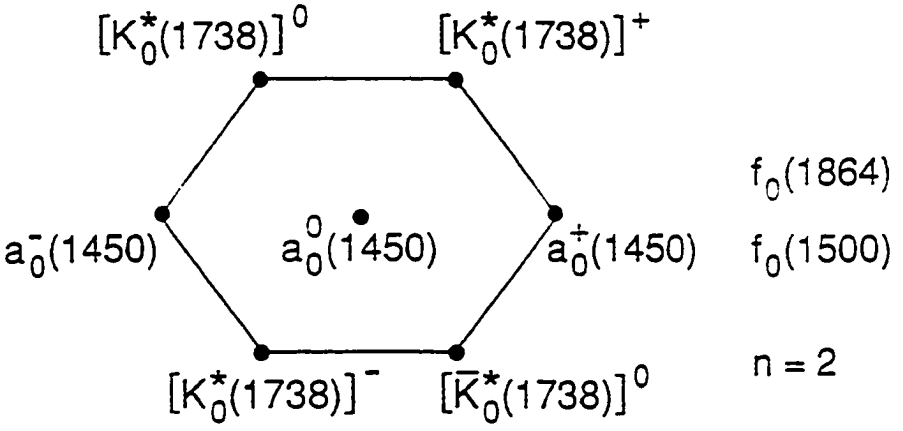

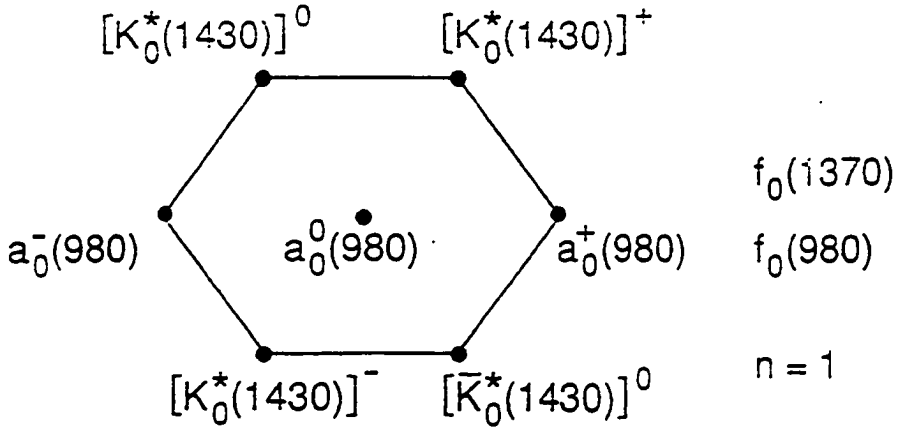

Fig. 6.2

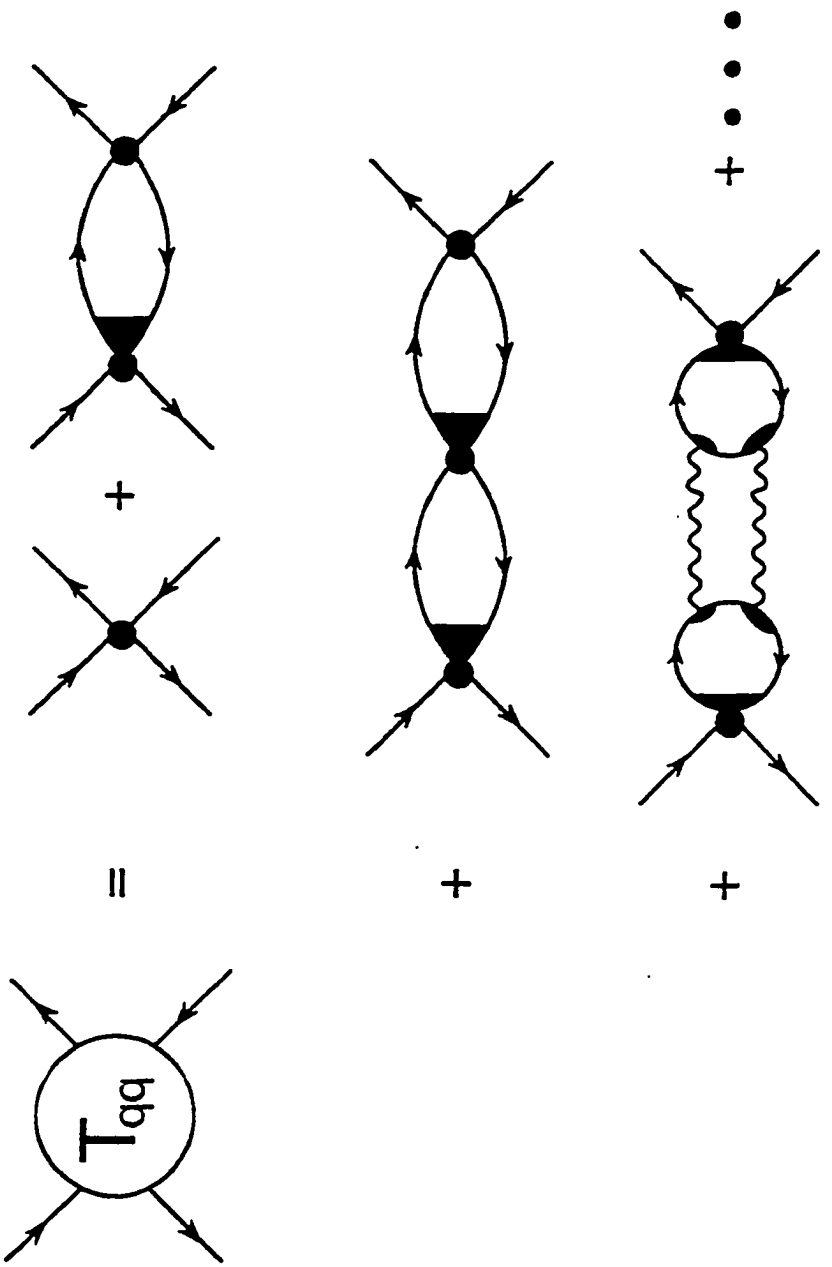

Fig. 6.3

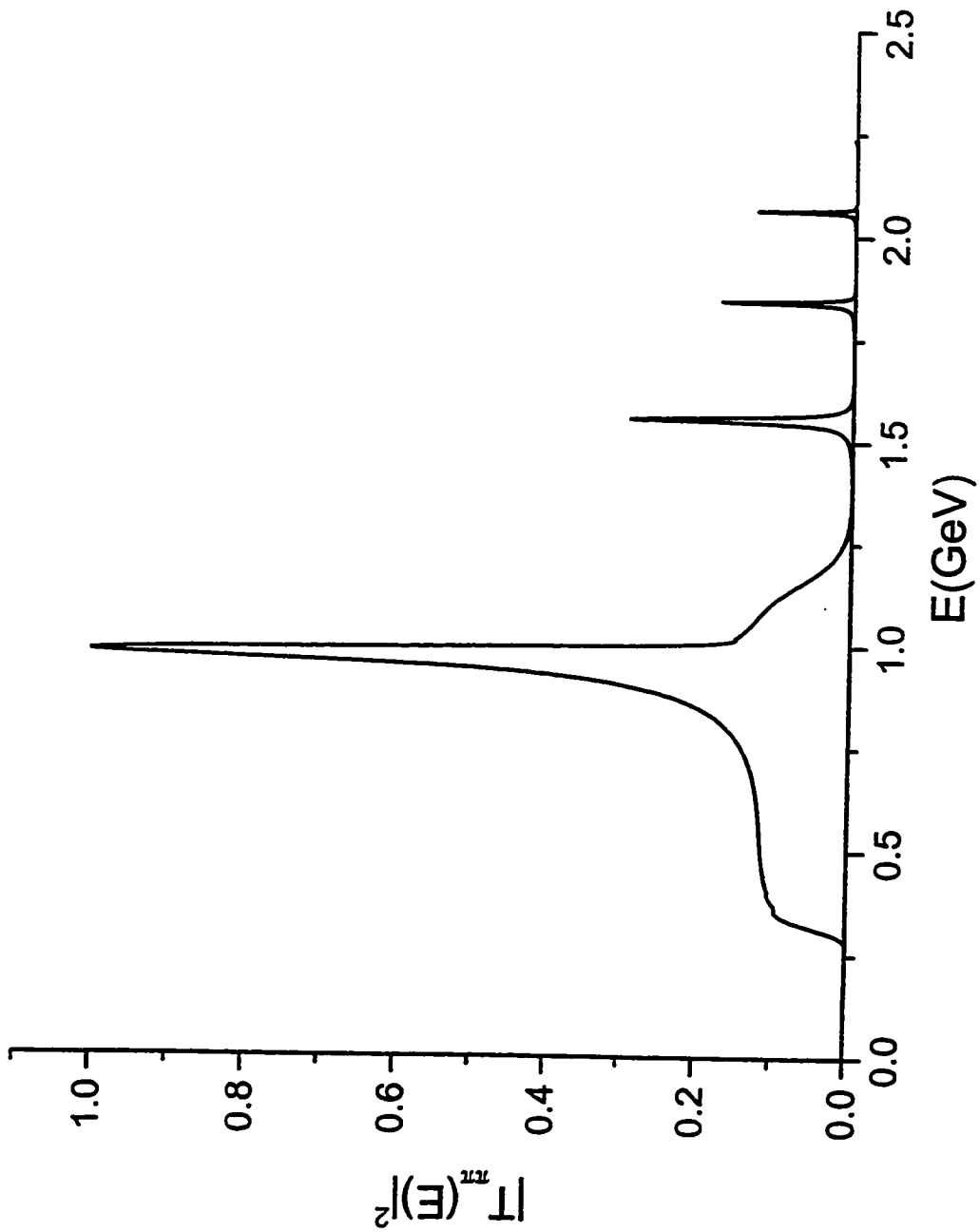

Fig. 6.4

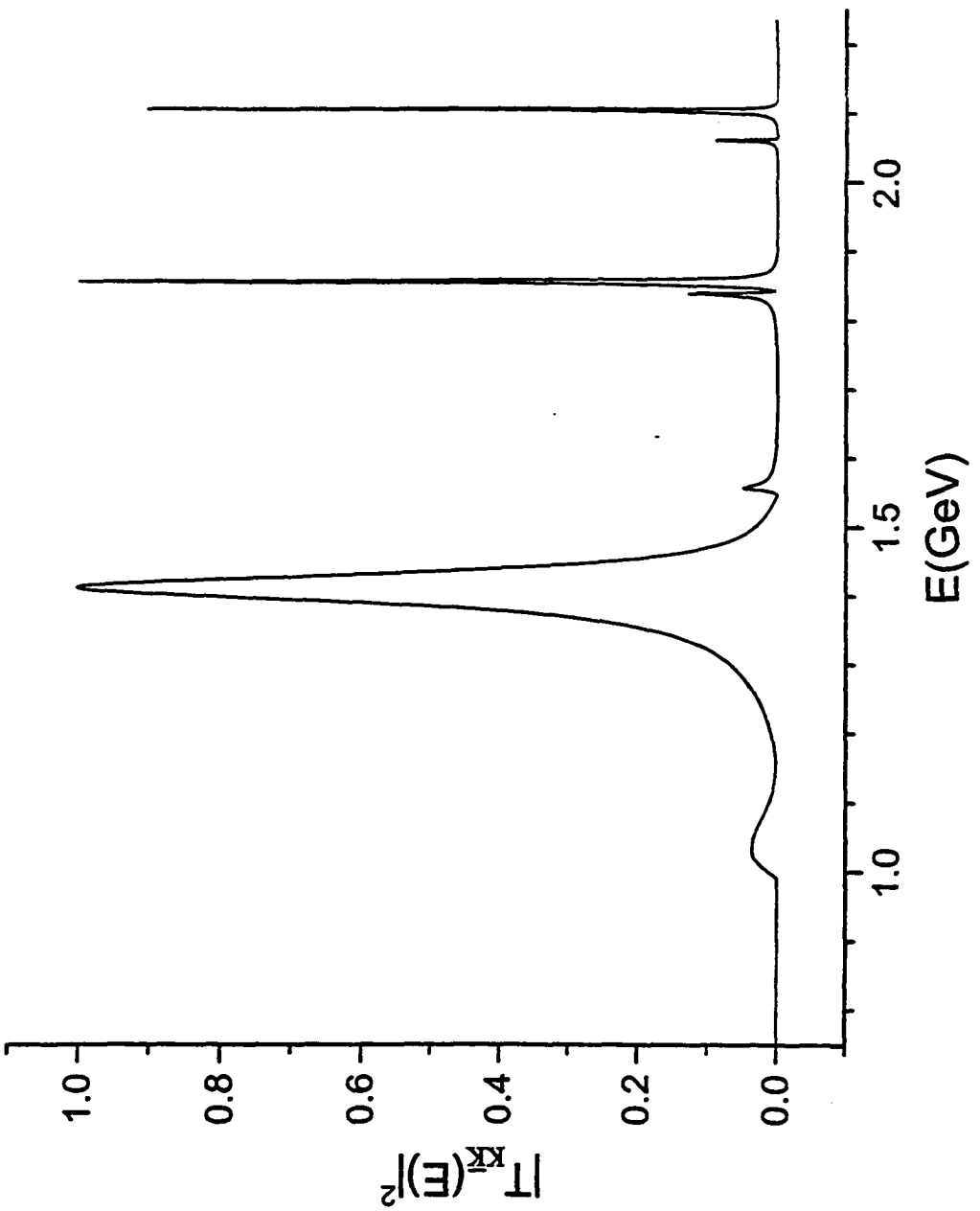

Fig. 6.5

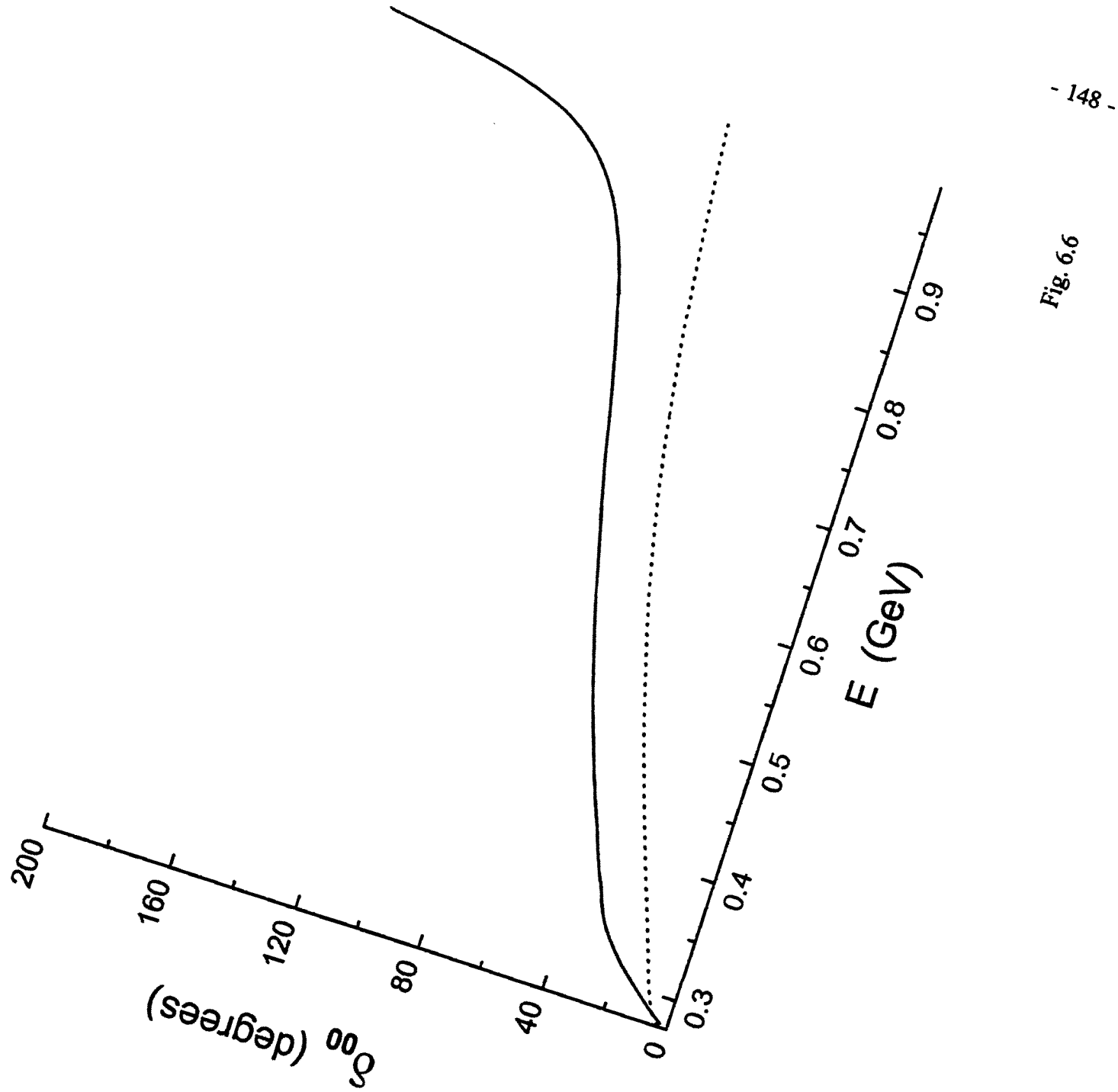

Fig. 6.6

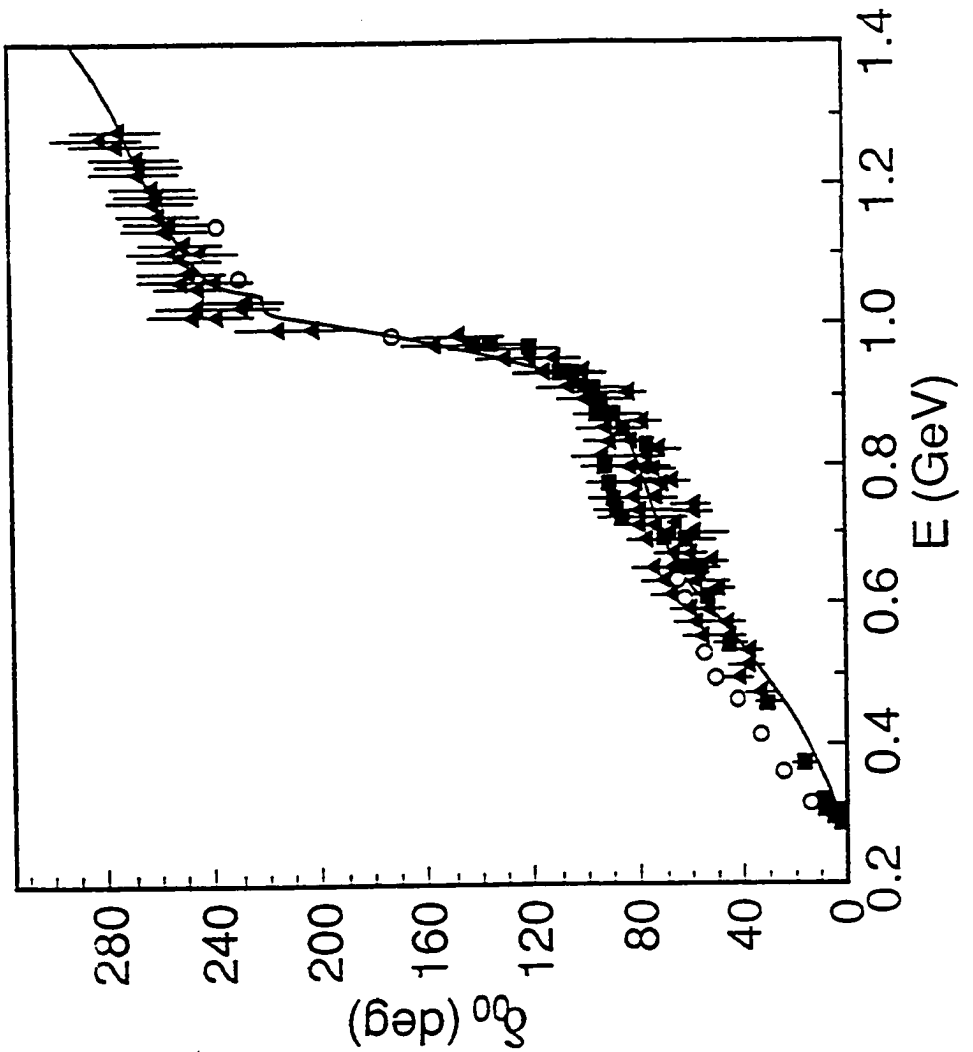

Fig. 6.7

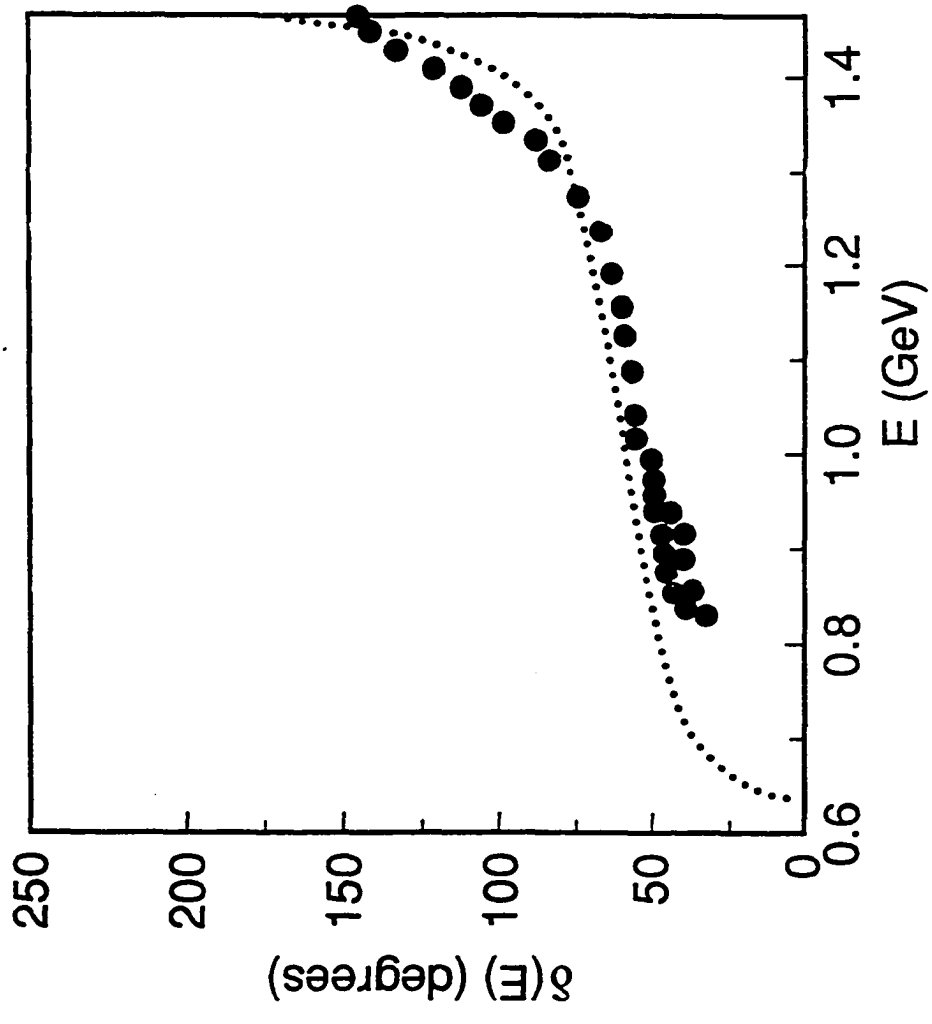

Fig. 6.8

References

[An00] A.V. Anisovich, V.V. Anisovich, and A.V. Sarantsev, arXiv: hep-ph/0003313 (March, 2000).

[As88] D. Aston *et al.* [LASS Collaboration] Nucl. Phys. B296, 493(1988).

[Bl98] D. Black, A.H. Fariborz, F. Sannino, and J. Schechter, Phys. Rev. D58, 054012(1998).

[Bl99] D. Black, A.H. Fariborz, F. Sannino, and J. Schechter, Phys. Rev. D59, 074026(1999).

[Bl00] D. Black, A.H. Fariborz, and J. Schechter, Phys. Rev. D61, 074001(2000).

[Bu00] D. Bugg, private communication.

[Ce97] L.S. Celenza, Xiang-Dong Li, and C.M. Shakin, Phys. Rev. C55, 1492(1997).

[Ce99a] L.S. Celenza, Bo Huang, Huangsheng Wang, and C.M. Shakin, Phys. Rev. C60, 025202(1999); (E) C60, 039901(1999).

[Ce99b] L.S. Celenza, Bo Huang, Huangsheng Wang, and C.M. Shakin, Phys. Rev. C60, 065210(1999).

[Ce99c] L.S. Celenza, Bo Huang, Huangsheng Wang, and C.M. Shakin, Phys. Rev. C60, 065209(1999).

[Ce99d] L.S. Celenza, Bo Huang, and C.M. Shakin, Phys. Rev. C59, 1030(1999).

[Ce99e] L.S. Celenza, Bo Huang, Huangsheng Wang, and C.M. Shakin, Phys. Rev. C60, 035206(1999).

[Ce99f] L.S. Celenza, Bo Huang, Huangsheng Wang, and C.M. Shakin, Brooklyn College Report: BCCNT 99/111/283R3 (1999).

[Ce00] L.S. Celenza, Shun-fun Gao, Bo Huang, Huangsheng Wang, and C.M. Shakin, Phys. Rev. C61, 035201 (2000).

[Ch00] S.N. Cherry and M.R. Pennington, "There is no $\kappa(900)$", arXiv: hep-ph/0005208 (May, 2000).

[Cl00] F.E. Close and A. Kirk, The mixing of the $f_0(1370)$, $f_0(1500)$ and $f_0(1710)$ and the search for the scalar glueball, arXiv: hep-ph/0004241(2000).

[Co00] S.R.Cotanch and F.J. Llanes-Estrada, arXiv: hep-ph/0009191(2000).

[El98] V. Elias, A.H. Fariborz, Fang Shi, and T.G. Steele, Nucl. Phys. A633, 279(1998).

[Fe71] A.L. Fetter, and J.D. Walecka, *Quantum Theory of Many-Particle Systems*, (McGraw-Hill, New York, 1971) [See Chapter 15.]

[Ha90] T. Hatsuda, Phys. Rev. Lett. 65, 543(1990).

[Ha94] T. Hatsuda and T. Kunihiro, Phys. Rep. 247, 221(1994).

[Ha96] M. Harada, F.Sannino, and J. Schechter, Phys. Rev. D54, 1991(1996).

[Ha99] T. Hannah, Phys. Rev. D60, 017502(1999).

[Ja77] R.Jaffe, Phys. Rev. D15, 281(1977).

[Ja95] G. Janssen, B. C. Pearce, K. Holinde and J. Speth, Phys. Rev. D52, 2690(1995).

[Ja00] M. Jamin, J.A. Oller and A. Pich, arXiv: hep-ph/0006045 (June, 2000).

[Ka00] Joachim Kambor and Kim Maltman, Phys. Rev. D62, 093023(2000).

[Ko00] M. Koll, R. Ricken, D. Merten, B. Metsch, and H. Petry, arXiv: hep-ph/0008220(2000).

[Ku90] T. Kunihiro and T. Hatsuda, Phys. Lett. B240, 209(1990).

[Ku99] T. Kunihiro, Invited talk presented at the Workshop on Hadron Spectroscopy (WHS99), Frascati, March 1999; arXiv: hep-ph/9905262 (1999).

[Le99a] W. Lee and D. Weingarten,Nucl. Phys. Proc. Suppl. 73, 249(1999).

[Le99b] W. Lee and Weingarten, Phys. Rev. D59, 094508(1999).

[Le00] W. Lee and D. Weingarten, Phys. Rev.D61, 014015(2000).

[Ll00] F.J.Llanes-Estrada and S.R. Cotanch, Phys. Rev. Lett. 84, 1102(2000).

[Ma99] K. Maltman, Phys. Lett. B462, 14(1999).

[Ma00] K. Maltman, Scalar decay constants and the nature of the $a_0(980)$, Presented at the International Conference on Quark Nuclear Physics, Adelaide (Feb. 21-25, 2000)-arXiv: hep-ph/0005155(2000).

[Me96] B. Metsch and H.R. Petry, Acta Phys. Polon. B27, 3307(1996).

[Me00] Ulf-G. Meissner, Contribution to the III Workshop on Physics and Detectors for DAΦNE, Frascati, Nov. 16-19(1999); arXiv: hep-ph/0001066 (Jan 2000).

[Mü94] C.R. Münz, J. Resay, B.C. Metsch, and H.R. Petry, Nucl. Phys. A578, 418(1994).

[Na89] S. Narison, *QCD Spectral Sum Rules*, (World Scientific, Singapore, 1989).

[Ol99a] J.A. Oller and E. Oset, Phys. Rev. D60, 074023(1999).

[Ol99b] J.A. Oller, E. Oset and J.R. Pelaez, Phys. Rev. D59, 074001(1999); (E) Phys. Rev. D59, 099906(1999).

[Pe99] M.R. Pennington, Riddle of the scalars: Where is the σ ? Talk given at the Workshop on Hadron Spectroscopy (WHS99), Frascati (March, 1999); arXiv: hep-ph/9905241 (May, 1999).

[Ri00] R. Ricken, M. Koll, D. Merten, B. Metsch, and H.R. Petry, arXiv: hep-ph/0008221(2000).

[Ro70] D.J.Rowe, *Nuclear Collective Motion: Models and Theory* (Mcthuen, London, 1970). [See Fig.14.3.]

[Sa95] F. Sannino and J. Schechter, Phys. Rev. D52, 96(1995).

[Sh00] C.M.Shakin and Huangsheng Wang, Brooklyn College Report: BCCNT 00/081/294 (2000).

[Sh00a] C.M. Shakin and Huangsheng Wang, Brooklyn College Report: BCCNT 00/061/291(2000).

[Sh00b] F. Shi, T.G. Steele, V. Elias, K.B. Speaque, Ying Xue, and A.H. Fariborz, Nucl. Phys. A671, 416(2000).

[Sh01] C.M.Shakin and Huangsheng Wang, Phys. Rev. D63, 014019(2001).

[Tö95] N.A. Törnqvist, Z. Phys. C68, 647(1995).

[Vo98] M.K.Volkov , D. Ebert and M. Nagy, Int. J. Mod. Phys. A13, 5443(1998).

[Vo99] M.K.Volkov and V.L.Yudichev, Int. J. Mod. Phys. A14, 4621(1999).

[Vo00] M.K.Volkov and V.L.Yudichev, Phys. Part. Nucl. 31, 282(2000).

[We82] J.Weinstein and N.Isgur, Phys. Rev. Lett. 48, 659(1982).

[We97] D. Weingarten, Nucl. Phys. Suppl. 53, 232(1997).

[Zo94] B.S.Zou and D.V. Bugg, Phys. Rev. D50, 591(1994).